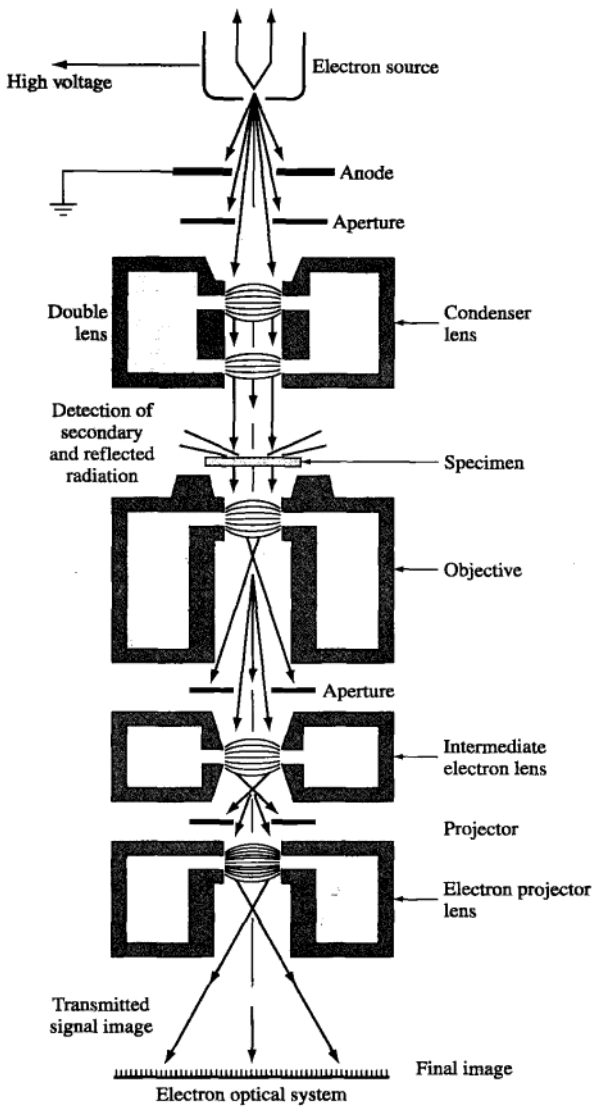

Figure 4.32
Schematic arrangement of electron lens system in a transmission electron microscope. All the lenses are enclosed in a column that is evacuated during operation. The path of the electron beam from the electron source to the final projected transmitted image is indicated by arrows. A specimen thin enough to allow an electron beam to be transmitted through it is placed between the condenser and objective lenses as indicated.
(After L.E. Murr, "Electron and Ion Microscopy and Microanalysis," Marcel Decker, 1982, p. 105.)

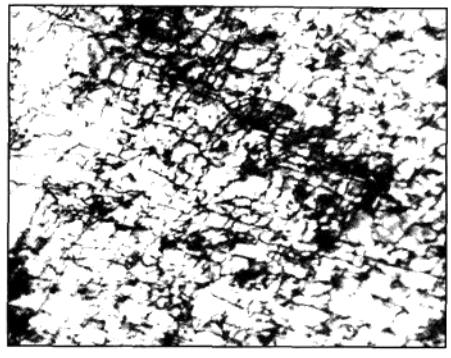

Figure 4.33
Dislocation structure in iron deformed 14 percent at −195°C. The dislocations appear as dark lines because electrons have been scattered along the linear irregular atomic arrangements of the dislocations. (Thin foil specimen; magnification 40,000×.)
(Electron and Ion Microscopy and Microanalysis: Principles and Applications by Murr, Lawrence Eugene. Copyright 1982 by CRC Press LLC (J). Reproduced with permission of CRC Press LLC (J) in the format Textbook via Copyright Clearance Center.)

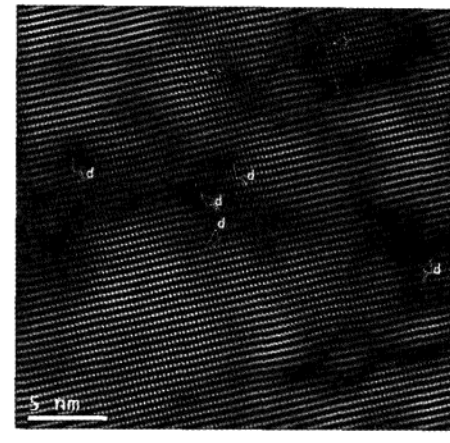

Figure 4.34
HRTEM image of AℓN atomic structure. The image shows two types of defects: (1) dislocations represented by arrows and the letter "d", and (2) stacking fault represented by two opposing arrows (top of the image).
(Courtesy of Dr. Jharna Chavdhuri, Department of Mechanical Engineering, Texas Tech University.)

similar to those of the TEM. However, the sample must be significantly thinner—on the order of 10 to 15 nm. In some situations, it is possible to view a two-dimensional projection of a crystal with the accompanying defects. To achieve this, the thin sample is tilted so that a low-index direction in the plane is perpendicular to the direction of electron beam (atoms are exactly on top of each other relative to the beam). The diffraction pattern is representative of the periodic potential for the electrons in two dimensions. The interference of all the diffracted beams and the primary beam, when brought together again using the objective lens, provides an enlarged picture of the periodic potential. Figure 4.34 shows the HRTEM image of several dislocations (marked by "d") and some stacking faults (marked by arrows) in AℓN thin film. In the figure, the periodic order of the atoms in the undisturbed regions is clearly observed (lower left). Dislocations create a wavy pattern in atomic structure. One can clearly see the disturbance in the atomic structure as a result of defects such as dislocations and stacking faults. It should be noted that due to limitations in the objective lens in HRTEM, accurate quantitative analysis of images is not easy to achieve and must be done with care.

4.5.5 Scanning Probe Microscopes and Atomic Resolution

Scanning tunneling microscope (STM) and *atomic force microscope* (AFM) are two of many recently developed tools that allow scientists to analyze and image materials at the atomic level. These instruments and others with similar capabilities are collectively classified as *scanning probe microscopy* (SPM). The SPM systems have the ability to magnify the features of a surface to the subnanometer scale, producing an atomic-scale topographic map of the surface. These instruments have important applications in many areas of science including but not limited to surface sciences where the arrangement of atoms and their bonding are important; metrology where surface roughness of materials needs to be analyzed; and nanotechnology where the position of individual atoms or molecules may be manipulated and new nanoscale phenomena may be investigated. It is appropriate to discuss these systems, how they function, the nature of information they provide, and their applications.

Scanning Tunneling Microscope IBM researchers G. Binnig and H. Rohrer developed the STM technique in the early 1980s and later received the Nobel Prize in Physics in 1986 for their invention. In this technique, an extremely sharp tip (Fig. 4.35), traditionally made of metals such as tungsten, nickel, platinum-iridium, or gold, and more recently out of carbon nanotubes (see Sec. 11.11), is used to probe the surface of a sample.

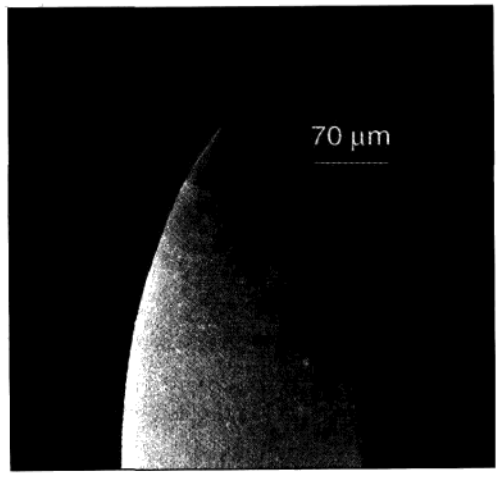

Figure 4.35
STM tip made of Pt-Ir alloy. The tip is sharpened using chemical etching techniques. (*Courtesy of Molecular Corp.*)

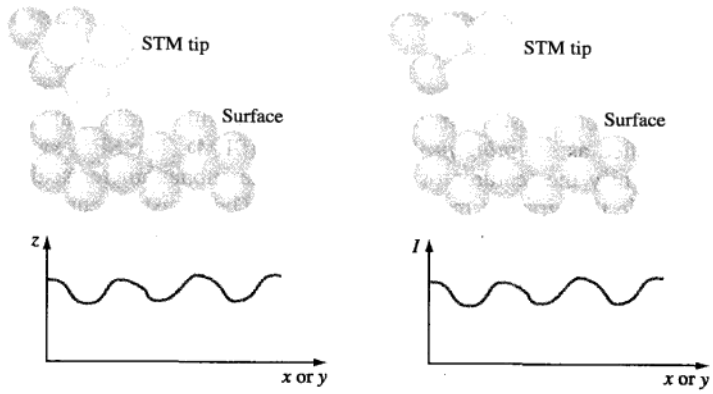

(*a*) Constant current mode (*b*) Constant height mode

Figure 4.36
Schematics showing the STM modes of operation. (*a*) Adjust the *z* coordinate of the tip to maintain constant current (record *z* adjustments), (*b*) Adjust the current in the tip to maintain constant height (record *I* adjustments).

Figure 4.37
STM image of the surface of platinum showing outstanding atomic resolution.
(*IBM Research, Almaden Research Center.*)

The tip is first positioned a distance in the order of an atom diameter ($\cong$0.1 to 0.2 nm) from the surface of the sample. At such proximity, the electron clouds of the atoms in the tip of the probe interact with the electron clouds of the atoms on the surface of the sample. If at this point, a small voltage is applied across the tip and the surface, the electrons will "tunnel" the gap and, therefore, produce a small current that

may be detected and monitored. Generally, the sample is analyzed under ultrahigh vacuum to avoid contamination and oxidation of its surface.

The produced current is extremely sensitive to the gap size between the tip and the surface. Small changes in the gap size produce an exponential increase in the detected current. As a result, small changes (less than 0.1 nm) in the position of the tip relative to the surface may be detected. The magnitude of current is measured when the tip is positioned directly above an atom (its electron cloud). This current is maintained at the same level as the tip moves over the atoms and valleys between the atoms (*constant current mode*) (Fig. 4.36*a*). This is accomplished by adjusting the vertical position of the tip. The small movements required to adjust and maintain the current through the tip is then used to map the surface. The surface may also be mapped using a *constant height mode* in which the relative distance between the tip and the surface is maintained at a constant value and the changes in current are monitored (Fig. 4.36*b*). The quality of the surface topography achieved by STM is striking as observed in the STM images of the surface of platinum (Fig. 4.37).

Clearly, what is extremely important here is that the diameter of the tip should be of the order of a single atom to maintain atomic-scale resolution. The conventional metal tips can easily be worn and damaged during the scanning process, which results in poor image quality. More recently, carbon nanotubes of about one to tens of nanometer in diameter are being used as nanotips for STM and AFM applications because of their slender structure and strength. The STM is primarily used for topography purposes, and it offers no quantitative insight into the bonding nature and properties of the material. Because the apparatus's function is based on creating and monitoring small amounts of current, only those materials that can conduct electricity may be mapped, including metals and semiconductors. However, many materials of high interest to the research community, such as biological materials or polymers, are not conductive and, therefore, cannot be analyzed using this technique. For nonconducting materials, the AFM techniques are applied.

Atomic Force Microscope The AFM uses a similar approach as the STM in that it uses a tip to probe the surface. However, in this case, the tip is attached to a small cantilever beam. As the tip interacts with the surface of the sample, the forces (Van der Waals forces) acting on the tip deflect the cantilever beam. The interaction may be a short-range repulsive force (*contact mode AFM*) or a long-range attractive force (*non–contact-mode AFM*). The deflection of the beam is monitored using a laser and a photodetector set up as shown in Fig. 4.38. The deflection is used to calculate the force acting on the tip. During scanning, the force will be maintained at a constant level (similar to the constant current mode in STM), and the displacement of the tip will be monitored. The surface topography is determined from these small displacements. Unlike STM, the AFM approach does not rely on a current tunneling through the tip and can therefore be applied to all materials even nonconductors. This is the main advantage of AFM over its predecessor, STM. There are currently numerous other AFM-based techniques available with various imaging modes, including magnetic and acoustic. AFM in various imaging modes is being used in areas such as DNA research, in situ monitoring of corrosion in material, in situ annealing of polymers, and polymer-coating technology. The fundamental understanding of important issues in the above areas has been significantly enhanced because of the application of such techniques.

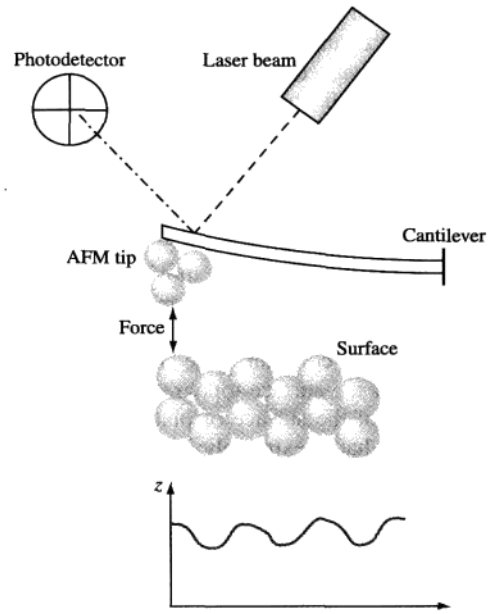

Figure 4.38
A schematic showing the basic AFM technique.

Understanding the behavior of advanced materials at the atomic level drives the state-of-the-art in high-resolution electron microscopy, which in turn provides an opportunity for the development of new materials. Electron and scanning probe microscopy techniques are and will be particularly important in nanotechnology and nanostructured materials.

4.6 SUMMARY

Most metals and alloys are melted and cast into semifinished or finished shapes. During the solidification of a metal into a casting, nuclei are formed that grow into grains, creating solidified cast metal with a polycrystalline grain structure. For most industrial applications, a very small grain size is desirable. The grain size may be indirectly determined by ASTM grain-size number n or directly determined by finding the average grain diameter. Large single crystals are rarely made in industry. However, an exception is the large single crystals of silicon produced for the semiconductor industry. For this material, special solidification conditions must be used, and the silicon must be of very high purity.

Crystal imperfections are present in all real crystalline materials, even at the atomic or ionic size level. Vacancies or empty atomic sites in metals can be explained in terms of the thermal agitation of atoms and are considered equilibrium lattice defects. Dislocations (line

defects) occur in metal crystals and are created in large numbers by the solidification process. Dislocations are not equilibrium defects and increase the internal energy of the metal. Images of dislocations can be observed in the transmission electron microscope. Grain boundaries are surface imperfections in metals created by crystals of different orientations meeting each other during solidification. Other important types of defects that affect the properties of materials are twins, low angle boundaries, high angle boundaries, twists, stacking faults, and precipitates.

Materials scientists and engineers use high-tech instruments to learn about the internal structure (including defect structure), behavior, and failure of materials. Instruments such as metallographs, SEM, TEM (HRTEM), and SPM allow analysis of materials from macro- to nanorange. Without such instruments, understanding the behavior of materials would be impossible.

4.7 DEFINITIONS

Sec. 4.1

Nuclei: small particles of a new phase formed by a phase change (e.g., solidification) that can grow until the phase change is complete.

Homogeneous nucleation (as pertains to the solidification of metals): the formation of very small regions of a new solid phase (called *nuclei*) in a pure metal that can grow until solidification is complete. The pure homogeneous metal itself provides the atoms that make up the nuclei.

Embryos: small particles of a new phase formed by a phase change (e.g., solidification) that are not of critical size and that can redissolve.

Critical radius r^* of nucleus: the minimum radius that a particle of a new phase formed by nucleation must have to become a stable nucleus.

Heterogeneous nucleation (as pertains to the solidification of metals): the formation of very small regions (called *nuclei*) of a new solid phase at the interfaces of solid impurities. These impurities lower the critical size at a particular temperature of stable solid nuclei.

Grain: a single crystal in a polycrystalline aggregate.

Equiaxed grains: grains that are approximately equal in all directions and have random crystallographic orientations.

Columnar grains: long, thin grains in a solidified polycrystalline structure. These grains are formed in the interior of solidified metal ingots when heat flow is slow and uniaxial during solidification.

Sec. 4.2

Polycrystalline structure: a crystalline structure that contains many grains.

Sec. 4.3

Alloy: a mixture of two or more metals or a metal (metals) and a nonmetal (nonmetals).

Solid solution: an alloy of two or more metals or a metal(s) and a nonmetal(s) that is a single-phase atomic mixture.

Substitutional solid solution: a solid solution in which solute atoms of one element can replace those of solvent atoms of another element. For example, in a Cu–Ni solid solution, the copper atoms can replace the nickel atoms in the solid-solution crystal lattice.

Interstitial solid solution: a solid solution formed in which the solute atoms can enter the interstices or holes in the solvent-atom lattice.

Sec. 4.4

Vacancy: a point imperfection in a crystal lattice where an atom is missing from an atomic site.

Interstitialcy (self-interstitial): a point imperfection in a crystal lattice where an atom of the same kind as those of the matrix lattice is positioned in an interstitial site between the matrix atoms.

Frenkel imperfection: a point imperfection in an ionic crystal in which a cation vacancy is associated with an interstitial cation.

Schottky imperfection: a point imperfection in an ionic crystal in which a cation vacancy is associated with an anion vacancy.

Dislocation: a crystalline imperfection in which a lattice distortion is centered around a line. The displacement distance of the atoms around the dislocation is called the *slip* or *Burgers vector* **b.** For an *edge dislocation*, the slip vector is perpendicular to the dislocation line, while for a *screw dislocation*, the slip vector is parallel to the dislocation line. A *mixed dislocation* has both edge and screw components.

Grain boundary: a surface imperfection that separates crystals (grains) of different orientations in a polycrystalline aggregate.

Grain-size number: a nominal (average) number of grains per unit area at a particular magnification.

Twin boundary: a mirror image misorientation of the crystal structure which is considered a surface defect.

Low-angle boundary (tilt): an array of dislocations forming angular mismatch inside a crystal.

Twist boundary: an array of screw dislocations creating mismatch inside a crystal.

Stacking fault: a surface defect formed due to improper (out of place) stacking of atomic planes.

Sec. 4.5

Scanning electron microscope (SEM): an instrument used to examine the surface of a material at very high magnifications by impinging electrons.

Transmission electron microscope (TEM): an instrument used to study the internal defect structures based on passage of electron through a thin films of materials.

High-resolution transmission electron microscope (HRTEM): a technique based on TEM but with significantly higher resolution by using significantly thinner samples.

Scanning probe microscopy (SPM): microscopy techniques such as STM and AFM that allow mapping of the surface of a material at the atomic level.

4.8 PROBLEMS

Answers to problems marked with an asterisk are given at the end of the book.

Knowledge and Comprehension Problems

4.1 Describe and illustrate the solidification process of a pure metal in terms of the nucleation and growth of crystals.

4.2 Define the homogeneous nucleation process for the solidification of a pure metal.

4.3 In the solidification of a pure metal, what are the two energies involved in the transformation? Write the equation for the total free-energy change involved in the transformation of liquid to produce a strain-free solid nucleus by homogeneous nucleation. Also illustrate graphically the energy changes associated with the formation of a nucleus during solidification.

4.4 In the solidification of a metal, what is the difference between an embryo and a nucleus? What is the critical radius of a solidifying particle?

4.5 During solidification, how does the degree of undercooling affect the critical nucleus size? Assume homogeneous nucleation.

4.6 Distinguish between homogeneous and heterogeneous nucleation for the solidification of a pure metal.

4.7 Describe the grain structure of a metal ingot that was produced by slow-cooling the metal in a stationary open mold.

4.8 Distinguish between equiaxed and columnar grains in a solidified metal structure.

4.9 How can the grain size of a cast ingot be refined? How is grain refining accomplished industrially for aluminum alloy ingots?

4.10 What special techniques must be used to produce single crystals?

4.11 How are large silicon single crystals for the semiconductor industry produced?

4.12 What is a metal alloy? What is a solid solution?

4.13 Distinguish between a substitutional solid solution and an interstitial solid solution.

4.14 What are the conditions that are favorable for extensive solid solubility of one element in another (Hume-Rothery rules)?

4.15 Describe an interstitial site.

4.16 Describe and illustrate the following types of point imperfections that can be present in metal lattices: (*a*) vacancy, (*b*) divacancy, and (*c*) interstitialcy.

4.17 Describe and illustrate the following imperfections that can exist in crystal lattices: (*a*) Frenkel imperfection and (*b*) Schottky imperfection.

4.18 Describe and illustrate the edge- and screw-type dislocations. What type of strain fields surround both types of dislocations?

4.19 Describe the structure of a grain boundary. Why are grain boundaries favorable sites for the nucleation and growth of precipitates?

4.20 Describe and illustrate the following planar defects: (*a*) twins, (*b*) low-angle tilt boundaries, (*c*) small-angle twist boundaries, (*d*) external surfaces, and (*e*) stacking faults. For each defect, express the impact on the properties of the material.

4.21 Describe the concept of volume or three dimensional defects.

4.22 Describe the optical metallography technique. What qualitative and quantitative information can this technique provide? What levels of magnification can be achieved by this technique?

4.23 Why are grain boundaries easily observed in the optical microscope?

4.24 How is the grain size of polycrystalline materials measured by the ASTM method?

4.25 Describe various ranges of grain size. What do these ranges tell you about a metal?

4.26 Explain how one can measure the average grain size of a metal using a micrograph at a known magnification.

4.27 What is a scanning electron microscope (SEM)? What magnifications can it achieve? How does it work (draw a schematic). What information can it provide?

4.28 What is a transmission electron microscope (TEM)? How does it work (draw a schematic). What is the dimensional resolution that it can achieve? What information can it provide?

4.29 What is a high resolution transmission electron microscope (HRTEM)? What is the dimensional resolution that it can achieve? What information can it provide?

4.30 Describe the scanning tunneling microscope (STM). What are its modes of operation (draw a schematic)? What is the dimensional resolution that they can achieve? What information can it provide?

4.31 Describe the atomic force microscope (AFM). What are the modes of operation (draw a schematic)? What is the dimensional resolution that it can achieve? What information can it provide?

Application and Analysis Problems

***4.32** Calculate the size (radius) of the critically sized nucleus for pure platinum when homogeneous nucleation takes place.

4.33 Calculate the number of atoms in a critically sized nucleus for the homogeneous nucleation of pure platinum.

4.34 Calculate the size (radius) of the critical nucleus for pure iron when nucleation takes place homogeneously.

4.35 Calculate the number of atoms in a critically sized nucleus for the homogeneous nucleation of pure iron.

4.36 (*a*) The alloy used for the gold medal awarded to the first place winner in Salt Lake City Olympics had a composition of 92.0 a/o silver, 7.5 a/o copper, and 0.5 a/o gold (the medal is gold-plated). Determine the absolute mass of each metal in a 253-gram medal. Repeat the same calculation for (*b*) the silver medal: 92.5 a/o silver and 7.5 a/o copper, and (*c*) the bronze medal: 90 a/o copper and 10 a/o tin.

4.37 Assume that Figure 4.14 shows a representative image of the overall atomic composition of a substitutional solid solution of an alloy of nickel (dark spheres) and copper (light spheres) and estimate (*a*) the a/o of each element in overall crystal, (*b*) the defect density in a/o, and (*c*) the wt/o of each metal?

***4.38** (*a*) Calculate the radius of the largest interstitial void in the BCC α iron lattice. The atomic radius of the iron atom in this lattice is 0.124 nm, and the largest interstitial voids occur at the $(\frac{1}{4}, \frac{1}{2}, 0)$; $(\frac{1}{2}, \frac{3}{4}, 0)$; $(\frac{3}{4}, \frac{1}{2}, 0)$; $(\frac{1}{2}, \frac{1}{4}, 0)$, etc., type positions. (*b*) If an iron atom occupies this interstitial void, how many iron atom neighbors will it have, or in other words, what will its coordination number be?

4.39 In Example Problem 4.3, if a carbon atom occupies the interstitial void, how many iron neighbors will it have, or in other words, what will its coordination number be?

4.40 Consider a copper lattice with an excessive average of one vacancy in every 100 unit cells. What will be its density? Compare this to the theoretical density of copper.

***4.41** If there are 600 grains per square inch on a photomicrograph of a metal at 100×, what is its ASTM grain-size number?

4.42 If there are 400 grains per square inch on a photomicrograph of a ceramic material at 200×, what is the ASTM grain-size number of the material?

4.43 Determine, by counting, the ASTM grain-size number of the low-carbon sheet steel shown in Fig. P4.43. This micrograph is at 100×. Classify the grain size according to the value of *n*, i.e., coarse, medium, fine, or ultrafine grain size. Measure the area of the image for your calculations.

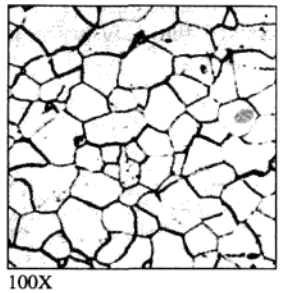

100X

Figure P4.43
(After "Metals Handbook," vol. 7, 8th ed., American Society for Metals, 1972, p. 4.)

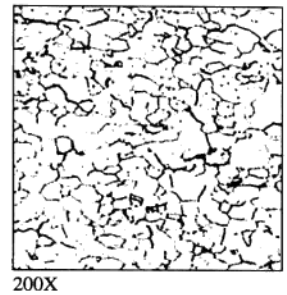

200X

Figure P4.44
(After "Metals Handbook," vol. 7, 8th ed., American Society for Metals, 1972, p. 4.)

4.44 Determine the ASTM grain-size number of the type 430 stainless steel micrograph shown in Fig. P4.44. This micrograph is at 200×. Classify the grain size according to the value of n, i.e., coarse, medium, fine, or ultrafine grain size. Measure the area of the image for your calculations.

***4.45** For the grain structure in Problem 4.43, estimate the average grain diameter.

4.46 For the grain structure in Problem 4.44, estimate the average grain diameter.

Synthesis and Evaluation Problems

4.47 It is easier for the iron lattice to house carbon atoms at temperatures slightly higher than 912°C than slightly lower temperatures. Use the results in Example Problem 4.3 and Problem 4.38 (solve this problem first if you have not already done so) to explain why.

***4.48** The γ iron and silver both possess FCC crystal structures. The location for interstitial voids will be the same for both. Will the size of the interstitial voids be different? If yes, what will be the interstitial void size for silver? Hint: Example Problem 4.3.

4.49 The chemical formula for an intermetallics compound of Cu and Al is Cu_2Al. According to the formula, the atom percent of Al should be exactly 33.33% (one out of three atoms should be aluminum). However, in practice, one can find a range of 31% to 37% for Al. How do you explain this discrepancy?

4.50 Iron oxide, FeO, is an ionic compound made up of Fe^{2+} cations and O^{2-} anions. However, when available, a small number of Fe^{3+} cations may replace Fe^{2+} cations. How will this substitution affect the atomic structure of the compound, if at all? (Consult Sec. 2.5.1 related to packing of ionic compounds.)

4.51 In chapter 3 (example 3.11), we calculated the theoretical density of copper to be 8.98 g/cm^3. Determine the experimentally measured density of copper by referring to Appendix II. To what do you attribute this difference?

4.52 The following pairs of elements can form solid solution alloys. Predict which ones will form substitutional and which ones interstitial alloys. Justify your answers.

(*a*) Copper and tin (bronze)
(*b*) Aluminum and silicon
(*c*) Iron and nitrogen
(*d*) Titanium and hydrogen

Element	Atom radius (nm)	Crystal structure	Electro-negativity	Valence
Aluminum	0.143	FCC	1.5	+3
Copper	0.128	FCC	1.8	+2
Manganese	0.112	Cubic	1.6	+2, +3, +6, +7
Magnesium	0.160	HCP	1.3	+2
Zinc	0.133	HCP	1.7	+2
Silicon	0.117	Diamond cubic	1.8	+4


Tutorial

4.53 Using the data in the following table, predict the relative degree of solid solubility of the following elements in aluminum:

(*a*) Copper
(*b*) Manganese
(*c*) Magnesium
(*d*) Zinc
(*e*) Silicon

Use the scale: very high, 70%–100%; high, 30%–70%; moderate, 10%–30%, low, 1%–10%; and very low, <1%.

Element	Atom radius (nm)	Crystal structure	Electro-negativity	Valence
Iron	0.124	BCC	1.7	+2, +3
Nickel	0.125	FCC	1.8	+2
Chromium	0.125	BCC	1.6	+2, +3, +6
Molybdenum	0.136	BCC	1.3	+3, +4, +6
Titanium	0.147	HCP	1.3	+2, +3, +4
Manganese	0.112	Cubic	1.6	+2, +3, +6, +7

***4.54** Using the data in the following table, predict the relative degree of atomic solid solubility of the following elements in iron:

(*a*) Nickel
(*b*) Chromium
(*c*) Molybdenum
(*d*) Titanium
(*e*) Manganese

Use the scale: very high, 70%–100%; high, 30%–70%; moderate, 10%–30%, low, 1%–10%; and very low, <1%.

4.55 Comment, based on calculations and comparisons, on the extent of solubility of copper in nickel based on the Hume-Rothery rules.

***4.56** (*a*) Estimate the density of a 75 wt% copper-25 wt% Ni alloy (use Appendix II for density data). (*b*) What will be the most probable crystal structure for this alloy? (*c*) Determine the mass in grams of the atoms inside a unit cell of this alloy. (*d*) Determine the lattice constant for this alloy.

4.57 (*a*) What is the theoretical atom % of each element in the compound FeO? What is the corresponding wt% of each element in the compound? What is your conclusion?

4.58 Sterling silver consists of approximately 93 wt% silver and 7 wt% copper. Discuss all the ways by which the addition of 7 wt% copper is beneficial.

4.59 What is the significance or impact of Schottky and/or Frenkel imperfection of the properties and behavior of ionic materials?

***4.60** When the magnification in a metallurgical microscope is increased by a factor of 2, what happens to the size of the area that you are observing (area magnification)?

4.61 For a given application, you would need to select the metal with larger grain size between copper (n = 7) and mild steel (n = 4). (*a*) Which one would you pick? (*b*) If strength is an important consideration, which alloy would you pick and why? (*c*) What if the application was at elevated temperatures; would your answer in part *b* change, and why?

4.62 The image below is an SEM micrograph (500×) and shows the fracture surface of a gear. Describe all the features that you are observing in this micrograph. Can you estimate the average grain diameter (assume C = 1.5)?

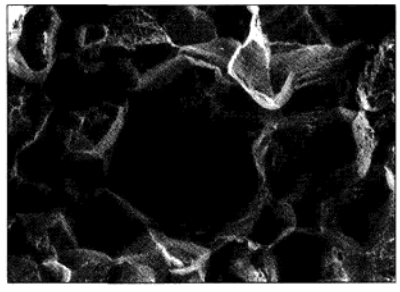

Figure P4.62
(Courtesy of met-tech)

4.63 The image below is an optical micrograph of 1018 steel (200×) made of mostly iron and a small amount of carbon (only 0.18 wt%). Describe all the features that you observe in this micrograph. What do you think the different colors represent?

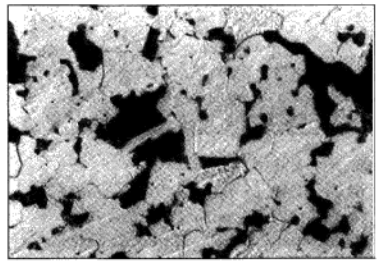

Figure P4.63

4.64 The image below is a TEM image and shows the structure of a cold-worked aluminum alloy. Describe all the features that you are observing in this micrograph. Speculate as to what happened.

Figure P4.64
(Handbook of Metallography. p 693, Fig 7. Reprinted with permission of ASM International. All rights reserved. www.asminternational.org.)

4.65 The image below is a TEM image and shows the annealed structure of heavily cold-worked iron. Describe the features of the image. Speculate as to what happened during annealing.

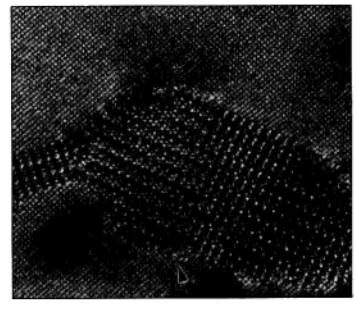

Figure P4.65
(After W.M. Rainforth, "Opportunities and pitfalls in characterization of nanoscale features," Materials Science and Technology, vol. 16 (2000) 1349–1355.)

4.66 A low carbon steel bar of circular cross-section is cast such that its grain structure is equiaxed. Your application requires that the diameter of the bar be reduced and the grain dimensions be longer along the longitudinal axis of the bar. How would you accomplish this?

4.67 In Fig. 4.34, the HRTEM image of AlM is presented. In the figure, the dislocations are highlighted with arrows and the letter "d." Can you verify that what the scientist designates as an edge dislocation is in fact an edge dislocation (hint: compare Fig. 4.34 to Fig. 4.18*a*)? Also, discuss how the scientist knows that a stacking fault exists at the top of the image.

CHAPTER 5

Thermally Activated Processes and Diffusion in Solids

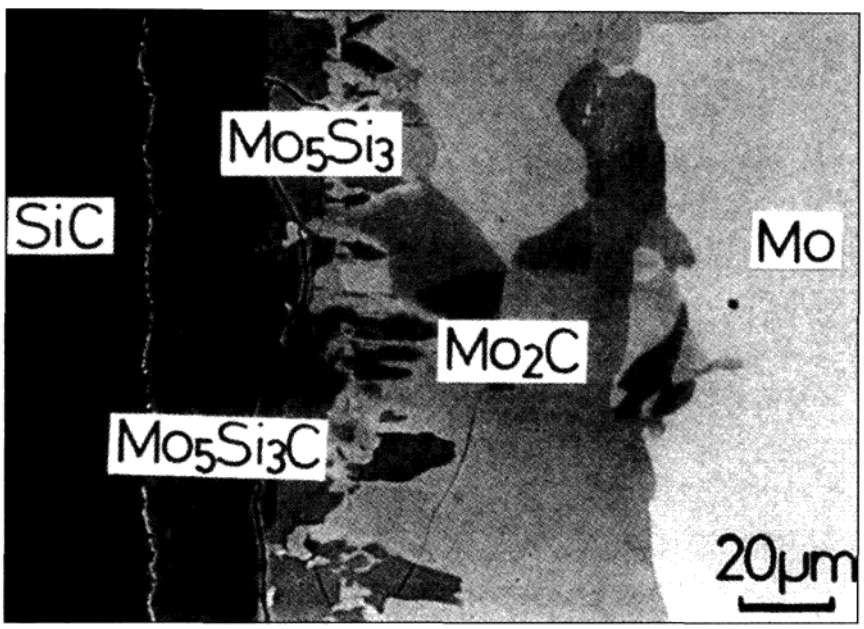

(After "Engineered Materials Handbook vol. 4: Ceramics and Glasses", American Society for Metals, p. 525. ISBN 0-87170-282-7. Reprinted with permission from ASM International. All rights reserved. www.asminternational.org.)

Automobile engine components are often made from a combination of metals and ceramics. Metals offer high strength and ductility, and ceramics offer high temperature strength, chemical stability, and low wear. In many situations, it is necessary to join a metallic part to a thin layer of ceramic to make the best part for the application. The ceramic layer will serve to protect the inner metallic part from corrosive environments at high temperature. One method of joining metallic and ceramic components together is through solid-state bonding. The process works based on the simultaneous application of pressure and high temperature. Externally applied pressure assures contact between the joining surfaces, and high temperature facilitates diffusion across the contact surface. The figure shows the interfacial microstructure when the metal molybdenum (Mo) is joined with a thin layer of silicon carbide (SiC) at a bonding temperature of 1700°C and a pressure of 100 MPa for a period of one hour. Note that a transition region exists that contains a layer of mostly Mo_2C (carbide) and Mo_5Si_3 (silicide). These products form due to diffusion and form a strong bond. ■

LEARNING OBJECTIVES

By the end of this chapter, students will be able to . . .

1. Describe rate processes in solids involving the movement of atoms in a solid state based on Boltzmann's relationship. Explain the concept of activation energy, E*, and determine the fraction of atoms or molecules having energy greater than E* at a given temperature.
2. Describe the effect of temperature on reaction rates based on the Arrhenius rate equation.
3. Describe the two main mechanisms of diffusion.
4. Distinguish between steady and nonsteady diffusion and apply Fick's first and second law to the solution of related problems.
5. Describe the industrial applications of the diffusion process.

5.1 RATE PROCESSES IN SOLIDS

Many processes involved in the production and utilization of engineering materials are concerned with the rate at which atoms move in the solid state. In many of these processes, reactions occur in the solid state that involve the spontaneous rearrangement of atoms into new and more stable atomic arrangements. In order for these reactions to proceed from the unreacted to the reacted state, the reacting atoms must have sufficient energy to overcome an activation energy barrier. The additional energy required above the average energy of the atoms is called the **activation energy** ΔE^*, which is usually measured in joules per mole or calories per mole. Figure 5.1 illustrates the activation energy for a thermally activated solid-state reaction. Atoms possessing an energy level E_r (energy of the reactants) $+\Delta E^*$ (activation energy) will have sufficient energy to react spontaneously to reach the reacted state E_p (energy of the products). The reaction shown in Fig. 5.1 is exothermic since energy is given off in the reaction.

At any temperature, only a fraction of the molecules or atoms in a system will have sufficient energy to reach the activation energy level of E^*. As the temperature of the system is increased, more and more molecules or atoms will attain the activation energy level. Boltzmann studied the effect of temperature on increasing the energies of gas molecules. On the basis of statistical analysis, Boltzmann's results showed that the probability of finding a molecule or atom at an energy level E^* greater than the average energy E of all the molecules or atoms in a system at a particular temperature T in kelvins was

$$\text{Probability} \propto e^{-(E^*-E)/kT} \tag{5.1}$$

where k = Boltzmann's constant = 1.38×10^{-23} J/(atom · K).

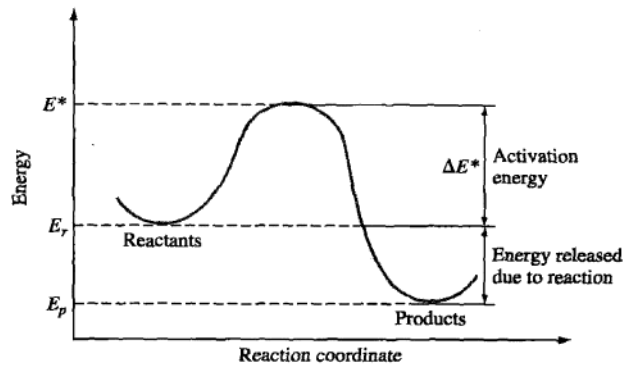

Figure 5.1
Energy of reacting species as it proceeds from the unreacted to the reacted state.

The fraction of atoms or molecules in a system having energies greater than E^*, where E^* is much greater than the average energy of any atom or molecule, can be written as

$$\frac{n}{N_{\text{total}}} = Ce^{-E^*/kT} \tag{5.2}$$

where n = number of atoms or molecules with an energy greater than E^*
N_{total} = total number of atoms or molecules present in system
k = Boltzmann's constant = 8.62×10^{-5} eV/K
T = temperature, K
C = a constant

The number of vacancies at equilibrium at a particular temperature in a metallic crystal lattice can be expressed by the following relationship, which is similar to Eq. 5.2:

$$\frac{n_v}{N} = Ce^{-E_v/kT} \tag{5.3}$$

where n_v = number of vacancies per cubic meter of metal
N = total number of atom sites per cubic meter of metal
E_v = activation energy to form a vacancy (eV)
T = absolute temperature (K)
k = Boltzmann's constant = 8.62×10^{-5} eV/K
C = constant

In Example Problem 5.1, the equilibrium concentration of vacancies present in pure copper at 500°C is calculated by using Eq. 5.3 and assuming that $C = 1$. According to this calculation, there is only about one vacancy for every one million atoms!

EXAMPLE PROBLEM 5.1

Calculate (*a*) the equilibrium number of vacancies per cubic meter in pure copper at 500°C and (*b*) the vacancy fraction at 500°C in pure copper. Assume the energy of formation of a vacancy in pure copper is 0.90 eV. Use Eq. 5.3 with $C = 1$. (Boltzmann's constant $k = 8.62 \times 10^{-5}$ eV/K)

■ Solution

a. The equilibrium number of vacancies per cubic meter in pure copper at 500°C is

$$n_v = Ne^{-E_v/kT} \qquad \text{(assume } C = 1\text{)} \tag{5.3a}$$

where n_v = no. of vacancies/m^3
N = no. of atom sites/m^3
E_v = energy of formation of a vacancy in pure copper at 500°C (eV)
k = Boltzmann's constant
T = temperature (K)

First, we determine a value for N by using the equation

$$N = \frac{N_0 \rho_{Cu}}{\text{at. mass Cu}} \tag{5.4}$$

where N_0 = Avogadro's number and ρ_{Cu} = density of Cu = 8.96 Mg/m^3. Thus,

$$N = \frac{6.02 \times 10^{23} \text{ atoms}}{\text{at. mass}} \times \frac{1}{63.54 \text{ g/at. mass}} \times \frac{8.96 \times 10^6 \text{ g}}{\text{m}^3}$$
$$= 8.49 \times 10^{28} \text{ atoms/m}^3$$

Substituting the values of N, E_v, k, and T into Eq. 5.3*a* gives

$$n_v = Ne^{-E_v/kT}$$
$$= (8.49 \times 10^{28})\left\{\exp\left[-\frac{0.90 \text{ eV}}{(8.62 \times 10^{-5} \text{ eV/K})(773 \text{ K})}\right]\right\}$$
$$= (8.49 \times 10^{28})(e^{-13.5}) = (8.49 \times 10^{28})(1.37 \times 10^{-6})$$
$$= 1.2 \times 10^{23} \text{ vacancies/m}^3 \blacktriangleleft$$

b. The vacancy fraction in pure copper at 500°C is found from the ratio n_v/N from Eq. 5.3*a*:

$$\frac{n_v}{N} = \exp\left[-\frac{0.90 \text{ eV}}{(8.62 \times 10^{-5} \text{ eV/K})(773 \text{ K})}\right]$$
$$= e^{-13.5} = 1.4 \times 10^{-6} \blacktriangleleft$$

Thus, there is only one vacancy in every 10^6 atom sites!

A similar expression to the Boltzmann relationship for the energies of molecules in a gas was arrived at by Arrhenius[1] experimentally for the effect of temperature on chemical reaction rates. Arrhenius found that the rate of many chemical reactions

[1]Svante August Arrhenius (1859–1927). Swedish physical chemist who was one of the founders of modern physical chemistry and who studied reaction rates.

as a function of temperature could be expressed by the relationship

$$\textbf{Arrhenius rate equation:} \qquad \text{Rate of reaction} = Ce^{-Q/RT} \tag{5.5}$$

where Q = activation energy, J/mol or cal/mol
R = molar gas constant
= 8.314 J/(mol · K) or 1.987 cal/(mol · K)
T = temperature (K)
C = rate constant, independent of temperature

In working with liquids and solids, the activation energy is usually expressed in terms of a mole, or 6.02×10^{23} atoms or molecules. The activation energy is also usually given the symbol Q and expressed in joules per mole or calories per mole.

The Boltzmann equation (5.2) and the Arrhenius equation (5.5) both imply that the reaction rate among atoms or molecules in many cases depends on the number of reacting atoms or molecules that have activation energies of E^* or greater. The rates of many solid-state reactions of particular interest to materials scientists and engineers obey the Arrhenius rate law, and so the Arrhenius equation is often used to analyze experimental solid-state rate data.

The Arrhenius equation (5.5) is commonly rewritten in natural logarithmic form as

$$\ln \text{ rate} = \ln C - \frac{Q}{RT} \tag{5.6}$$

This equation is that of a straight line of the type

$$y = b + mx \tag{5.7}$$

where b is the y intercept and m is the slope of the line. The ln rate term of Eq. 5.6 is equivalent to the y term of Eq. 5.7, and the ln constant term of Eq. 5.6 is equivalent to the b term of Eq. 5.7. The $-Q/R$ quantity of Eq. 5.6 is equivalent to the slope m of Eq. 5.7. Thus, a plot of ln rate versus $1/T$ produces a straight line of slope $-Q/R$.

The Arrhenius equation (5.5) can also be rewritten in common logarithmic form as

$$\log_{10} \text{ rate} = \log_{10} C - \frac{Q}{2.303\,RT} \tag{5.8}$$

The 2.303 is the conversion factor from natural to common logarithms. This equation is also an equation of a straight line. A schematic plot of $\log_{10}$ rate versus $1/T$ is given in Fig. 5.2.

Thus, if a plot of experimental ln reaction rate versus $1/T$ data produces a straight line, an activation energy for the process involved can be calculated from the slope of the line. We shall use the Arrhenius equation to explore the effects of temperature on the diffusion of atoms and the electrical conductivity of pure elemental semiconductors later.

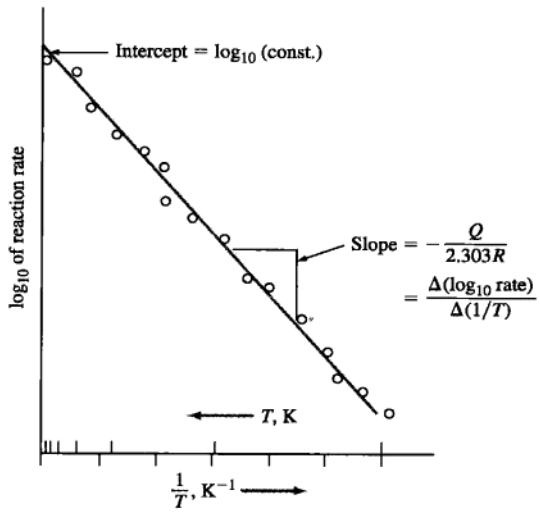

Figure 5.2
Typical Arrhenius plot of experimental rate data.
(From Wulff et al., Structure and Properties of Materials, Vol. II, J.H. Brophy, R.M. Rose, and J. Wulff, "Thermodynamics of Structure," Wiley, 1966, p. 64.)

5.2 ATOMIC DIFFUSION IN SOLIDS

5.2.1 Diffusion in Solids in General

Diffusion can be defined as the mechanism by which matter is transported through matter. Atoms in gases, liquids, and solids are in constant motion and migrate over a period of time. In gases, atomic movement is relatively rapid, as indicated by the rapid movement of cooking odors or smoke particles. Atomic movements in liquids are in general slower than in gases, as evidenced by the movement of colored dye in liquid water. In solids, atomic movements are restricted due to bonding to equilibrium positions. However, thermal vibrations occurring in solids do allow some atoms to move. Diffusion of atoms in metals and alloys is particularly important since most solid-state reactions involve atomic movements. Examples of solid-state reactions are the precipitation of a second phase from solid solution (Sec. 9.5.1) and the nucleation and growth of new grains in the recrystallization of a cold-worked metal (Sec. 6.8).

5.2.2 Diffusion Mechanisms

There are two main mechanisms of diffusion of atoms in a crystalline lattice: (1) the *vacancy or substitutional mechanism* and (2) the *interstitial mechanism.*

Vacancy or Substitutional Diffusion Mechanism Atoms can move in crystal lattices from one atomic site to another if there is enough activation energy provided by the thermal vibration of the atoms and if there are vacancies or other crystal defects in the lattice for atoms to move into. Vacancies in metals and alloys are equilibrium defects, and therefore some are always present to enable **substitutional diffusion** of atoms to take place. As the temperature of the metal increases, more vacancies are present and more thermal energy is available, and so the diffusion rate is higher at higher temperatures.

Consider the example of vacancy diffusion shown in Fig. 5.3 on a (111) plane of copper atoms in a copper crystal lattice. If an atom next to the vacancy has sufficient activation energy, it can move into the vacant site and thereby contribute to the **self-diffusion** of copper atoms in the lattice. The activation energy for self-diffusion is equal to the sum of the activation energy to form a vacancy and the activation energy to move the vacancy. Table 5.1 lists some activation energies for self-diffusion in pure metals. Note that in general as the melting point of the metal is increased, the activation energy is also. This relationship exists because the higher-melting-temperature metals tend to have stronger bonding energies between their atoms.

During self-diffusion or substitutional solid-state diffusion, atoms must break the original bonds among atoms and replace these with new bonds. This process is assisted by having vacancies present, and thus it can occur at lower activation energies (Fig. 5.3). In order for this process to occur in alloys, there must exist solid solubility of one type of atom in another. Thus, this process is dependent on the rules of solid solubility, which are listed in Sec. 4.3. Because of these differences in chemical bonding and solid solubility and other factors, substitutional diffusion data must be obtained experimentally. With time, these measurements are made more precisely, and hence these data may change with time.

One of the major breakthroughs in diffusion measurements occurred in the 1940s when the Kirkendall effect was discovered. This effect showed that the markers at the diffusion interface moved slightly in the opposite direction to the most rapidly moving (faster diffusing) species of a binary diffusion couple (Fig. 5.4*a*). After much discussion, it was concluded that the presence of vacancies allowed this phenomenon to occur.

Diffusion can also occur by the vacancy mechanism in solid solutions. Atomic size differences and bonding energy differences between the atoms are factors that affect the diffusion rate.

Table 5.1 Self-diffusion activation energies for some pure metals

Metal	Melting point (°C)	Crystal structure	Temperature range studied (°C)	Activation energy	
				kJ/mol	kcal/mol
Zinc	419	HCP	240–418	91.6	21.9
Aluminum	660	FCC	400–610	165	39.5
Copper	1083	FCC	700–990	196	46.9
Nickel	1452	FCC	900–1200	293	70.1
α iron	1530	BCC	808–884	240	57.5
Molybdenum	2600	BCC	2155–2540	460	110

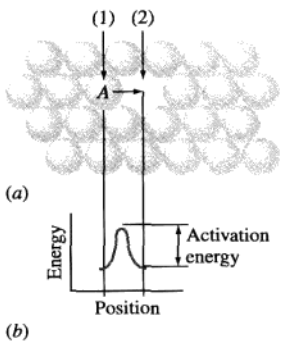

Figure 5.3
Activation energy associated with the movement of atoms in a metal. (*a*) Diffusion of copper atom *A* at position 1 on the (111) plane of a copper crystal lattice to position 2 (a vacancy site) if sufficient activation energy is provided as indicated in (*b*).

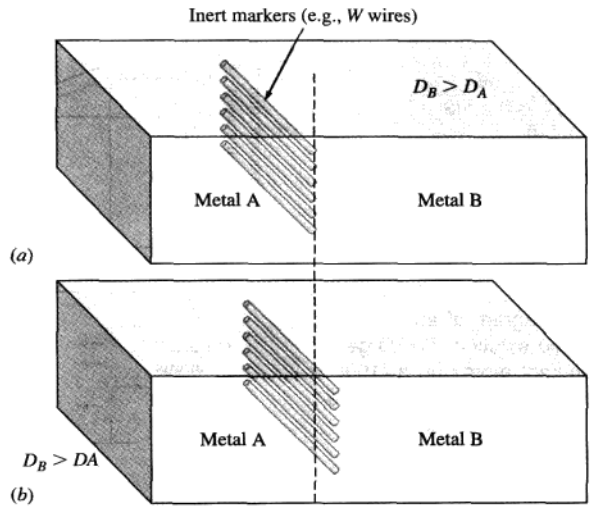

Figure 5.4
Experiment to illustrate the Kirkendall effect. (*a*) At start of diffusion experiment ($t = 0$). (*b*) After time t, markers move in the direction opposite the most rapidly diffusing species, *B*.


Animation

Interstitial Diffusion Mechanisms The **interstitial diffusion** of atoms in crystal lattices takes place when atoms move from one interstitial site to another neighboring interstitial site without permanently displacing any of the atoms in the matrix crystal lattice (Fig. 5.5). For the interstitial mechanism to be operative, the size of the diffusing atoms must be relatively small compared to the matrix atoms. Small atoms such as hydrogen, oxygen, nitrogen, and carbon can diffuse interstitially in some metallic crystal lattices. For example, carbon can diffuse interstitially in BCC α iron and FCC γ iron (see Fig. 4.15*a*). In the interstitial diffusion of carbon in iron, the carbon atoms must squeeze between the iron matrix atoms.

5.2.3 Steady-State Diffusion

Consider the diffusion of solute atoms in the x direction between two parallel atomic planes perpendicular to the paper separated by a distance x as shown in Fig. 5.6. We will assume that over a period of time the concentration of atoms at plane 1 is C_1 and that of plane 2 is C_2. That is, there is no change in the concentration of solute atoms at these planes for the system with time. Such diffusion conditions are said to be **steady-state conditions.** This type of diffusion takes place when a nonreacting gas diffuses through a metal foil. For example, steady-state diffusion conditions are attained when hydrogen gas diffuses through a foil of palladium if the hydrogen gas is at high pressure on one side and low pressure on the other.

If in the diffusion system shown in Fig. 5.6 no chemical interaction occurs between the solute and solvent atoms, because there is a concentration difference between planes 1 and 2, there will be a net flow of atoms from the higher concentration to the

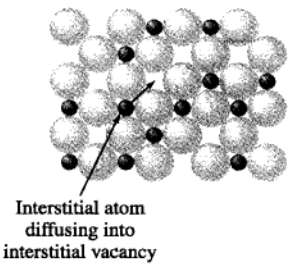

Figure 5.5
A schematic diagram of an interstitial solid solution. The large circles represent atoms on a (100) plane of an FCC crystal lattice. The small, dark circles are interstitial atoms that occupy interstitial sites. The interstitial atoms can move into adjacent interstitial sites that are vacant. There is an activation energy associated with interstitial diffusion.


Animation

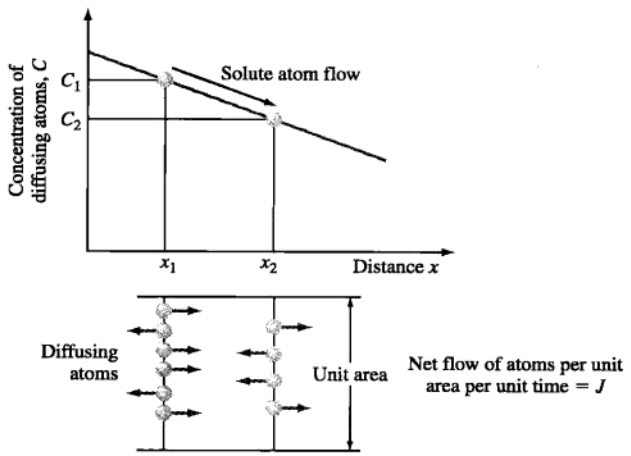

Figure 5.6
Steady-state diffusion of atoms in a concentration gradient. An example is hydrogen gas diffusing through a palladium metal foil.

lower concentration. The *flux* or flow of atoms in this type of system can be represented by the equation

$$J = -D\frac{dC}{dx} \tag{5.9}$$

where J = flux or net flow of atoms

D = proportionality constant called the **diffusivity** (atomic conductivity) or *diffusion coefficient*

$\frac{dC}{dx}$ = concentration gradient

A negative sign is used because the diffusion is from a higher to a lower concentration; i.e., there is a negative diffusion gradient.

This equation is called **Fick's[2] first law of diffusion** and states that for steady-state diffusion conditions (i.e., no change in system with time), the net flow of atoms by atomic diffusion is equal to the diffusivity D times the diffusion gradient dC/dx. The SI units for this equation are

$$J\left(\frac{\text{atoms}}{\text{m}^2 \cdot \text{s}}\right) = D\left(\frac{\text{m}^2}{\text{s}}\right)\frac{dC}{dx}\left(\frac{\text{atoms}}{\text{m}^3} \times \frac{1}{\text{m}}\right) \tag{5.10}$$

[2]Adolf Eugen Fick (1829–1901). German physiologist who first put diffusion on a quantitative basis by using mathematical equations. Some of his work was published in the *Annals of Physics (Leipzig)*, **170**:59 (1855).

Table 5.2 lists some values of atomic diffusivities of selected interstitial and substitutional diffusion systems. The diffusivity values depend on many variables, of which the following are important:

1. *The type of diffusion mechanism.* Whether the diffusion is interstitial or substitutional will affect the diffusivity. Small atoms can diffuse interstitially in the crystal lattice of larger solvent atoms. For example, carbon diffuses interstitially in the BCC or FCC iron lattices. Copper atoms diffuse substitutionally in an aluminum solvent lattice since both the copper and the aluminum atoms are about the same size.
2. *The temperature at which the diffusion takes place* greatly affects the value of the diffusivity. As the temperature is increased, the diffusivity also increases, as shown in Table 5.2 for all the systems by comparing the 500°C values with those for 1000°C. The effect of temperature on diffusivity in diffusion systems will be discussed further in Sec. 5.4.
3. *The type of crystal structure of the solvent lattice* is important. For example, the diffusivity of carbon in BCC iron is 10^{-12} m^2/s at 500°C, which is much *greater* than 5×10^{-15} m^2/s, the value for the diffusivity of carbon in FCC iron at the same temperature. The reason for this difference is that the BCC crystal structure has a lower atomic packing factor of 0.68 as compared to that of the FCC crystal structure, which is 0.74. Also, the interatomic spaces between the iron atoms are wider in the BCC crystal structure than in the FCC one, and so the carbon atoms can diffuse between the iron atoms in the BCC structure more easily than in the FCC one.
4. *The type of crystal imperfections present* in the region of solid-state diffusion is also important. More open structures allow for more rapid diffusion of atoms. For

Table 5.2 Diffusivities at 500°C and 1000°C for selected solute-solvent diffusion systems

Solute	Solvent (host structure)	Diffusivity (m^2/s) 500°C (930°F)	1000°C (1830°F)
1. Carbon	FCC iron	(5×10^{-15})*	3×10^{-11}
2. Carbon	BCC iron	10^{-12}	(2×10^{-9})
3. Iron	FCC iron	(2×10^{-23})	2×10^{-16}
4. Iron	BCC iron	10^{-20}	(3×10^{-14})
5. Nickel	FCC iron	10^{-23}	2×10^{-16}
6. Manganese	FCC iron	(3×10^{-24})	10^{-16}
7. Zinc	Copper	4×10^{-18}	5×10^{-13}
8. Copper	Aluminum	4×10^{-14}	10^{-10} M†
9. Copper	Copper	10^{-18}	2×10^{-13}
10. Silver	Silver (crystal)	10^{-17}	10^{-12} M
11. Silver	Silver (grain boundary)	10^{-11}	
12. Carbon	HCP titanium	3×10^{-16}	(2×10^{-11})

*Parentheses indicate that the phase is metastable.
†M—Calculated, although temperature is above melting point.
Source: L.H. Van Vlack, "Elements of Materials Science and Engineering," 5th ed., Addison-Wesley, 1985.

example, diffusion takes place more rapidly along grain boundaries than in the grain matrix in metals and ceramics. Excess vacancies will increase diffusion rates in metals and alloys.

5. *The concentration of the diffusing species* is important in that higher concentrations of diffusing solute atoms will affect the diffusivity. This aspect of solid-state diffusion is very complex.

5.2.4 Non–Steady-State Diffusion

Steady-state diffusion in which conditions do not change with time is not commonly encountered with engineering materials. In most cases, **non–steady-state diffusion** in which the concentration of solute atoms at any point in the material changes with time takes place. For example, if carbon is being diffused into the surface of a steel camshaft to harden its surface, the concentration of carbon under the surface at any point will change with time as the diffusion process progresses. For cases

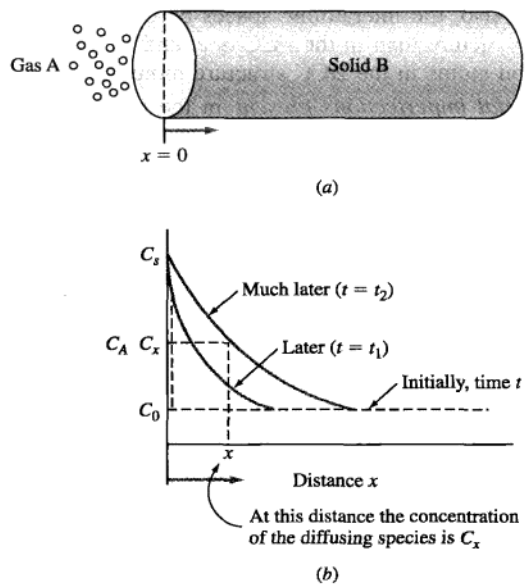

Figure 5.7
Diffusion of a gas into a solid. (*a*) Gas A diffuses into solid B at the surface where $x = 0$. The gas maintains a concentration of A atoms, called C_s, on this surface. (*b*) Concentration profiles of element A at various times along the solid in the x direction. The solid contains a uniform concentration of element A, called C_0, before diffusion starts.

of non–steady-state diffusion in which the diffusivity is independent of time, **Fick's second law of diffusion** applies, which is

$$\frac{dC_x}{dt} = \frac{d}{dx}\left(D\frac{dC_x}{dx}\right) \tag{5.11}$$

This law states that the rate of compositional change is equal to the diffusivity times the rate of change of the concentration gradient. The derivation and solving of this differential equation is beyond the scope of this book. However, the particular solution to this equation in which a gas is diffusing into a solid is of great importance for some engineering diffusion processes and will be used to solve some practical industrial diffusion problems.

Let us consider the case of a gas A diffusing into a solid B, as illustrated in Fig. 5.7*a*. As the time of diffusion increases, the concentration of solute atoms at any point in the x direction will also increase, as indicated for times t_1 and t_2 in Fig. 5.7*b*. If the diffusivity of gas A in solid B is independent of position, then the solution to Fick's second law (Eq. 5.11) is

$$\frac{C_s - C_x}{C_s - C_0} = \text{erf}\left(\frac{x}{2\sqrt{Dt}}\right) \tag{5.12}$$

where C_s = surface concentration of element in gas diffusing into the surface
C_0 = initial uniform concentration of element in solid
C_x = concentration of element at distance x from surface at time t
x = distance from surface
D = diffusivity of diffusing solute element
t = time
erf is a mathematical function called error function.

The error function, erf, is a mathematical function existing by agreed definition and is used in some solutions of Fick's second law. The error function can be found in standard tables in the same way as sines and cosines. Table 5.3 is an abbreviated table of the error function.

Table 5.3 Table of the error function

z	erf z	z	erf z	z	erf z	z	erf z
0	0	0.40	0.4284	0.85	0.7707	1.6	0.9763
0.025	0.0282	0.45	0.4755	0.90	0.7970	1.7	0.9838
0.05	0.0564	0.50	0.5205	0.95	0.8209	1.8	0.9891
0.10	0.1125	0.55	0.5633	1.0	0.8427	1.9	0.9928
0.15	0.1680	0.60	0.6039	1.1	0.8802	2.0	0.9953
0.20	0.2227	0.65	0.6420	1.2	0.9103	2.2	0.9981
0.25	0.2763	0.70	0.6778	1.3	0.9340	2.4	0.9993
0.30	0.3286	0.75	0.7112	1.4	0.9523	2.6	0.9998
0.35	0.3794	0.80	0.7421	1.5	0.9661	2.8	0.9999

Source: R.A. Flinn and P.K. Trojan, "Engineering Materials and Their Applications," 2nd ed., Houghton Mifflin, 1981, p. 137.

5.3 INDUSTRIAL APPLICATIONS OF DIFFUSION PROCESSES

Many industrial manufacturing processes utilize solid-state diffusion. In this section, we will consider the following two diffusion processes: (1) case hardening of steel by gas carburizing and (2) the impurity doping of silicon wafers for integrated electronic circuits.

5.3.1 Case Hardening of Steel by Gas Carburizing

Many rotating or sliding steel parts such as gears and shafts must have a hard outside case for wear resistance and a tough inner core for fracture resistance. In the manufacture of a carburized steel part, usually the part is machined first in the soft condition, and then, after machining, the outer layer is hardened by some casehardening treatment such as gas carburizing. Carburized steels are low-carbon steels that have about 0.10% to 0.25% C. However, the alloy content of the carburized steels can vary considerably depending on the application for which the steel will be used. Some typical gas-carburized parts are shown in Fig. 5.8.

In the first part of the gas-carburizing process, the steel parts are placed in a furnace in contact with gases containing methane or other hydrocarbon gases at about 927°C (1700°F). The carbon from the atmosphere diffuses into the surface of the gears so that after subsequent heat treatments the gears are left with high-carbon hard cases as indicated, for example, by the darkened surface areas of the macrosection of the gear shown in Fig. 5.9.

Figure 5.10 shows some typical carbon gradients in test bars of AISI 1022 (0.22% C) plain-carbon steel carburized at 1685°F (918°C) by a carburizing atmosphere with 20% CO. Notice how the carburizing time greatly affects the carbon content versus distance-below-the-surface profile. Example Problems 5.2 and 5.3 illus-

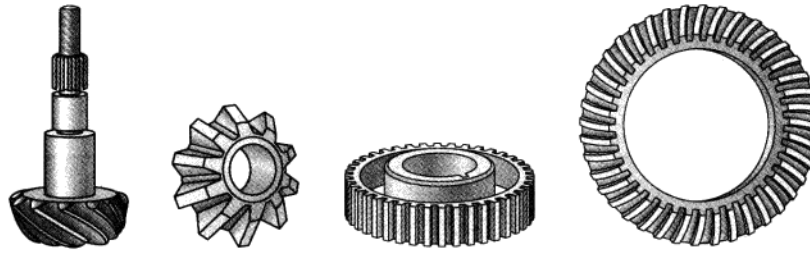

Figure 5.8
Typical gas-carburized steel parts.
(From Metals Handbook, vol. 2, "Heat Treating," 8th ed., American Society for Metals, 1964, p. 108. ASM International.)

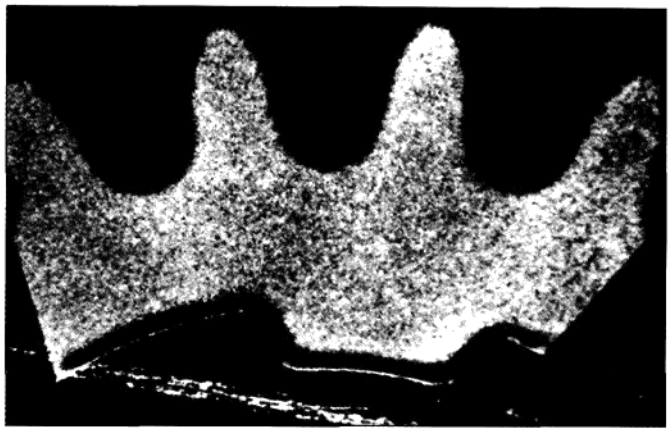

Figure 5.9
Macrosection of nitrogen-methanol-carburized SAE 8620 final-drive pinion gear.
(After B.J. Sheehy, Met. Prog., September 1981, p. 120.Reprinted with permission from ASM International. All rights reserved. www.asminternational.org.)

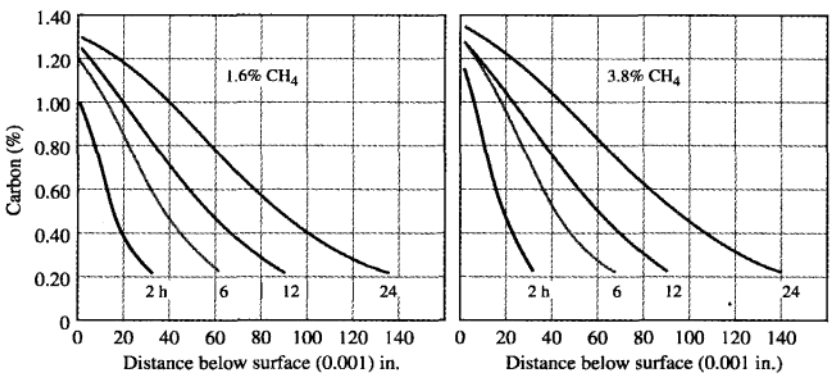

Figure 5.10
Carbon gradients in test bars of 1022 steel carburized at 918°C (1685°F) in a 20% CO–40% H_2 gas with 1.6% and 3.8% methane (CH_4) added.
(From Metals Handbook, vol. 2, "Heat Treating," 8th ed., American Society for Metals, 1964, p. 100. Used by permission of ASM International.)

trate how the diffusion equation (5.11) can be used to determine one unknown variable, such as time of diffusion or carbon content at a particular depth below the surface of the part being carburized.

EXAMPLE PROBLEM 5.2

Consider the gas carburizing of a gear of 1020 steel at 927°C (1700°F). Calculate the time in minutes necessary to increase the carbon content to 0.40% at 0.50 mm below the surface. Assume that the carbon content at the surface is 0.90% and that the steel has a nominal carbon content of 0.20%.

$$D_{927°C} = 1.28 \times 10^{-11}\ \text{m}^2/\text{s}$$

■ Solution

$$\frac{C_s - C_x}{C_s - C_0} = \text{erf}\left(\frac{x}{2\sqrt{Dt}}\right) \tag{5.12}$$

$C_s = 0.90\%$ $\quad x = 0.5\ \text{mm} = 5.0 \times 10^{-4}\ \text{m}$

$C_0 = 0.20\%$ $\quad D_{927°C} = 1.28 \times 10^{-11}\ \text{m}^2/\text{s}$

$C_x = 0.40\%$ $\quad t = ?\ \text{s}$

Substituting these values in Eq. 5.12 gives

$$\frac{0.90 - 0.40}{0.90 - 0.20} = \text{erf}\left[\frac{5.0 \times 10^{-4}\ \text{m}}{2\sqrt{(1.28 \times 10^{-11}\ \text{m}^2/\text{s})(t)}}\right]$$

$$\frac{0.50}{0.70} = \text{erf}\left(\frac{69.88}{\sqrt{t}}\right) = 0.7143$$

Let

$$Z = \frac{69.88}{\sqrt{t}} \quad \text{then erf } Z = 0.7143$$

We need a number for Z whose error function (erf) is 0.7143. From Table 5.3 we find this number by interpolation to be 0.755:

erf Z	Z
0.7112	0.75
0.7143	x
0.7421	0.80

$$\frac{0.7143 - 0.7112}{0.7421 - 0.7112} = \frac{x - 0.75}{0.80 - 0.75}$$

$$x - 0.75 = (0.1003)(0.05)$$

$$x = 0.75 + 0.005 = 0.755$$

Thus,

$$Z = \frac{69.88}{\sqrt{t}} = 0.755$$

$$\sqrt{t} = \frac{69.88}{0.755} = 92.6$$

$$t = 8567\ \text{s} = 143\ \text{min} \blacktriangleleft$$

EXAMPLE PROBLEM 5.3

Consider the gas carburizing of a gear of 1020 steel at 927°C (1700°F) as in Example Problem 5.2. Only in this problem calculate the *carbon content* at 0.50 mm beneath the surface of the gear after 5 h carburizing time. Assume that the carbon content of the surface of the gear is 0.90% and that the steel has a nominal carbon content of 0.20%.

■ **Solution**

$$D_{927°C} = 1.28 \times 10^{-11}\ \text{m}^2/\text{s}$$

$$\frac{C_s - C_x}{C_s - C_0} = \text{erf}\left(\frac{x}{2\sqrt{Dt}}\right) \tag{5.12}$$

$C_s = 0.90\%$ $\quad x = 0.50\ \text{mm} = 5.0 \times 10^{-4}\ \text{m}$

$C_0 = 0.20\%$ $\quad D_{927°C} = 1.28 \times 10^{-11}\ \text{m}^2/\text{s}$

$C_x = ?\%$ $\quad t = 5\ \text{h} = 5\ \text{h} \times 3600\ \text{s/h} = 1.8 \times 10^4\ \text{s}$

$$\frac{0.90 - C_x}{0.90 - 0.20} = \text{erf}\left[\frac{5.0 \times 10^{-4}\ \text{m}}{2\sqrt{(1.28 \times 10^{-11}\ \text{m/s})(1.8 \times 10^4\ \text{s})}}\right]$$

$$\frac{0.90 - C_x}{0.70} = \text{erf}\ 0.521$$

Let $Z = 0.521$. We need to know what is the corresponding error function for the Z value of 0.521. To determine this number from Table 5.3, we must interpolate the data as shown in the accompanying table.

Z	erf Z
0.500	0.5205
0.521	x
0.550	0.5633

$$\frac{0.521 - 0.500}{0.550 - 0.500} = \frac{x - 0.5205}{0.5633 - 0.5205}$$

$$0.42 = \frac{x - 0.5205}{0.0428}$$

$$x - 0.5205 = (0.42)(0.0428)$$

$$x = 0.0180 + 0.5205$$

$$= 0.538$$

Therefore,

$$\frac{0.90 - C_x}{0.70} = \text{erf}\ 0.521 = 0.538$$

$$C_x = 0.90 - (0.70)(0.538)$$

$$= 0.52\% \blacktriangleleft$$

Note that by increasing the carburizing time from about 2.4 to 5 h for the 1020 steel, the carbon content at 0.5 mm below the surface of the gear is increased from 0.4% to only 0.52%.

5.3.2 Impurity Diffusion into Silicon Wafers for Integrated Circuits

Impurity diffusion into silicon wafers to change their electrical conducting characteristics is an important phase in the production of modern integrated electronic circuits. In one method of impurity diffusion into silicon wafers, the silicon surface is exposed to the vapor of an appropriate impurity at a temperature above about 1100°C in a quartz tube furnace, as shown schematically in Fig. 5.11. The part of the silicon surface not to be exposed to the impurity diffusion must be masked off so that the impurities diffuse into the parts selected by the design engineer for conductivity change. Figure 5.12 shows a technician loading a rack of silicon wafers into a tube furnace for impurity diffusion.

As in the case of the gas carburizing of a steel surface, the concentration of impurities diffused into the silicon surface decreases as the depth of penetration increases, as shown in Fig. 5.13. Changing the time of diffusion will also change the concentration of impurities versus depth-of-penetration profile, as shown qualitatively in Fig. 5.7. Example Problem 5.4 illustrates how Eq. 5.12 can be used quantitatively to determine one unknown variable, such as time of diffusion or depth of penetration at a particular concentration level.

EXAMPLE PROBLEM 5.4

Consider the impurity diffusion of gallium into a silicon wafer. If gallium is diffused into a silicon wafer with no previous gallium in it at a temperature of 1100°C for 3 h, what is the depth below the surface at which the concentration is 10^{22} atoms/m^3 if the surface concentration is 10^{24} atoms/m^3? For gallium diffusing into silicon at 1100°C the solution is as follows:

■ **Solution**

$$D_{1100°C} = 7.0 \times 10^{-17}\ \text{m}^2/\text{s}$$

$$\frac{C_s - C_x}{C_s - C_0} = \text{erf}\left(\frac{x}{2\sqrt{Dt}}\right) \qquad (5.12)$$

$C_s = 10^{24}$ atoms/m^3 $\qquad$ x = ?m (depth at which $C_x = 10^{22}$ atoms/m^3)

$C_x = 10^{22}$ atoms/m^3 $\qquad$ $D_{1100°C} = 7.0 \times 10^{-17}$ m^2/s

$C_0 = 0$ atoms/m^3 $\qquad$ $t = 3\ \text{h} = 3\ \text{h} \times 3600\ \text{s/h} = 1.08 \times 10^4\ \text{s}$

Substituting these values into Eq. 5.12 gives

$$\frac{10^{24} - 10^{22}}{10^{24} - 0} = \text{erf}\left[\frac{x\ \text{m}}{2\sqrt{(7.0 \times 10^{-17}\ \text{m}^2/\text{s})(1.08 \times 10^4\ \text{s})}}\right]$$

$$1 - 0.01 = \text{erf}\left(\frac{x\ \text{m}}{1.74 \times 10^{-6}\ \text{m}}\right) = 0.99$$

Let $$Z = \frac{x}{1.74 \times 10^{-6}\ \text{m}}$$

Thus, $$\text{erf}\, Z = 0.99 \quad \text{and} \quad Z = 1.82$$

(from Table 5.3 using interpolation). Therefore,

$$x = (Z)(1.74 \times 10^{-6}\ \text{m}) = (1.82)(1.74 \times 10^{-6}\ \text{m})$$
$$= 3.17 \times 10^{-6}\ \text{m} \blacktriangleleft$$

Note: Typical diffusion depths in silicon wafers are of the order of a few micrometers (i.e., about 10^{-6} m), while the wafer is usually several hundred micrometers thick.

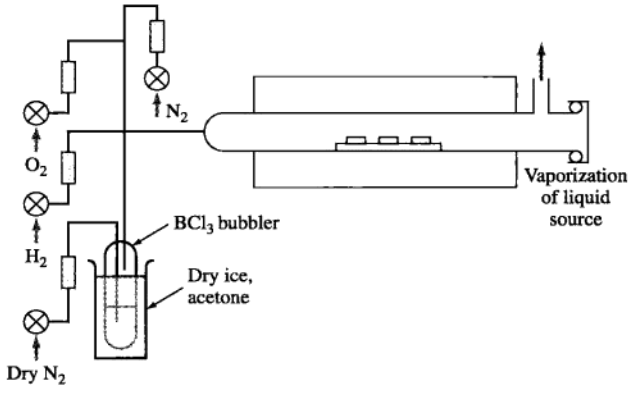

Figure 5.11
Diffusion method for diffusing boron into silicon wafers.
(From W.R. Runyan, "Silicon Semiconductor Technology," McGraw-Hill, 1965. Reproduced with permission of The McGraw-Hill Companies.)

Figure 5.12
Loading a rack of silicon wafers into a tube furnace for impurity diffusion.
(Getty/RF.)

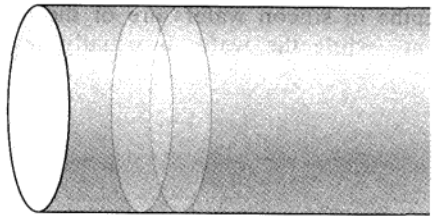

(*a*)

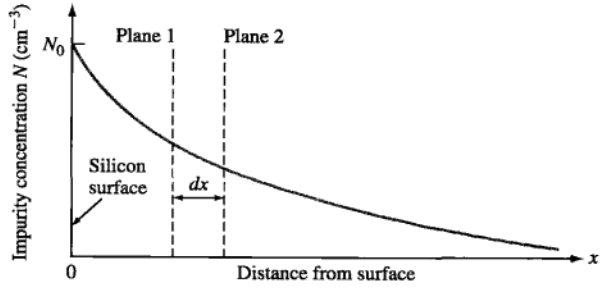

(*b*)

Figure 5.13
Impurity diffusion into a silicon wafer from one face. (*a*) A silicon wafer with thickness greatly exaggerated having an impurity concentration that diminishes from the left face toward the interior. (*b*) Graphical representation of the same impurity distribution.
(After R.M. Warner, "Integrated Circuits," McGraw-Hill, 1965, p. 70.)

5.4 EFFECT OF TEMPERATURE ON DIFFUSION IN SOLIDS

Since atomic diffusion involves atomic movements, it is to be expected that increasing the temperature of a diffusion system will increase the diffusion rate. By experiment, it has been found that the temperature dependence of the diffusion rate of many diffusion systems can be expressed by the following Arrhenius-type equation:

$$D = D_0 e^{-Q/RT} \tag{5.13}$$

where D = diffusivity, m^2/s

D_0 = proportionality constant, m^2/s, independent of temperature in range for which equation is valid

Q = activation energy of diffusing species, J/mol or cal/mol

R = molar gas constant
= 8.314 J/(mol · K) or 1.987 cal/(mol · K)
T = temperature, K

Example Problem 5.5 applies Eq. 5.13 to determine the diffusivity of carbon diffusing in γ iron at 927°C when given values for D_0 and the activation energy Q.

EXAMPLE PROBLEM 5.5

Calculate the value of the diffusivity D in meters squared per second for the diffusion of carbon in γ iron (FCC) at 927°C (1700°F). Use values of $D_0 = 2.0 \times 10^{-5}$ m^2/s, $Q = 142$ kJ/mol, and $R = 8.314$ J/(mol · K).

■ **Solution**

$$D = D_0 e^{-Q/RT} \tag{5.13}$$

$$= (2.0 \times 10^{-5}\ \text{m}^2/\text{s}) \left\{ \exp \frac{-142{,}000\ \text{J/mol}}{[8.314\ \text{J/(mol} \cdot \text{K)}](1200\ \text{K})} \right\}$$

$$= (2.0 \times 10^{-5}\ \text{m}^2/\text{s})(e^{-14.23})$$

$$= (2.0 \times 10^{-5}\ \text{m}^2/\text{s})(0.661 \times 10^{-6})$$

$$= 1.32 \times 10^{-11}\ \text{m}^2/\text{s} \blacktriangleleft$$

The diffusion equation $D = D_0 e^{-Q/RT}$ (Eq. 5.13) can be written in logarithmic form as the equation of a straight line as was done in Eqs. 5.6 and 5.8 for the general Arrhenius rate law equation:

$$\ln D = \ln D_0 - \frac{Q}{RT} \tag{5.14}$$

or

$$\log_{10} D = \log_{10} D_0 - \frac{Q}{2.303RT} \tag{5.15}$$

If diffusivity values for a diffusion system are determined at two temperatures, values for Q and D_0 can be determined by solving two simultaneous equations of the Eq. 5.14 type. If these Q and D_0 values are substituted into Eq. 5.15, a general equation for $\log_{10} D$ versus $1/T$ over the temperature range investigated can be created. Example Problem 5.6 shows how the activation energy for a binary diffusion system can be calculated directly by using the relationship $D = D_0 e^{-Q/RT}$ (Eq. 5.13) when the diffusivities are known for two temperatures.

Table 5.4 lists D_0 and Q values for some metallic systems used to produce the Arrhenius diffusivity plots in Fig. 5.14. Figure 5.15 shows similar plots for the diffusion of impurity elements into silicon, which are useful for the fabrication of integrated circuits for the electronics industry.

Table 5.4 Diffusivity data for some metallic systems

Solute	Solvent	D_0 (m^2/s)	Q kJ/mol	Q kcal/mol
Carbon	FCC iron	2.0×10^{-5}	142	34.0
Carbon	BCC iron	22.0×10^{-5}	122	29.3
Iron	FCC iron	2.2×10^{-5}	268	64.0
Iron	BCC iron	20.0×10^{-5}	240	57.5
Nickel	FCC iron	7.7×10^{-5}	280	67.0
Manganese	FCC iron	3.5×10^{-5}	282	67.5
Zinc	Copper	3.4×10^{-5}	191	45.6
Copper	Aluminum	1.5×10^{-5}	126	30.2
Copper	Copper	2.0×10^{-5}	197	47.1
Silver	Silver	4.0×10^{-5}	184	44.1
Carbon	HCP titanium	51.0×10^{-5}	182	43.5

Source: Data from L.H. Van Vlack, "Elements of Materials Science and Engineering," 5th ed., Addison-Wesley, 1985.

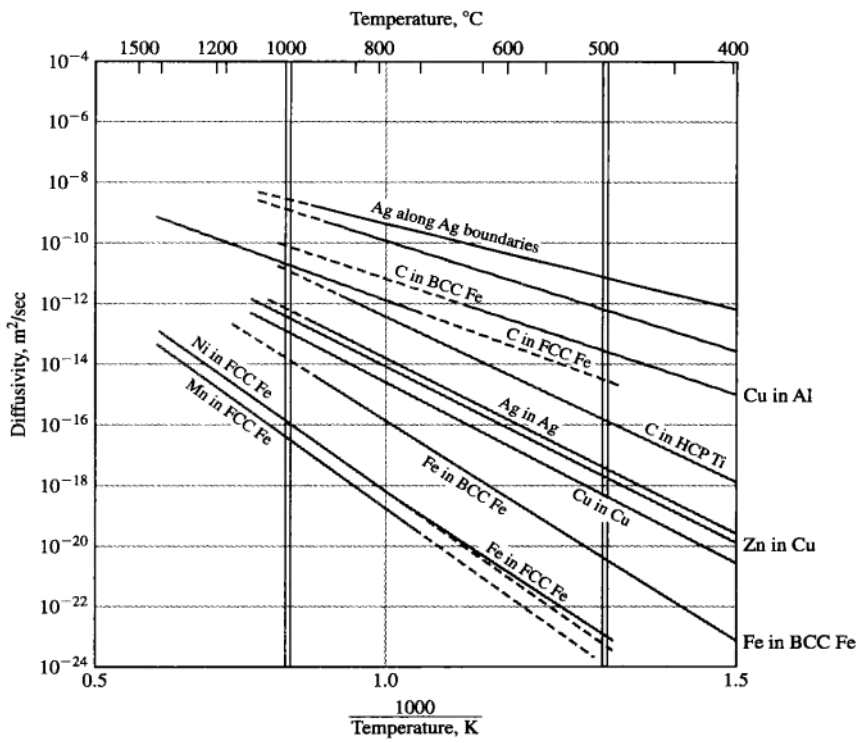

Figure 5.14
Arrhenius plots of diffusivity data for some metallic systems.
(From Van Vlack, L.H., "Elements Materials Science Engineering," 5th ed., 1985. Electronically reproduced by permission of Pearson Education, Inc., Upper Saddle River, New Jersey.)

EXAMPLE PROBLEM 5.6

The diffusivity of silver atoms in solid silver metal is 1.0×10^{-17} m^2/s at 500°C and 7.0×10^{-13} m^2/s at 1000°C. Calculate the activation energy (joules per mole) for the diffusion of Ag in Ag in the temperature range 500°C to 1000°C.

■ Solution

Using Eq. 5.13, $T_2 = 1000°C + 273 = 1273$ K, $T_1 = 500°C + 273 = 773$ K, and $R = 8.314$ J/(mol · K):

$$\frac{D_{1000°C}}{D_{500°C}} = \frac{\exp(-Q/RT_2)}{\exp(-Q/RT_1)} = \exp\left[-\frac{Q}{R}\left(\frac{1}{T_2} - \frac{1}{T_1}\right)\right]$$

$$\frac{7.0 \times 10^{-13}}{1.0 \times 10^{-17}} = \exp\left\{-\frac{Q}{R}\left[\left(\frac{1}{1273\text{ K}} - \frac{1}{773\text{ K}}\right)\right]\right\}$$

$$\ln(7.0 \times 10^4) = -\frac{Q}{R}(7.855 \times 10^{-4} - 12.94 \times 10^{-4}) = \frac{Q}{8.314}(5.08 \times 10^{-4})$$

$$11.16 = Q(6.11 \times 10^{-5})$$

$$Q = 183{,}000\text{ J/mol} = 183\text{ kJ/mol} \blacktriangleleft$$

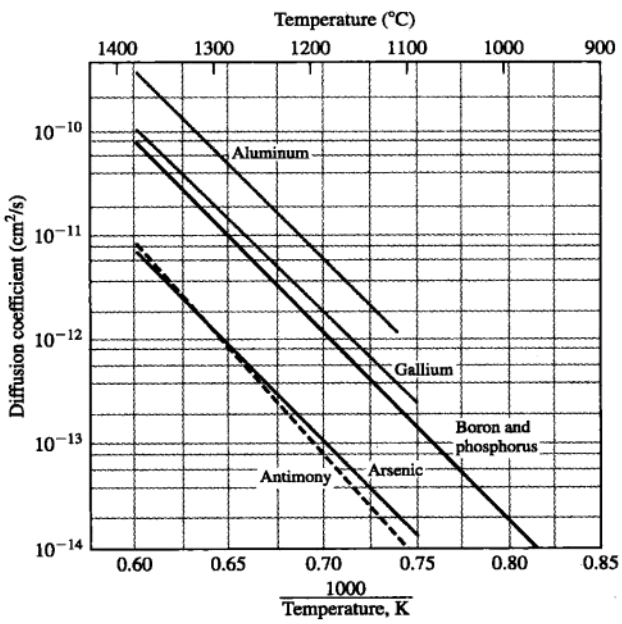

Figure 5.15
Diffusion coefficients as a function of temperature for some impurity elements in silicon.
[*From C.S. Fuller and J.A. Ditzenberger, J. Appl. Phys., 27:544(1956).*]

5.5 SUMMARY

Atomic diffusion occurs in metallic solids mainly by (1) a vacancy or substitution mechanism and (2) an interstitial mechanism. In the vacancy mechanism, atoms of about the same size jump from one position to another, using the vacant atomic sites. In the interstitial mechanism very small atoms move through the interstitial spaces between the larger atoms of the parent matrix. Fick's first law of diffusion states that diffusion takes place because of a difference in concentration of a diffusing species from one place to another and is applicable for steady-state conditions (i.e., conditions that do not change with time). Fick's second law of diffusion is applicable for non–steady-state conditions (i.e., conditions in which the concentrations of the diffusing species change with time). In this book, the use of Fick's second law has been restricted to the case of a gas diffusing into a solid. The rate of diffusion depends greatly on temperature, and this dependence is expressed by the diffusivity, a measure of the diffusion rate: Diffusivity $D = D_0 e^{-Q/RT}$. Diffusion processes are used commonly in industry. In this chapter, we have examined the diffusion-gas-carburizing process for surface-hardening steel and the diffusion of controlled amounts of impurities into silicon wafers for integrated circuits.

5.6 DEFINITIONS

Sec. 5.1

Activation energy: the additional energy required above the average energy for a thermally activated reaction to take place.

Arrhenius rate equation: an empirical equation that describes the rate of a reaction as a function of temperature and an activation energy barrier.

Sec. 5.2

Substitutional diffusion: the migration of solute atoms in a solvent lattice in which the solute and solvent atoms are approximately the same size. The presence of vacancies makes the diffusion possible.

Self-diffusion: the migration of atoms in a pure material.

Interstitial diffusion: the migration of interstitial atoms in a matrix lattice.

Steady-state conditions: for a diffusing system there is no change in the concentration of the diffusing species with time at different places in the system.

Diffusivity: a measure of the rate of diffusion in solids at a constant temperature. Diffusivity D can be expressed by the equation $D = D_0 e^{-Q/RT}$, where Q is the activation energy and T is the temperature in Kelvins. D_0 and R are constants.

Fick's first law of diffusion in solids: the flux of a diffusing species is proportional to the concentration gradient at constant temperature.

Non–steady-state conditions: for a diffusing system the concentration of the diffusing species changes with time at different places in the system.

Fick's second law of diffusion in solids: the rate of change of composition is equal to the diffusivity times the rate of change of the concentration gradient at constant temperature.

5.7 PROBLEMS

Answers to problems marked with an asterisk are given at the end of the book.

Knowledge and Comprehension Problems

5.1 What is a thermally activated process? What is the activation energy for such a process?

5.2 Write an equation for the number of vacancies present in a metal at equilibrium at a particular temperature, and define each of the terms. Give the units for each term, and use electron volts for the activation energy.

5.3 Write the Arrhenius rate equation in the (*a*) exponential and (*b*) common logarithmic forms.

5.4 Draw a typical Arrhenius plot of log10 of the reaction rate versus reciprocal absolute temperature, and indicate the slope of the plot.

5.5 Describe the substitutional and interstitial diffusion mechanisms in solid metals.

5.6 Write the equation for Fick's first law of diffusion, and define each of the terms in SI units.

5.7 What factors affect the diffusion rate in solid metal crystals?

5.8 Write the equation for Fick's second law of diffusion in solids, and define each of the terms.

5.9 Write the equation for the solution to Fick's second law for the diffusion of a gas into the surface of a solid metal crystal lattice.

5.10 Describe the gas-carburizing process for steel parts. Why is the carburization of steel parts carried out?

Application and Analysis Problems

***5.11** (*a*) Calculate the equilibrium concentration of vacancies per cubic meter in pure copper at 850°C. Assume that the energy of formation of a vacancy in pure copper is 1.0 eV. (*b*) What is the vacancy fraction at 800°C?

5.12 (*a*) Calculate the equilibrium concentration of vacancies per cubic meter in pure silver at 750°C. Assume that the energy of formation of a vacancy in pure silver is 1.10 eV. (*b*) What is the vacancy fraction at 700°C?

***5.13** Determine the diffusion flux of zinc atoms in a solid solution of zinc in copper between two points A and B, 20 μm apart, at 500°C. $C_A = 10^{26}$ atoms/m^3 and $C_B = 10^{24}$ atoms/m^3.

5.14 The diffusion flux of copper solute atoms in aluminum solvent from point A to point B, 10 μm apart, is $4 \times 10^{17} \frac{\text{atoms}}{\text{m}^2 \cdot \text{s}}$ at 500°C. Determine (*a*) the concentration gradient and (*b*) difference in the concentration levels of copper between the two points.

***5.15** Consider the gas carburizing of a gear of 1018 steel (0.18 wt %) at 927°C (1700°F). Calculate the time necessary to increase the carbon content to 0.35 wt % at 0.40 mm below the surface of the gear. Assume the carbon content at the surface to be 1.15 wt % and that the nominal carbon content of the steel gear before carburizing is 0.18 wt %. D (C in γ iron) at 927°C $= 1.28 \times 10^{-11}$ m^2/s.

5.16 The surface of a steel gear made of 1022 steel (0.22 wt % C) is to be gas-carburized at 927°C (1700°F). Calculate the time necessary to increase the carbon content to 0.30 wt % at 0.030 in. below the surface of the gear. Assume the carbon content of the surface to be 1.20 wt %. D (C in γ iron) at 927°C = 1.28×10^{-11} m²/s.

5.17 A gear made of 1020 steel (0.20 wt % C) is to be gas-carburized at 927°C (1700°F). Calculate the carbon content at 0.90 mm below the surface of the gear after a 4.0-h carburizing time. Assume the carbon content at the surface of the gear is 1.00 wt %. D (C in γ iron) at 927°C = 1.28×10^{-11} m²/s.

5.18 A gear made of 1020 steel (0.20 wt % C) is to be gas-carburized at 927°C (1700°F). Calculate the carbon content at 0.040 in. below the surface of the gear after a 7.0-h carburizing time. Assume the carbon content at the surface of the gear is 1.15 wt %. D (C in γ iron) at 927°C = 1.28×10^{-11} m²/s.

***5.19** The surface of a steel gear made of 1018 steel (0.18 wt % C) is to be gas-carburized at 927°C. Calculate the time necessary to increase the carbon content to 0.35 wt % at 1.00 mm below the surface of the gear after an 8.0-h carburizing time. Assume the carbon content at the surface of the gear is 1.20 wt %. D (C in γ iron) at 927°C = 1.28×10^{-11} m²/s.

5.20 The surface of a steel gear made of 1020 steel (0.20 wt % C) is to be gas-carburized at 927°C. Calculate the carbon content at 0.95 mm below the surface of the gear after an 8.0-h carburizing time. Assume the carbon content at the surface of the gear is 1.25 wt %. D (C in γ iron) at 927°C = 1.28×10^{-11} m²/s.

5.21 A steel gear made of 1018 steel (0.18 wt % C) is to be gas-carburized at 927°C. If the carburizing time is 7.5 h, at what depth in millimeters will the carbon content be 0.040 wt %? Assume the carbon content at the surface of the gear is 1.20 wt %. D (C in γ iron) at 927°C = 1.28×10^{-11} m²/s.

***5.22** If boron is diffused into a thick slice of silicon with no previous boron in it at a temperature of 1100°C for 5 h, what is the depth below the surface at which the concentration is 10^{17} atoms/cm³ if the surface concentration is 10^{18} atoms/cm³? $D = 4 \times 10^{-13}$ cm²/s for boron diffusing in silicon at 1100°C.

5.23 If aluminum is diffused into a thick slice of silicon with no previous aluminum in it at a temperature of 1100°C for 6 h, what is the depth below the surface at which the concentration is 10^{16} atoms/cm³ if the surface concentration is 10^{18} atoms/cm³? $D = 2 \times 10^{-12}$ cm²/s for aluminum diffusing in silicon at 1100°C.

5.24 Phosphorus is diffused into a thick slice of silicon with no previous phosphorus in it at a temperature of 1100°C. If the surface concentration of the phosphorus is 1×10^{18} atoms/cm³ and its concentration at 1 μm is 1×10^{15} atoms/cm³, how long must be the diffusion time? $D = 3.0 \times 10^{-13}$ cm²/s for P diffusing in Si at 1100°C.

***5.25** If the diffusivity in Prob. 5.24 had been 1.5×10^{-13} cm²/s, at what depth in micrometers would the phosphorus concentration be 1×10^{15} atoms/cm³?

5.26 Arsenic is diffused into a thick slice of silicon with no previous arsenic in it at 1100°C. If the surface concentration of the arsenic is 5.0×10^{18} atoms/cm³ and its concentration at 1.2 μm below the silicon surface is 1.5×10^{16} atoms/cm³, how long must be the diffusion time? $D = 3.0 \times 10^{-14}$ cm²/s for As diffusing in Si at 1100°C.

5.27 Calculate the diffusivity D in square meters per second for the diffusion of nickel in FCC iron at 1100°C. Use values of $D_0 = 7.7 \times 10^{-5}$ cm²/s; $Q = 280$ kJ/mol; $R = 8.314$ J/(mol · K).

5.28 Calculate the diffusivity in square meters per second of carbon in HCP titanium at 700°C. Use $D_0 = 5.10 \times 10^{-4}$ m²/s; $Q = 182$ kJ/mol; $R = 8.314$ J/(mol · K).

5.29 Calculate the diffusivity in square meters per second for the diffusion of zinc in copper at 350°C. Use $D_0 = 3.4 \times 10^{-5}$ m²/s; $Q = 191$ kJ/(mol), $R = 8.314$ J/(mol · K).

5.30 The diffusivity of manganese atoms in the FCC iron lattice is 1.50×10^{-14} m²/s at 1300°C and 1.50×10^{-15} m²/s at 400°C. Calculate the activation energy in kJ/mol for this case in this temperature range. $R = 8.314$ J/(mol · K).

5.31 The diffusivity of copper atoms in the aluminum lattice is 7.50×10^{-13} m²/s at 600°C and 2.50×10^{-15} m²/s at 400°C. Calculate the activation energy for this case in this temperature range. $R = 8.314$ J/(mol · K).

5.32 The diffusivity of iron atoms in the BCC iron lattice is 4.5×10^{-23} m²/s at 400°C and 5.9×10^{-16} m²/s at 800°C. Calculate the activation energy in kJ/mol for this case in this temperature range. $R = 8.314$ J/(mol · K).

Synthesis and Evaluation Problems

***5.33** The concentration of Manganese (Mn) at 500°C on the surface of an iron sample is 0.6 a%. At a distance of 2 mm below the surface, the concentration is 0.1 a/o. Determine the flux of Mn atoms between the surface and plane 2 mm deep. Hint: convert a% to atoms/m³ using information in Table 3.2.

5.34 The concentration of carbon on the surface of a 1018 steel gear is 0.8 wt% at 1000°C. Determine the flux of carbon atoms from the surface to a plane 25 μm below the surface where carbon concentration is unaffected by the surface concentration. Hint: convert wt% to atoms/m³ using information in Table 3.2.

5.35 A copper-zinc alloy (85wt% Cu-10wt% zinc) is coupled with pure copper (interfaced). The diffusion couple is then heated to a temperature of 1000°C. (*a*) How long will it take for the concentration of zinc to reach 0.2%, 2.5 mm below the interface? (*b*) How much will the zinc concentration at the same point be in twice the time calculated in part a?

***5.36** A bar of pure nickel is coupled with a bar of pure iron (interfaced). The diffusion couple is then heated to a temperature of 1000°C. (*a*) How long will it take for the concentration of nickel to reach 0.1wt%, 1.0 μm below the interface? (*b*) How long will it take for the concentration of nickel to reach 0.1wt%, 1.0 mm below the interface? (*c*) What does the comparison of the two answers show?

5.37 The proportionality constant, $D_{o,}$ of carbon in HCP titanium is 25.5 times higher than carbon in FCC iron. The activation energy of carbon in HCP titanium is 1.28 times of carbon in FCC iron. Determine Q and D_o for carbon in FCC iron. Verify your answers with those in Table 5.4.

***5.38** The proportionality constant, $D_{o,}$ of iron in BCC iron is 9.1 times higher than in FCC iron. The activation energy of iron in BCC iron is 86% that of iron in FCC iron. Determine Q and D_o for iron in FCC iron. Verify your answers with those in Table 5.4.

5.39 The activation energy of nickel atoms in FCC iron is 280 kJ/mol and carbon atoms in FCC iron is 142 kJ/mol. (*a*) What does this tell you about the comparative diffusion of nickel and carbon in iron? (*b*) Can you explain why the activation energies are so drastically different? (*c*) Find a way to qualitatively explain how much energy is 142 kJ to a non-engineer or a non-scientist.

5.40 The melt temperatures of copper and aluminum are 1083°C and 657°C respectively. Compare the diffusivities of copper in copper and copper in aluminum at 500°C (use Table 5.2). Can you explain why a drastic difference exists?

5.41 The self-diffusion of iron atoms in BCC iron is significantly higher than in FCC iron (See Table 5.2). Explain why.

5.42 Would you expect the diffusion rate of copper (self diffusion) to be lower or higher in copper with ASTM grain size 4 than in copper with ASTM grain size 8? Explain your answer.

5.43 Would you expect the diffusion rate of copper (self-diffusion) to be lower in a pure copper sample that is loaded with dislocations or in a pure copper sample that is free of dislocations (refer to Sec. 4.4.2 for characteristics of dislocations)? Explain your answer.

5.44 In NaCl, would you expect the activation energy of cation (Na^+) to be higher or the anion (Cl^-)? Why?

5.45 Is the non-steady diffusion process more sensitive to temperature or time? Explain using appropriate equations.

5.46 Show, using equations only, that as time increases in the gas carburization process, the concentration C_x increases.

5.47 If hydrogen diffuses in ferrous alloys, it will make the material significantly more brittle and susceptible to fracture. The activation energy of hydrogen in steel is 3.6 Kcal/mol. Should we worry about hydrogen embrittlement of steels (is it very likely to occur)? Explain.

5.48 In powder metallurgy, solid parts are formed by first densifying powder through pressure/compaction at room temperature. The particles are pressed against each other and form necks at the point of contact with each other (see Fig. P5.48*a*). The next stage is then sintering in which the densified compact is heated to elevated temperatures. The sintering stages are between 1000°C (Fig. P5.48*b*) and 1050°C (Fig. P5.48*d*). What observation can you make regarding the physical features of the compact going from the room temperature compact to sintering at 1050°C? What is the reason for this change?

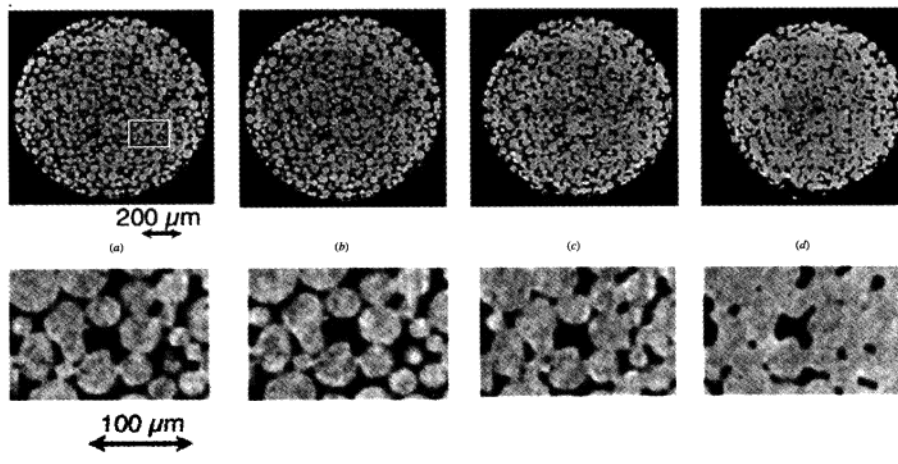

Figure P5.48
(© 2009 ESRF.)

CHAPTER 6

Mechanical Properties of Metals I

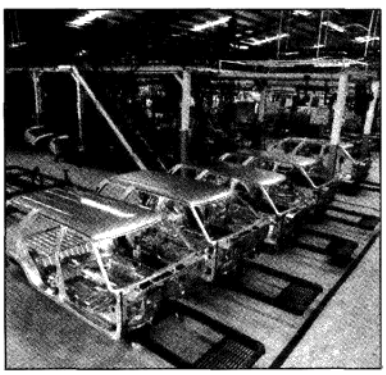

(*Getty/RF.*)

(*Getty/RF.*)

Metals are formed into functional shapes using a wide variety of metal-forming operations under both cold and hot conditions. Perhaps one of the most important examples, revealing the use of metal-forming operations, is in manufacturing of automobile parts (both body and engine). The engine block is usually made of cast iron or aluminum alloys; the cylinder and other openings in the block are made by drilling, boring, and tapping operations; the cylinder heads are also cast of aluminum alloys; connecting rods, crankshafts, and cams are forged (sometimes cast) and are then finish ground; the body panels including the roof, trunk lid, doors, and side panels are stamped from steel sheets and are then spot-welded together (left figure). As the number of operations to produce a part increases, so does the cost of the part and therefore the overall product. To reduce the cost, manufacturers follow the "Near Net Shape" manufacturing concepts, in which the product is formed with the least number of operations and with the least amount of finish machining or grinding required. Automotive parts with complex and nonsymmetrical shapes such as bevel gears or universal joints are forged almost ready-to-install (right figure). ■

LEARNING OBJECTIVES

By the end of this chapter, students will be able to . . .

1. Describe the forming operations that are used to shape metals into functional shapes. Differentiate between wrought alloy and cast products. Differentiate between hot- and cold-forming processes.
2. Explain the engineering and true definition of stress and strain.
3. Explain the differences between elastic and plastic deformation at the atomic, micro-, and macro-scales.
4. Explain the differences between normal and sharing stresses and strains.
5. Explain what a tensile test is, what type of machine is used to perform the tensile tests, and what information regarding the properties of a material can be extracted from such tests.
6. Define hardness and explain how is it measured. Describe various available hardness scales.
7. Describe the plastic deformation of a single crystal at the atomic level. Describe the concept of slip, dislocations, and twins, and their role in plastic deformation of a single crystal.
8. Define critical slip systems in BCC, FCC, and HCP single crystals.
9. Describe Schmid's law and its application in determination of the critical resolved shear stress.
10. Describe the effect of plastic deformation process on properties and grain structure of polycrystalline materials.
11. Explain the effect of grain size (Hall-Petch equation) and grain boundary on the plastic deformation and properties of a metal.
12. Describe various strengthening mechanisms used for metals.
13. Describe the annealing process and its impact on properties and microstructure of a cold-worked metal.
14. Describe the superplastic behavior in metals.
15. Describe what a nanocrystalline metal is and what advantages it may offer.

This chapter first examines some of the basic methods of processing metals and alloys into useful shapes. Then stress and strain in metals are defined, and the tensile test used to determine these properties is described. This is followed by a treatment of hardness and hardness testing of metals. Next, the plastic deformation of metal single crystals and polycrystalline metals is examined. The solid-solution strengthening of metals is considered, next followed by the annealing process and its impact on the cold-worked metal. Finally, superplasticity and nanocrystalline metals are introduced.

6.1 THE PROCESSING OF METALS AND ALLOYS

6.1.1 The Casting of Metals and Alloys

Most metals are processed by first melting the metal in a furnace that functions as a reservoir for the molten metal. Alloying elements can be added to the molten metal to produce various alloy compositions. For example, solid magnesium metal may be added to molten aluminum and, after melting, can be mechanically mixed with the aluminum to produce a homogeneous melt of an aluminum-magnesium alloy.

After oxide impurities and unwanted hydrogen gas are removed from the molten Al–Mg alloy, it is cast into a mold of a direct-chill semicontinuous casting unit, as shown in Fig. 4.8. Huge sheet ingots, such as those shown in Fig. 4.1, are produced in this way. Other types of ingots with different cross sections are cast in a similar way, for example, extrusion ingots are cast with circular cross sections.

Semifinished products are manufactured from the basic shaped ingots. Sheet[1] and plate[2] are produced by rolling sheet ingots to reduced thicknesses. Extruded shapes such as channels and structural shapes are produced from extrusion ingots, and rod and wire are manufactured from wire bar ingots. All these products that are manufactured by hot and cold working the metal from large ingots are called *wrought alloy products.* The effects of permanent deformation on the structure and properties of metals will be treated in Secs. 6.5 and 6.6.

On a smaller scale molten metal may be cast into a mold that is in the shape of the final product, and usually only a small amount of machining or other finishing operation is required to produce the final casting. Products made in this manner are called *cast products* and the alloys used to produce them, *casting alloys.* For example, pistons used in automobile engines are usually made by casting molten metal into a permanent steel mold. A schematic diagram of a simple permanent mold containing a casting is shown in Fig. 6.1. Figure 6.2*a* shows an operator pouring an aluminum alloy into a permanent

[1]For this book, *sheet* is defined as a rolled product rectangular in cross section and form of thickness 0.006 to 0.249 in. (0.015 to 0.063 cm).

[2]For this book, *plate* is defined as a rolled product rectangular in cross section and form of thickness 0.250 in. (0.635 cm) or more.

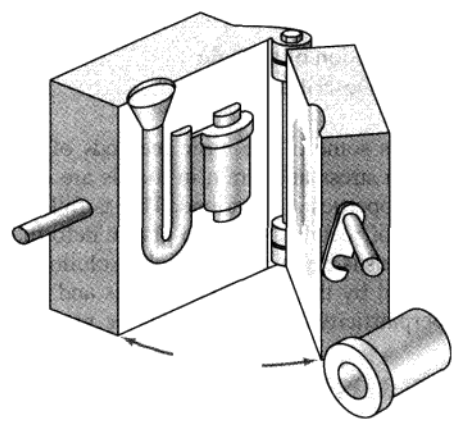

Figure 6.1
Permanent mold casting. Solidified casting with gate and metal core is shown in the left half of the mold. The completed casting is shown in front of the mold.
(After H.F. Taylor, M.C. Flemings, and J. Wulff, "Foundry Engineering," Wiley, 1959, p. 58.)

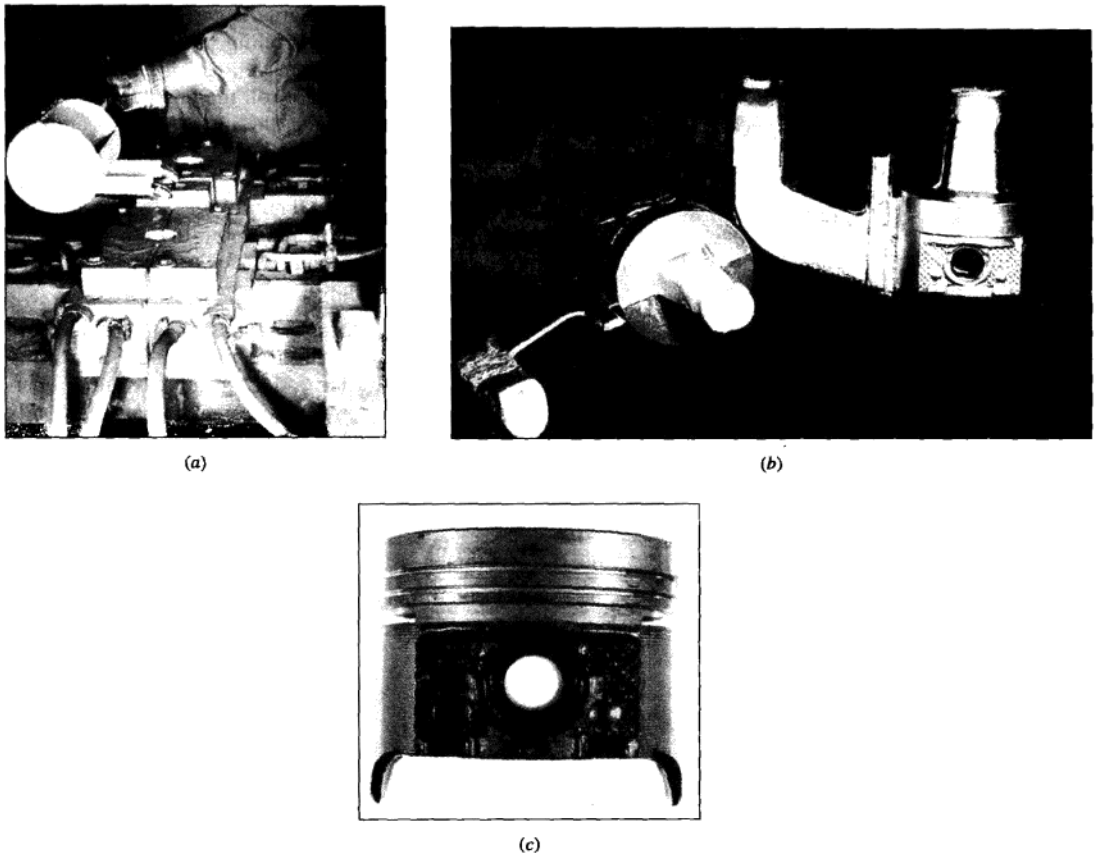

(a) (b)

(c)

Figure 6.2
(*a*) Simultaneous permanent mold casting of two aluminum alloy pistons. (*b*) Aluminum alloy permanent mold piston castings after being removed from the mold shown in (*a*). (*c*) An automobile piston after heat treatment and machining is ready for installation in an engine.
(*Courtesy of General Motors Corporation.*)

mold to produce a pair of piston castings; Fig. 6.2*b* shows the castings after they have been removed from the mold. After being trimmed, heat-treated, and machined, the finished piston (Fig. 6.2*c*) is ready for installation in an automobile engine.

6.1.2 Hot and Cold Rolling of Metals and Alloys

Hot and cold rolling are commonly used methods for fabricating metals and alloys. Long lengths of metal sheet and plate with uniform cross sections can be produced by these processes.

Hot Rolling of Sheet Ingots **Hot rolling** of sheet ingots is carried out first since greater reductions in thickness can be taken with each rolling pass when the metal is hot. Before hot rolling, sheet and plate ingots are preheated to a high temperature (about 1200°C). However, sometimes it is possible to hot roll the ingot-slabs directly from the caster. After removal from the preheat furnace, the ingot sections are usually hot rolled in a reversing break-down rolling mill (Fig. 6.3).

Hot rolling is continued until the temperature of the slab drops so low that continued rolling becomes too difficult. The slab is then reheated and hot rolling is continued, usually until the hot-rolled strip is thin enough to be wound into a coil. In most large-scale operations hot rolling of the slab is carried out by using a series of four-high rolling mills alone and in series, as shown for the hot rolling of steel strip in Fig. 6.4.

Cold Rolling of Metal Sheet[3] After hot rolling, which may also include some **cold rolling,** the coils of metal are usually given a reheating treatment called **annealing** to soften the metal to remove any cold work introduced during the hot-rolling operation. Cold rolling, which normally is done at room temperature, is again usually carried out with four-high rolling mills either alone or in series (Fig. 6.5). Figure 6.6 shows some sheet steel being cold-rolled on an industrial rolling mill.

The **percent cold reduction** of a plate or sheet of metal can be calculated as follows:

$$\%\ \text{cold reduction} = \frac{\text{initial metal thickness} - \text{final metal thickness}}{\text{initial metal thickness}} \times 100\% \tag{6.1}$$

EXAMPLE PROBLEM 6.1

Calculate the percent cold reduction in cold rolling an aluminum sheet alloy from 0.120 to 0.040 in.

■ **Solution**

$$\%\ \text{cold reduction} = \frac{\text{initial thickness} - \text{final thickness}}{\text{initial thickness}} \times 100\%$$

$$= \frac{0.120\ \text{in.} - 0.040\ \text{in.}}{0.120\ \text{in.}} \times 100\% = \frac{0.080\ \text{in.}}{0.120\ \text{in.}} \times 100\%$$

$$= 66.7\%$$

[3]Cold rolling of metals is usually carried out below the recrystallization temperature of the metal and results in the strain hardening of the metal.

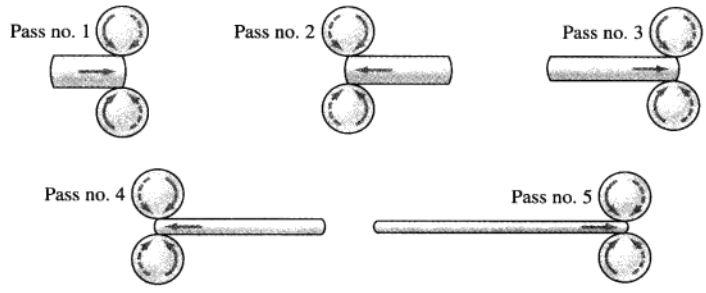

Figure 6.3
Diagrammatic representation of the sequence of hot-rolling operations involved in reducing an ingot to a slab on a reversing two-high mill.
(From H.E. McGannon (ed.), "The Making, Shaping, and Treating of Steel," 9th ed., United States Steel, 1971, p. 677. Courtesy of United States Steel Corporation.)

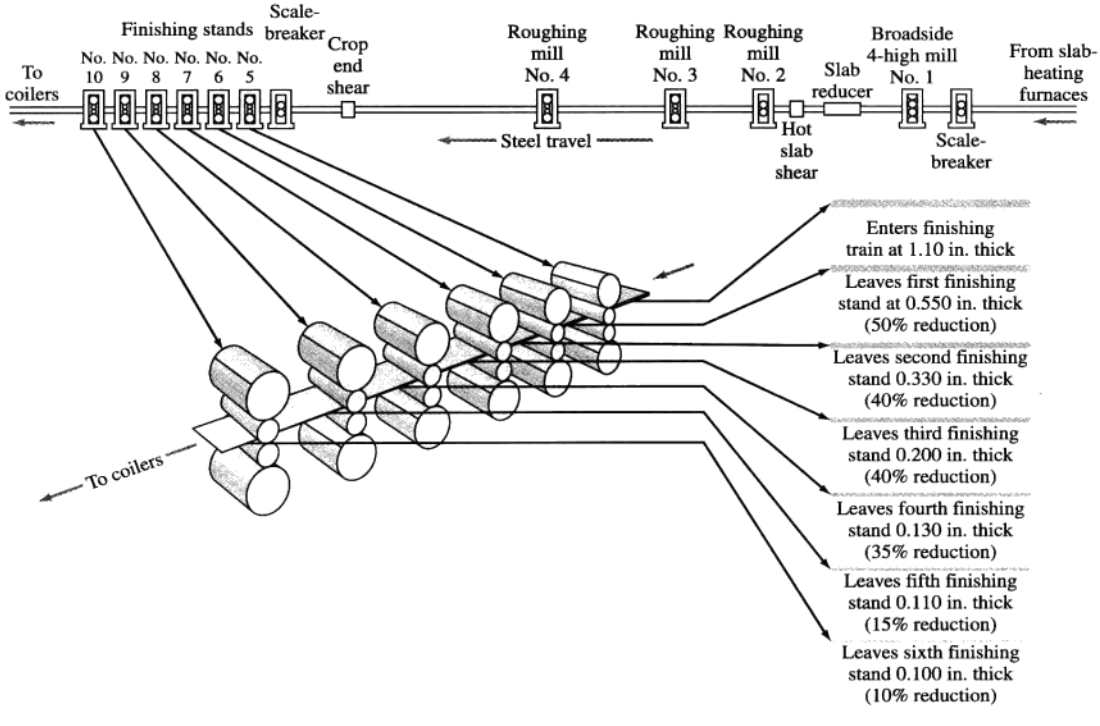

Figure 6.4
Typical reductions per pass in the finishing stands of a hot-strip mill equipped with four roughing stands and six finishing stands. Drawing is not to scale.
(From H.E. McGannon (ed.), "The Making, Shaping, and Treating of Steel," 9th ed., United States Steel, 1971, p. 937. Courtesy of United States Steel Corporation.)

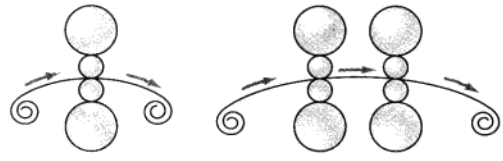

Figure 6.5
Schematic drawing illustrating the metal path during the cold rolling of metal sheet by four-high rolling mills: (*a*) single mill and (*b*) two mills in series.

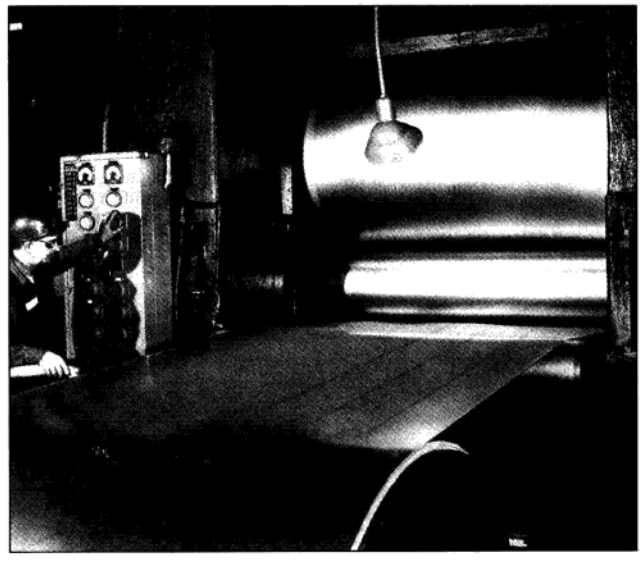

Figure 6.6
Cold rolling sheet steel. Mills of this type are used for cold rolling steel strip, tin plate, and nonferrous metals.
(*Courtesy of Bethlehem Steel Co.*)

EXAMPLE PROBLEM 6.2

A sheet of a 70% Cu–30% Zn alloy is cold-rolled 20 percent to a thickness of 3.00 mm. The sheet is then further cold-rolled to 2.00 mm. What is the total percent cold work?

■ **Solution**

We first determine the starting thickness of the sheet by considering the first cold reduction of 20 percent. Let x equal the starting thickness of the sheet. Then,

$$\frac{x - 3.00\text{ mm}}{x} = 0.20$$

or

$$x - 3.00 \text{ mm} = 0.20x$$
$$x = 3.75 \text{ mm}$$

We can now determine the *total* percent cold work from the starting thickness to the finished thickness from the relationship

$$\frac{3.75 \text{ mm} - 2.00 \text{ mm}}{3.75 \text{ mm}} = \frac{1.75 \text{ mm}}{3.75 \text{ mm}} = 0.466 \text{ or } 46.6\%$$

6.1.3 Extrusion of Metals and Alloys

Extrusion is a plastic-forming process in which a material under high pressure is reduced in cross section by forcing it through an opening in a die (Fig. 6.7). For most metals, the extrusion process is used to produce cylindrical bars or hollow tubes. For the more readily extrudable metals, such as aluminum and copper and some of their alloys, shapes with irregular cross sections are also commonly produced. Most metals are extruded hot since the deformation resistance of the metal is lower than if it is extruded cold. During extrusion, the metal of a billet in the container of an extrusion press is forced by a ram through a die so that the metal is continuously deformed into a long length of metal with a uniform desired cross section.

The two main types of extrusion processes are *direct extrusion* and *indirect extrusion.* In direct extrusion, the metal billet is placed in a container of an extrusion press and forced directly through the die by the ram (Fig. 6.7*a*). In indirect extrusion, a hollow ram holds the die, with the other end of the container of the extrusion press being closed by a plate (Fig. 6.7*b*). The frictional forces and power requirements for indirect extrusion are lower than those for direct extrusion. However, the loads that can be applied by using a hollow ram in the indirect process are more limited than those that can be used for direct extrusion.

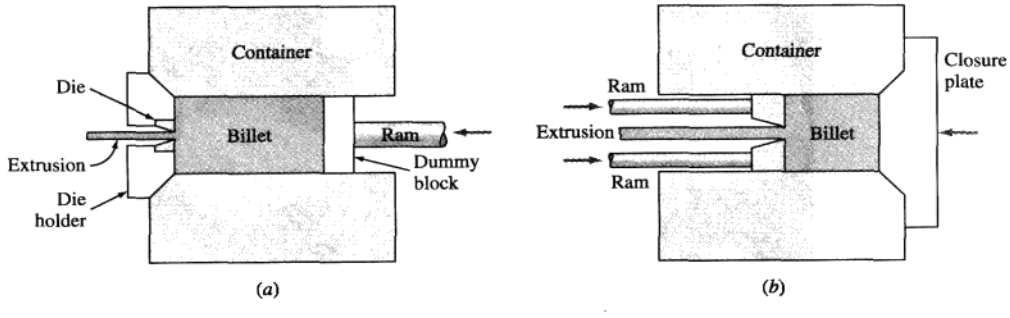

Figure 6.7
Two basic types of extrusion processes for metals: (*a*) direct and (*b*) indirect.
(G. Dieter, Mechanical Metallurgy, 2d ed., McGraw-Hill, 1976, p. 639. Reproduced with permission of The McGraw-Hill Companies.)

Animation

The extrusion process is used primarily for producing bar shapes, tube, and irregular shapes of the lower-melting nonferrous metals such as aluminum and copper and their alloys. However, with the development of powerful extrusion presses and improved lubricants such as glass, some carbon and stainless steels can also be hot-extruded.

6.1.4 Forging

Forging is another primary method for working metals into useful shapes. In the forging process the metal is hammered or pressed into a desired shape. Most forging operations are carried out with the metal in the hot condition, although in some cases the metal may be forged cold. There are two major types of forging methods: *hammer* and *press forging*. In hammer forging, a drop hammer repeatedly exerts a striking force against the surface of the metal. In press forging, the metal is subjected to a slowly moving compressive force (Fig. 6.8).

Forging processes can also be classified as *open-die forging* or *closed-die forging*. Open-die forging is carried out between two flat dies or dies with very simple shapes such as vees or semicircular cavities (Fig. 6.9) and is particularly useful for producing large parts such as steel shafts for electric steam turbines and generators. In closed-die forging, the metal to be forged is placed between two dies that have the upper and lower impressions of the desired shape of the forging. Closed-die forging can be carried out by using a single pair of dies or multiple-impression dies. An example of a closed-die forging in which multiple-impression dies are used is the automobile engine connecting rod (Fig. 6.10).

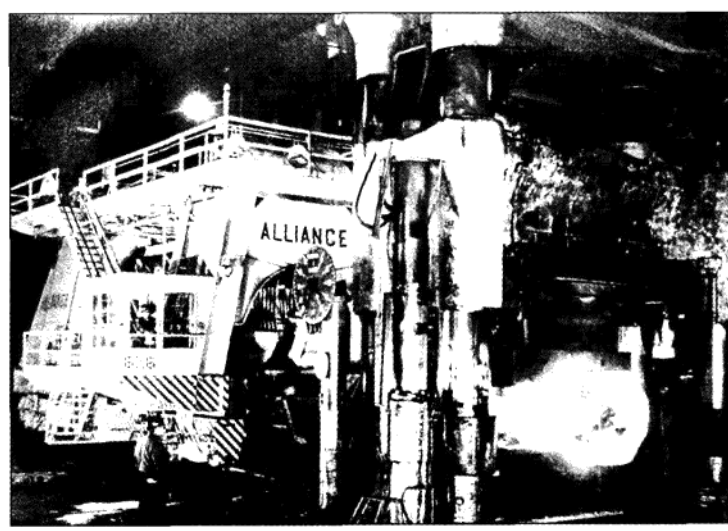

Figure 6.8
Heavy-duty manipulator holding an ingot in position while a 10,000-ton press squeezes the hot steel into the rough shape of the finished product. (*From H.E. McGannon [ed.], "The Making, Shaping, and Treating of Steel," 9th ed., United States Steel Corporation 1971, p. 1044.*)

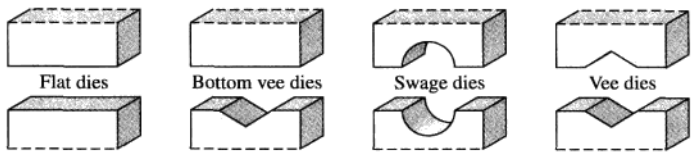

Figure 6.9
Basic shapes for open-die forging.
(From H.E. McGannon (ed.), "The Making, Shaping, and Treating of Steel," 9th ed., United States Steel, 1971, p. 1045. Courtesy of United States Steel Corporation.)

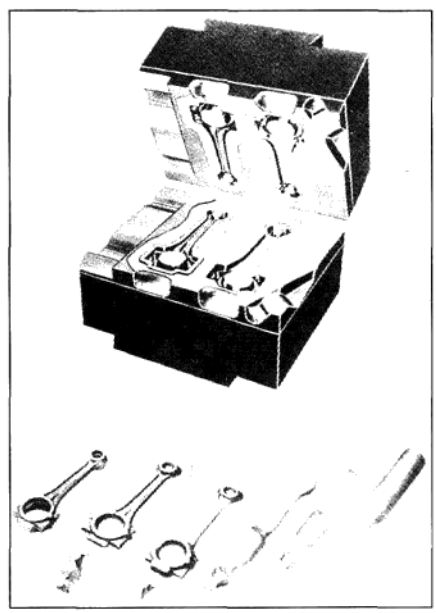

Figure 6.10
A set of closed forging dies used to produce an automobile connecting rod.
(Courtesy of the Forging Industry Association.)

In general, the forging process is used for producing irregular shapes that require working to improve the structure of the metal by reducing porosity and refining the internal structure. For example, a wrench that has been forged will be tougher and less likely to break than one that was simply cast into shape. Forging is also sometimes used to break down the as-cast ingot structure of some highly alloyed metals (e.g., some tool steels) so that the metal is made more homogeneous and less likely to crack during subsequent working.

6.1.5 Other Metal-Forming Processes

There are many types of secondary metal-forming processes whose descriptions are beyond the scope of this book. However, two of these processes, *wire drawing* and *deep drawing* of sheet metal, will be briefly described.

Wire drawing is an important metal-forming process. Starting rod or wire stock is drawn through one or more tapered wire-drawing dies (Fig. 6.11). For steel wire drawing, a tungsten carbide inner "nib" is inserted inside a steel casing. The hard carbide provides a wear-resistant surface for the reduction of the steel wire. Special precautions must be taken to make sure the surface of the stock to be drawn into wire is clean and properly lubricated. Intermediate softening heat treatments are sometimes necessary when the drawn wire work hardens during processing. The procedures used vary considerably, depending on the metal or alloy being drawn and the final diameter and temper desired.

EXAMPLE PROBLEM 6.3

Calculate the percent cold reduction when an annealed copper wire is cold-drawn from a diameter of 1.27 mm (0.050 in.) to a diameter of 0.813 mm (0.032 in.).

■ **Solution**

$$\%\ \text{cold reduction} = \frac{\text{change in cross-sectional area}}{\text{original area}} \times 100\% \tag{6.2}$$

$$= \frac{(\pi/4)(1.27\ \text{mm})^2 - (\pi/4)(0.813\ \text{mm})^2}{(\pi/4)(1.27\ \text{mm})^2} \times 100\%$$

$$= \left[1 - \frac{(0.813)^2}{(1.27)^2}\right](100\%)$$

$$= (1 - 0.41)(100\%) = 59\% \blacktriangleleft$$

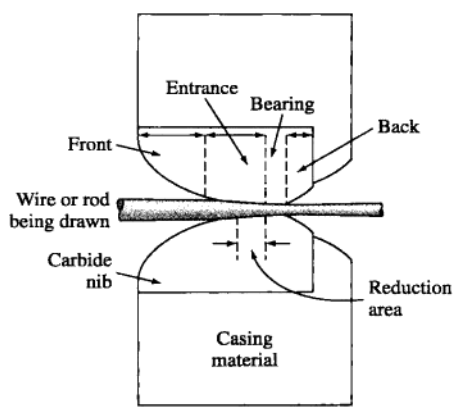

Figure 6.11
Section through a wire-drawing die.
(From "Wire and Rods, Alloy Steel," Steel Products Manual, American Iron and Steel Institute, 1975.)

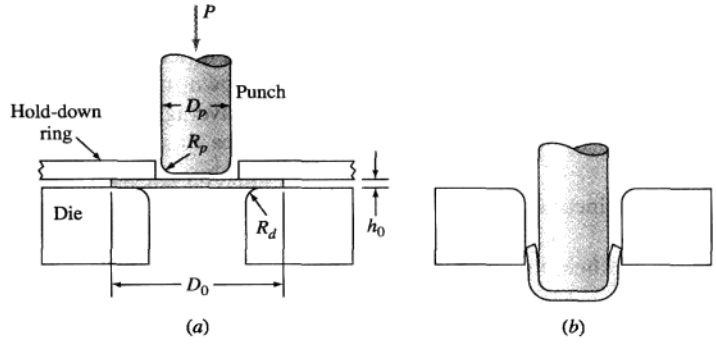

Figure 6.12
Deep drawing of a cylindrical cup (*a*) before drawing and (*b*) after drawing.
(G. Dieter, Mechanical Metallurgy, 2d ed., McGraw-Hill, 1976, p. 688. Reproduced with permission of The McGraw-Hill Companies.)

Deep drawing is another metal-forming process and is used for shaping flat sheets of metal into cup-shaped articles. A metal blank is placed over a shaped die and then is pressed into the die with a punch (Fig. 6.12). Usually a hold-down device is used to allow the metal to be pressed smoothly into the die to prevent wrinkling of the metal.

6.2 STRESS AND STRAIN IN METALS

In the first section of this chapter, we briefly examined most of the principal methods by which metals are processed into semifinished wrought and cast products. Let us now investigate how the mechanical properties of strength and ductility are evaluated for engineering applications.

6.2.1 Elastic and Plastic Deformation


Virtual Lab

When a piece of metal is subjected to a uniaxial tensile force, deformation of the metal occurs. If the metal returns to its original dimensions when the force is removed, the metal is said to have undergone **elastic deformation.** The amount of elastic deformation a metal can undergo is small, since during elastic deformation the metal atoms are displaced from their original positions but not to the extent that they take up new positions. Thus, when the force on a metal that has been elastically deformed is removed, the metal atoms return to their original positions and the metal takes back its original shape. If the metal is deformed to such an extent that it cannot fully recover its original dimensions, it is said to have undergone *plastic deformation.* During plastic deformation, the metal atoms are *permanently* displaced from their original positions and take up new positions. The ability of some metals to be extensively plastically deformed without fracture is one of the most useful engineering properties of metals. For example, the extensive plastic deformability of steel enables automobile parts such as fenders, hoods, and doors to be stamped out mechanically without the metal fracturing.

6.2.2 Engineering Stress and Engineering Strain

Engineering Stress Let us consider a cylindrical rod of length l_0 and cross-sectional area A_0 subjected to a uniaxial tensile force F, as shown in Fig. 6.13. By definition, the **engineering stress** σ on the bar is equal to the average uniaxial tensile force F on the bar divided by the original cross-sectional area A_0 of the bar. Thus,

$$\text{Engineering stress } \sigma = \frac{F \text{ (average uniaxial tensile force)}}{A_0 \text{ (original cross-sectional area)}} \tag{6.3}$$

The units for engineering stress are:

U.S. customary: pounds force per square inch ($lb_f/in.^2$, or psi);
lb_f = pounds force
SI: newtons per square meter (N/m^2) or pascals (Pa), where 1 N/m^2 = 1 Pa

The conversion factors for psi to pascals are

$$1 \text{ psi} = 6.89 \times 10^3 \text{ Pa}$$
$$10^6 \text{ Pa} = 1 \text{ megapascal} = 1 \text{ MPa}$$
$$1000 \text{ psi} = 1 \text{ ksi} = 6.89 \text{ MPa}$$

EXAMPLE PROBLEM 6.4

A 0.500-in.-diameter aluminum bar is subjected to a force of 2500 lb_f. Calculate the engineering stress in pounds per square inch (psi) on the bar.

■ **Solution**

$$\sigma = \frac{\text{force}}{\text{original cross-sectional area}} = \frac{F}{A_0}$$
$$= \frac{2500 \text{ lb}_f}{(\pi/4)(0.500 \text{ in})^2} = 12{,}700 \text{ lb}_f/\text{in.}^2 \blacktriangleleft$$

EXAMPLE PROBLEM 6.5

A 1.25-cm-diameter bar is subjected to a load of 2500 kg. Calculate the engineering stress on the bar in megapascals (MPa).

■ **Solution**

The load on the bar has a mass of 2500 kg. In SI units, the force on the bar is equal to the mass of the load times the acceleration of gravity (9.81 m/s^2), or

$$F = ma = (2500 \text{ kg})(9.81 \text{ m/s}^2) = 24{,}500 \text{ N}$$

The diameter d of the bar = 1.25 cm = 0.0125 m. Thus, the engineering stress on the bar is

$$\sigma = \frac{F}{A_0} = \frac{F}{(\pi/4)(d^2)} = \frac{24{,}500 \text{ N}}{(\pi/4)(0.0125 \text{ m})^2}$$
$$= (2.00 \times 10^8 \text{ Pa})\left(\frac{1 \text{ MPa}}{10^6 \text{ Pa}}\right) = 200 \text{ MPa} \blacktriangleleft$$

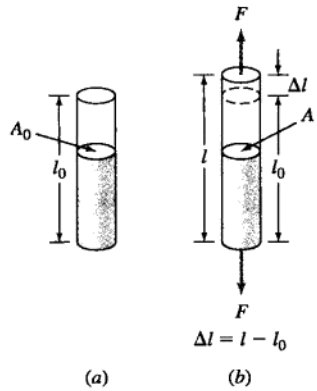

Figure 6.13
Elongation of a cylindrical metal rod subjected to a uniaxial tensile force *F*. (*a*) The rod with no force on it; and (*b*) the rod subjected to a uniaxial tensile force *F*, which elongates the rod from length l_0 to *l*.

Engineering Strain When a uniaxial tensile force is applied to a rod, such as that shown in Fig. 6.13, it causes the rod to be elongated in the direction of the force. Such a displacement is called *strain.* By definition, **engineering strain,** which is caused by the action of a uniaxial tensile force on a metal sample, is the ratio of the change in length of the sample in the direction of the force divided by the original length of sample considered. Thus, the engineering strain for the metal bar shown in Fig. 6.13 (or for a similar-type metal sample) is

$$\text{Engineering strain } \epsilon = \frac{l - l_0}{l_0} = \frac{\Delta l \,(\text{change in length of sample})}{l_0\,(\text{original length of sample})} \qquad \textbf{(6.4)}$$

where l_0 = original length of sample and l = new length of sample after being extended by a uniaxial tensile force. In most cases, engineering strain is determined by using a small length, usually 2 in., called the *gage length,* within a much longer, for example, 8 in., sample (see Example Problem 6.6).


Virtual Lab

The *units for engineering strain* ϵ are:

U.S. customary: inches per inch (in./in.)

SI: meters per meter (m/m)

Thus, engineering strain has *dimensionless units.* In industrial practice, it is common to convert engineering strain into *percent strain* or *percent elongation:*

$$\%\text{ engineering strain} = \text{engineering strain} \times 100\% = \%\text{ elongation}$$

EXAMPLE PROBLEM 6.6

A sample of commercially pure aluminum 0.500 in. wide, 0.040 in. thick, and 8 in. long that has gage markings 2.00 in. apart in the middle of the sample is strained so that the gage markings are 2.65 in. apart (Fig. 6.14). Calculate the engineering strain and the percent engineering strain elongation that the sample undergoes.

■ **Solution**

$$\text{Engineering strain } \epsilon = \frac{l - l_0}{l_0} = \frac{2.65 \text{ in.} - 2.00 \text{ in.}}{2.00 \text{ in.}} = \frac{0.65 \text{ in.}}{2.00 \text{ in.}} = 0.325 \blacktriangleleft$$

$$\% \text{ elongation} = 0.325 \times 100\% = 32.5\% \blacktriangleleft$$

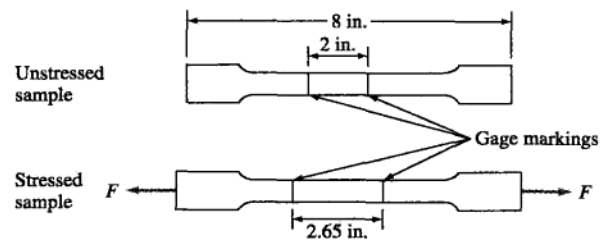

Figure 6.14
Flat tensile specimen before and after testing.

6.2.3 Poisson's Ratio

A longitudinal elastic deformation of a metal produces an accompanying lateral dimensional change. As shown in Fig. 6.15*b*, a tensile stress σ_z produces an axial strain $+\epsilon_z$ and lateral contractions of $-\epsilon_x$ and $-\epsilon_y$. For isotropic behavior,[4] ϵ_x and ϵ_y are equal. The ratio

$$\nu = -\frac{\epsilon \text{ (lateral)}}{\epsilon \text{ (longitudinal)}} = -\frac{\epsilon_x}{\epsilon_z} = -\frac{\epsilon_y}{\epsilon_z} \tag{6.5}$$

is called *Poisson's ratio.* For ideal materials, $\nu = 0.5$. However, for real materials, Poisson's ratio typically ranges from 0.25 to 0.4, with an average of about 0.3. Table 6.1 lists ν values for some metals and alloys.

6.2.4 Shear Stress and Shear Strain

Until now we have discussed the elastic and plastic deformation of metals and alloys under uniaxial tension stresses. Another important method by which a metal can be deformed is under the action of a **shear stress.** The action of a simple shear stress couple (shear stresses act in pairs) on a cubic body is shown in Fig. 6.15*c*, where a shearing force S acts over an area A. The shear stress τ is related to the shear force S by

$$\tau \text{ (shear stress)} = \frac{S \text{ (shear force)}}{A \text{ (area over which shear force acts)}} \tag{6.6}$$

[4] *Isotropic:* exhibiting properties with the same values when measured along axes in all directions.

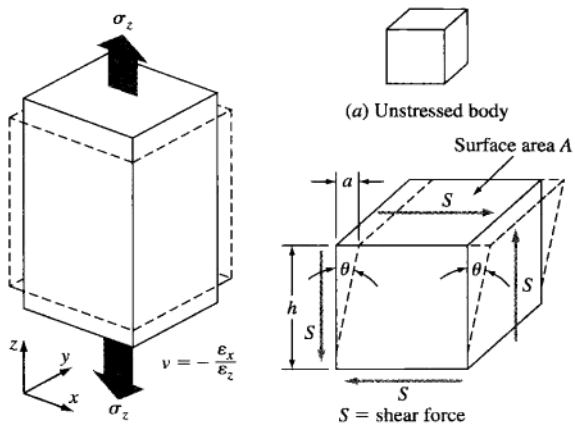

(*b*) Body under tensile stress (*c*) Body under shear stress

Virtual Lab

Figure 6.15
(*a*) Unstressed cubic body. (*b*) Cubic body subjected to tensile stress. The ratio of the elastic contraction perpendicular to the extension is designated Poisson's ratio ν. (*c*) Cubic body subjected to pure shear forces S acting over surface areas A. The shear stress τ acting on the body is equal to S/A.

Table 6.1 Typical room-temperature values of elastic constants for isotropic materials

Material	Modulus of elasticity, 10^6 psi (GPa)	Shear modulus, 10^6 psi (GPa)	Poisson's ratio
Aluminum alloys	10.5 (72.4)	4.0 (27.5)	0.31
Copper	16.0 (110)	6.0 (41.4)	0.33
Steel (plain carbon and low-alloy)	29.0 (200)	11.0 (75.8)	0.33
Stainless steel (18-8)	28.0 (193)	9.5 (65.6)	0.28
Titanium	17.0 (117)	6.5 (44.8)	0.31
Tungsten	58.0 (400)	22.8 (157)	0.27

Source: G. Dieter, "Mechanical Metallurgy," 3rd ed., McGraw-Hill, 1986.

The units for shear stress are the same as for uniaxial tensile stress:

U.S. customary: pounds force per square inch ($lb_f/in.^2$, or psi)

SI: newtons per square meter (N/m^2) or pascals (Pa)

The **shear strain** γ is defined in terms of the amount of the shear displacement a in Fig. 6.15*c* divided by the distance h over which the shear acts, or

$$\gamma = \frac{a}{h} = \tan \theta \tag{6.7}$$

For pure elastic shear, the proportionality between shear and stress is

$$\tau = G\gamma \tag{6.8}$$

where G is the elastic modulus.

We will be concerned with shear stresses when we discuss the plastic deformation of metals in Sec. 6.5.

6.3 THE TENSILE TEST AND THE ENGINEERING STRESS-STRAIN DIAGRAM

The *tensile test* is used to evaluate the strength of metals and alloys. In this test, a metal sample is pulled to failure in a relatively short time at a constant rate. Figure 6.16 is a picture of a modern tensile testing machine, and Fig. 6.17 illustrates schematically how the sample is tested in tension.

The force (load) on the specimen being tested is measured by the load cell while the strain is obtained from the extensometer attached to the specimen (Fig. 6.18) and the data is collected in a computer-control software package.

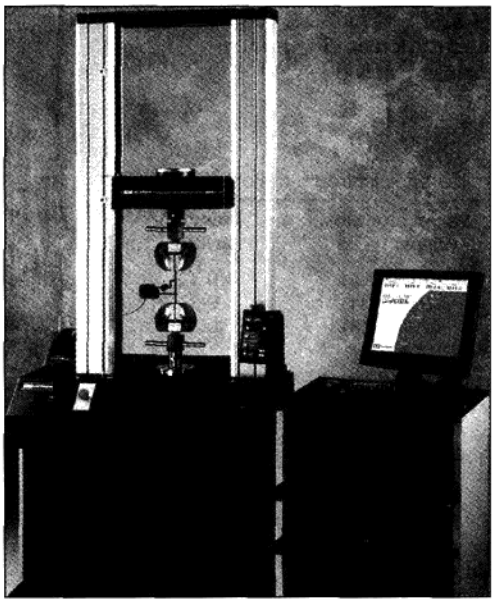

Virtual Lab

Figure 6.16
Modern tensile testing machine. The force (load) on the specimen is measured by the load cell while the strain is measured by the clip-on extensometer. The data is collected and analyzed by computer-controlled software.
(Courtesy of the Instron® Corporation.)

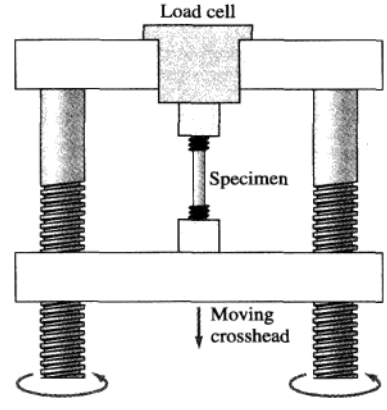

Figure 6.17
Schematic illustration showing how the tensile machine of Fig. 6.16 operates. Note, however, that the crosshead of the machine in Fig. 6.16 moves up.
(From H.W. Hayden, W.G. Moffatt and J. Wulff, The Structure and Properties of Materials, vol. III, "Mechanical Behavior," Wiley, 1965, Fig. 1.1, p. 2.)

The types of samples used for the tensile test vary considerably. For metals with a thick cross section such as plate, a 0.50-in.-diameter round specimen is commonly used (Fig. 6.19*a*). For metal with thinner cross sections such as sheet, a flat specimen is used (Fig. 6.19*b*). A 2-in. gage length within the specimen is the most commonly used gage length for tensile tests.

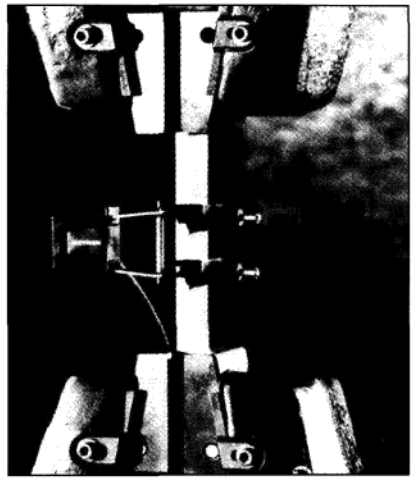

Figure 6.18
Close-up of the tensile machine extensometer that measures the strain that the sample undergoes during the tensile test. The extensometer is attached to the sample by small spring clamps.
(*Courtesy of the Instron Corporation.*)

Virtual Lab

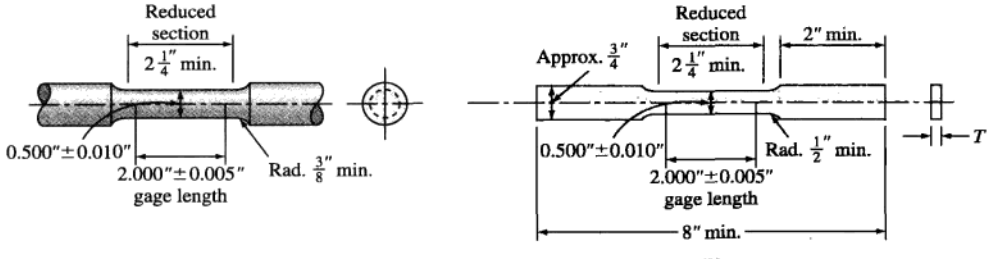

Figure 6.19
Examples of the geometrical shape of commonly used tension test specimens. (*a*) Standard round tension test specimen with 2-in. gage length. (*b*) Standard rectangular tension test specimen with 2-in. gage length.
(*From H.E. McGannon (ed.), "The Making, Shaping, and Treating of Steel," 9th ed., United States Steel, 1971, p. 1220. Courtesy of United States Steel Corporation.*)

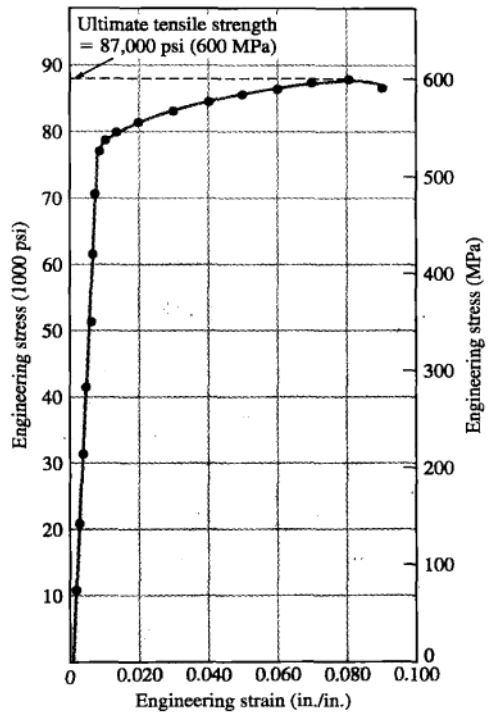

Figure 6.20
Engineering stress-strain diagram for a high-strength aluminum alloy (7075-T6). The specimens for the diagram were taken from ⅝-in. plate and had a 0.50-in. diameter with a 2-in. gage length.
(Courtesy of Aluminum Company of America.)


Virtual Lab

The force data obtained from the chart paper for the tensile test can be converted to engineering stress data, and a plot of engineering stress versus engineering strain can be constructed. Figure 6.20 shows an **engineering stress-strain diagram** for a high-strength aluminum alloy.

6.3.1 Mechanical Property Data Obtained from the Tensile Test and the Engineering Stress-Strain Diagram

The mechanical properties of metals and alloys that are of engineering importance for structural design and can be obtained from the engineering tensile test are:

1. Modulus of elasticity
2. Yield strength at 0.2 percent offset

3. Ultimate tensile strength
4. Percent elongation at fracture
5. Percent reduction in area at fracture

Modulus of Elasticity In the first part of the tensile test, the metal is deformed elastically. That is, if the load on the specimen is released, the specimen will return to its original length. For metals, the maximum elastic deformation is usually less than 0.5 percent. In general, metals and alloys show a linear relationship between stress and strain in the elastic region of the engineering stress-strain diagram, which is described by Hooke's law:[5]

$$\sigma \text{ (stress)} = E\epsilon \text{ (strain)} \tag{6.9}$$

or

$$E = \frac{\sigma \text{ (stress)}}{\epsilon \text{ (strain)}} \quad \text{(units of psi or Pa)}$$

Virtual Lab

where E is the **modulus of elasticity,** or *Young's modulus.*[6]

The modulus of elasticity is related to the bonding strength between the atoms in a metal or alloy. Table 6.1 lists the elastic moduli for some common metals. Metals with high elastic moduli are relatively stiff and do not deflect easily. Steels, for example, have high elastic moduli values of 30×10^6 psi (207 GPa),[7] whereas aluminum alloys have lower elastic moduli of about 10 to 11 $\times$ 10^6 psi (69 to 76 GPa). Note that in the elastic region of the stress-strain diagram, the modulus does not change with increasing stress.

Yield Strength The **yield strength** is a very important value for use in engineering structural design since it is the strength at which a metal or alloy shows significant plastic deformation. Because there is no definite point on the stress-strain curve where elastic strain ends and plastic strain begins, the yield strength is chosen to be that strength when a definite amount of plastic strain has occurred. For American engineering structural design, the yield strength is chosen when 0.2 percent plastic strain has taken place, as indicated on the engineering stress-strain diagram of Fig. 6.21.

The 0.2 percent yield strength, also called the *0.2 percent offset yield strength,* is determined from the engineering stress-strain diagram, as shown in Fig. 6.21. First, a line is drawn parallel to the elastic (linear) part of the stress-strain plot at 0.002 in./in. (m/m) strain, as indicated on Fig. 6.21. Then at the point where this line intersects the upper part of the stress-strain curve, a horizontal line is drawn to the stress axis. The 0.2 percent offset yield strength is the stress where the horizontal line intersects the stress axis, and in the case of the stress-strain

[5]Robert Hooke (1635–1703). English physicist who studied the elastic behavior of solids.

[6]Thomas Young (1773–1829). English physicist.

[7]SI prefix G = giga = 10^9.

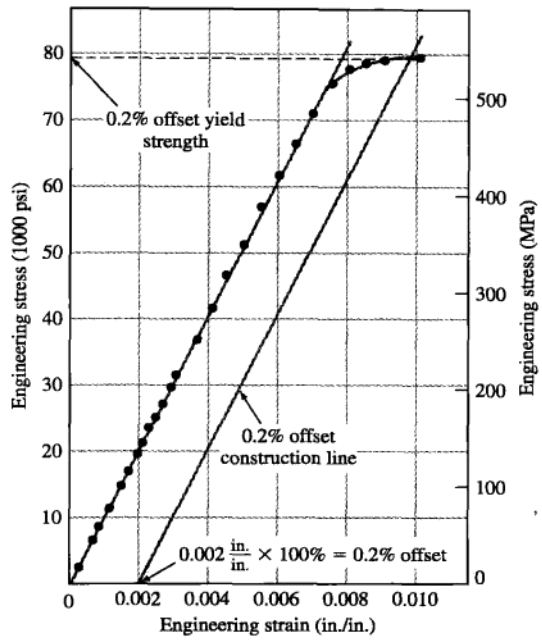

Figure 6.21
Linear part of engineering stress-strain diagram of Fig. 6.22 expanded on the strain axis to make a more accurate determination of the 0.2 percent offset yield stress.
(*Courtesy of Aluminum Company of America.*)

Virtual Lab

curve of Fig. 6.21, the yield strength is 78,000 psi. It should be pointed out that the 0.2 percent offset yield strength is arbitrarily chosen, and thus the yield strength could have been chosen at any other small amount of permanent deformation. For example, a 0.1 percent offset yield strength is commonly used in the United Kingdom.

Ultimate Tensile Strength The **ultimate tensile strength** (UTS) is the maximum strength reached in the engineering stress-strain curve. If the specimen develops a localized decrease in cross-sectional area (commonly called *necking*) (Fig. 6.22), the engineering stress will decrease with further strain until fracture occurs since the engineering stress is determined by using the *original* cross-sectional area of the specimen. The more ductile a metal is, the more the specimen will neck before fracture and hence the more the decrease in the stress on the

stress-strain curve beyond the maximum stress. For the high-strength aluminum alloy whose stress-strain curve is shown in Fig. 6.20, there is only a small decrease in stress beyond the maximum stress because this material has relatively low ductility.

An important point to understand with respect to engineering stress-strain diagrams is that the metal or alloy continues to increase in stress up to the stress at fracture. It is only because we use the original cross-sectional area to determine engineering stress that the stress on the engineering stress-strain diagram decreases at the latter part of the test.

The ultimate tensile strength of a metal is determined by drawing a horizontal line from the maximum point on the stress-strain curve to the stress axis. The stress where this line intersects the stress axis is called the *ultimate tensile strength,* or sometimes just the *tensile strength.* For the aluminum alloy of Fig. 6.20, the ultimate tensile strength is 87,000 psi.

The ultimate tensile strength is not used much in engineering design for ductile alloys since too much plastic deformation takes place before it is reached. However, the ultimate tensile strength can give some indication of the presence of defects. If the metal contains porosity or inclusions, these defects may cause the ultimate tensile strength of the metal to be lower than normal.

Percent Elongation The amount of elongation that a tensile specimen undergoes during testing provides a value for the ductility of a metal. Ductility of metals is most commonly expressed as percent elongation, starting with a gage length usually of 2 in. (5.1 cm) (Fig. 6.19). In general, the higher the ductility (the more deformable the metal is), the higher the percent elongation. For example, a sheet of 0.062-in. (1.6-mm) commercially pure aluminum (alloy 1100-0) in the soft condition has a high percent elongation of 35 percent, whereas the same thickness of the high-strength aluminum alloy 7075-T6 in the fully hard condition has a percent elongation of only 11 percent.

As previously mentioned, during the tensile test an extensometer can be used to continuously measure the strain of the specimen being tested. However, the percent elongation of a specimen after fracture can be measured by fitting the fractured specimen together and measuring the final elongation with calipers.

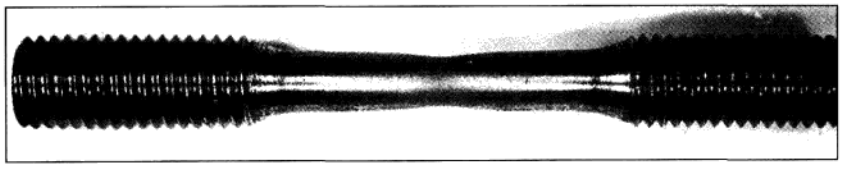

Figure 6.22
Necking in a mild-steel round specimen. The specimen was originally uniformly cylindrical. After being subjected to uniaxial tension forces up to almost fracture, the specimen decreased in cross section, or "necked" in the middle.

The percent elongation can then be calculated from the equation

$$\% \text{ elongation} = \frac{\text{final length*} - \text{initial length*}}{\text{initial length}} \times 100\%$$

$$= \frac{l - l_0}{l_0} \times 100\% \qquad \textbf{(6.10)}$$

Virtual Lab

The percent elongation at fracture is of engineering importance not only as a measure of ductility but also as an index of the quality of the metal. If porosity or inclusions are present in the metal or if damage due to overheating the metal has occurred, the percent elongation of the specimen tested may be decreased below normal.

Percent Reduction in Area The ductility of a metal or alloy can also be expressed in terms of the percent reduction in area. This quantity is usually obtained from a tensile test using a specimen 0.50 in. (12.7 mm) in diameter. After the test, the diameter of the reduced cross section at the fracture is measured. Using the measurements of the initial and final diameters, the percent reduction in area can be determined from the equation

$$\% \text{ reduction in area} = \frac{\text{initial area} - \text{final area}}{\text{initial area}} \times 100\%$$

$$= \frac{A_0 - A_f}{A_0} \times 100\% \qquad \textbf{(6.11)}$$

EXAMPLE PROBLEM 6.7

A 0.500-in.-diameter round sample of a 1030 carbon steel is pulled to failure in a tensile testing machine. The diameter of the sample was 0.343 in. at the fracture surface. Calculate the percent reduction in area of the sample.

■ **Solution**

$$\% \text{ reduction in area} = \frac{A_0 - A_f}{A_0} \times 100\% = \left(1 - \frac{A_f}{A_0}\right)(100\%)$$

$$= \left[1 - \frac{(\pi/4)(0.343 \text{ in.})^2}{(\pi/4)(0.500 \text{ in.})^2}\right](100\%)$$

$$= (1 - 0.47)(100\%) = 53\% \blacktriangleleft$$

The percent reduction in area, like the percent elongation, is a measure of the ductility of the metal and is also an index of quality. The percent reduction in area may be decreased if defects such as inclusions and/or porosity are present in the metal specimen.

*The initial length is the length between the gage marks on the specimen before testing. The final length is the length between these same gage marks after testing when the fractured surface of the specimen is fitted together (see Example Problem 6.6).

6.3.2 Comparison of Engineering Stress-Strain Curves for Selected Alloys

Engineering stress-strain curves for selected metals and alloys are shown in Fig. 6.23. Alloying a metal with other metals or nonmetals and heat treatment can greatly affect the tensile strength and ductility of metals. The stress-strain curves of Fig. 6.23 show a great variation in ultimate tensile strength. Elemental magnesium has a UTS of 35 ksi (1 ksi = 1000 psi), whereas SAE 1340 steel water-quenched and tempered at 700°F (370°C) has a UTS of 240 ksi.

6.3.3 True Stress and True Strain

The engineering stress is calculated by dividing the applied force F on a tensile test specimen by its original cross-sectional area A_0 (Eq. 6.3). Since the cross-sectional area of the test specimen changes continuously during a tensile test, the engineering stress calculated is not precise. During the tensile test, after necking of the sample occurs (Fig. 6.22), the engineering stress decreases as the strain increases, leading to a maximum engineering stress in the engineering stress-

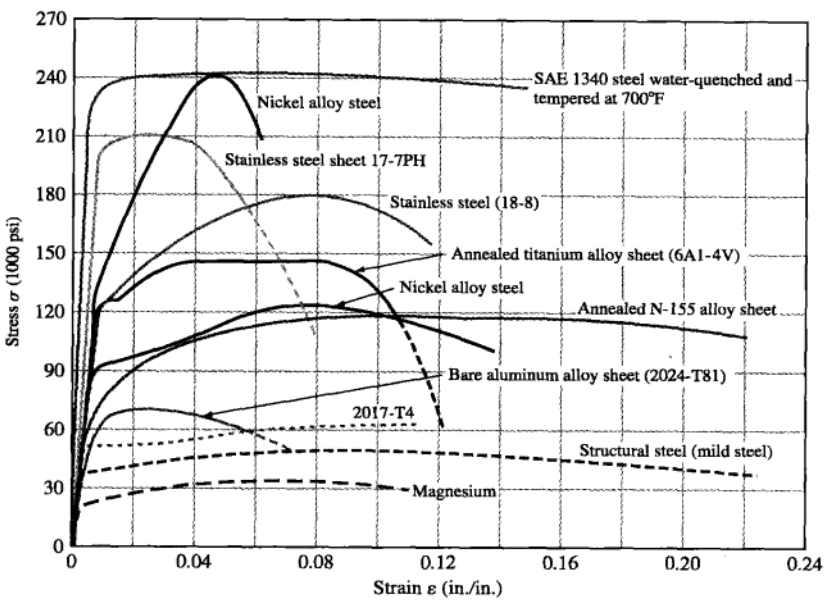

Figure 6.23
Engineering stress-strain curves for selected metals and alloys.
(Marin, Mechanical Behavior of Engineering Materials, 1st ed., 1962. Adapted by permission of Pearson Education, Inc., Upper Saddle River, NJ.)

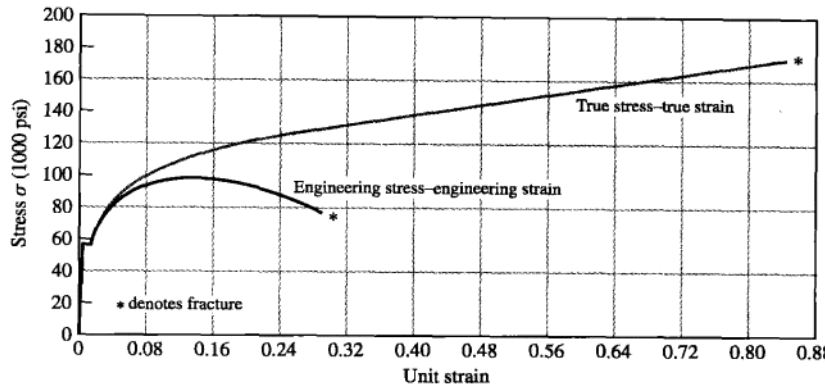

Virtual Lab

Figure 6.24
Comparison of the true stress–true strain curve with the engineering (nominal) stress-strain diagram for a low-carbon steel.
(From H.E. McGannon (ed.), The Making, Shaping, and Treating of Steel, 9th ed., United States Steel, 1971. Courtesy of United States Steel Corporation.)

strain curve (Fig. 6.24). Thus, once necking begins during the tensile test, the true stress is higher than the engineering stress. We define the true stress and true strain by the following:

$$\text{True stress } \sigma_t = \frac{F \text{ (average uniaxial force on the test sample)}}{A_i \text{ (instantaneous minimum cross-sectional area of sample)}} \tag{6.12}$$

$$\text{True strain } \epsilon_t = \int_{l_0}^{l_i} \frac{dl}{l} = \ln \frac{l_i}{l_0} \tag{6.13}$$

where l_0 is the original gage length of the sample and l_i is the instantaneous extended gage length during the test. If we assume constant volume of the gage-length section of the test specimen during the test, then $l_0 A_0 = l_i A_i$ or

$$\frac{l_i}{l_0} = \frac{A_0}{A_i} \qquad \text{and} \qquad \epsilon_t = \ln \frac{l_i}{l_0} = \ln \frac{A_0}{A_i} \tag{6.14}$$

Figure 6.24 compares engineering stress-strain and true stress-strain curves for a low-carbon steel.

Engineering designs are not based on true stress at fracture since as soon as the yield strength is exceeded, the material starts to deform. Engineers use instead the 0.2 percent offset engineering yield stress for structural designs with the proper safety factors. However, for research, sometimes the true stress-strain curves are needed.

EXAMPLE PROBLEM 6.8

Compare the engineering stress and strain with the true test and strain for the tensile test of a low-carbon steel that has the following test values.

Load applied to specimen = 17,000 lb_f Initial specimen diameter = 0.500 in.

Diameter of specimen under 17,000 lb_f load = 0.472 in.

■ **Solution**

$$\text{Area at start } A_0 = \frac{\pi}{4}d^2 = \frac{\pi}{4}(0.500 \text{ in.})^2 = 0.196 \text{ in.}^2$$

$$\text{Area under load } A_i = \frac{\pi}{4}(0.472 \text{ in.})^2 = 0.175 \text{ in.}^2$$

Assuming no volume change during extension, $A_0 l_0 = A_i l_i$ or $l_i/l_0 = A_0/A_i$.

$$\text{Engineering stress} = \frac{F}{A_0} = \frac{17{,}000 \text{ lb}_f}{0.196 \text{ in.}^2} = 86{,}700 \text{ psi} \blacktriangleleft$$

$$\text{Engineering strain} = \frac{\Delta l}{l} = \frac{l_i - l_0}{l_0} = \frac{A_0}{A_i} - 1 = \frac{0.196 \text{ in.}^2}{0.175 \text{ in.}^2} - 1 = 0.12$$

$$\text{True stress} = \frac{F}{A_i} = \frac{17{,}000 \text{ lb}_f}{0.175 \text{ in.}^2} = 97{,}100 \text{ psi} \blacktriangleleft$$

$$\text{True strain} = \ln\frac{l_i}{l_0} = \ln\frac{A_0}{A_i} = \ln\frac{0.196 \text{ in.}^2}{0.175 \text{ in.}^2} = \ln 1.12 = 0.113$$

6.4 HARDNESS AND HARDNESS TESTING

Hardness is a measure of the resistance of a metal to permanent (plastic) deformation. The hardness of a metal is measured by forcing an indenter into its surface. The indenter material, which is usually a ball, pyramid, or cone, is made of a material much harder than the material being tested. For example, hardened steel, tungsten carbide, or diamond are commonly used materials for indenters. For most standard hardness tests a known load is applied slowly by pressing the indenter at 90° into the metal surface being tested [Fig. 6.25*b* (2)]. After the indentation has been made, the indenter is withdrawn from the surface [Fig. 6.25*b* (3)]. An empirical hardness number is then calculated or read off a dial (or digital display), which is based on the cross-sectional area or depth of the impression.

Table 6.2 lists the types of indenters and types of impressions associated with four common hardness tests: Brinell, Vickers, Knoop, and Rockwell. The hardness number for each of these tests depends on the shape of the indentation and the applied load. Figure 6.25 shows a modern Rockwell hardness tester, which has a digital readout display.

The hardness of a metal depends on the ease with which it plastically deforms. Thus a relationship between hardness and strength for a particular metal can be determined empirically. The hardness test is much simpler than the tensile test and can

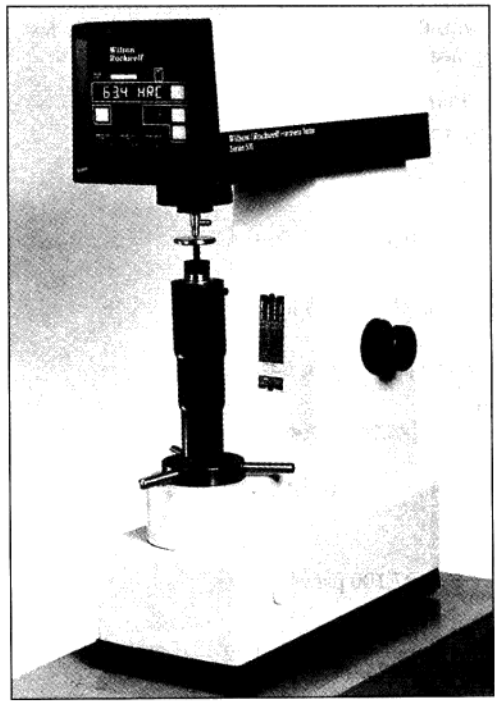

(a)

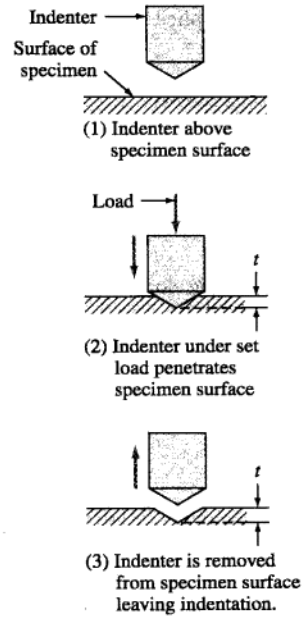

(b)

Virtual Lab

Figure 6.25
(*a*) A Rockwell hardness tester.
(*Courtesy of the Page-Wilson Co.*)
(*b*) Steps in the measurement of hardness with a diamond-cone identer. The depth t determines the hardness of the material. The lower the value of t, the harder the material.

be nondestructive (i.e., the small indentation of the indenter may not be detrimental to the use of an object). For these reasons, the hardness test is used extensively in industry for quality control.

6.5 PLASTIC DEFORMATION OF METAL SINGLE CRYSTALS

6.5.1 Slipbands and Slip Lines on the Surface of Metal Crystals

Let us first consider the permanent deformation of a rod of a zinc single crystal by stressing it beyond its elastic limit. An examination of the zinc crystal after the deformation shows that step markings appear on its surface, which are called

Table 6.2 Hardness tests

Test	Indenter	Shape of indentation: Side view	Shape of indentation: Top view	Load	Formula for hardness number
Brinell	10 mm sphere of steel or tungsten carbide	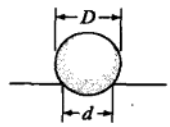		P	$\text{BHN} = \dfrac{2P}{\pi D(D - \sqrt{D^2 - d^2})}$
Vickers	Diamond pyramid	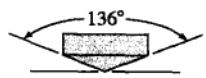		P	$\text{VHN} = \dfrac{1.72P}{d_1^2}$
Knoop microhardness	Diamond pyramid	 $l/b = 7.11$ $b/t = 4.00$	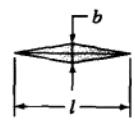	P	$\text{KHN} = \dfrac{14.2P}{l^2}$
Rockwell A C D	Diamond cone	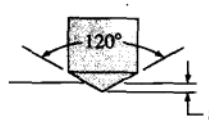		60 kg R_A = 150 kg R_C = 100 kg R_D =	100–500f
B F G	$\frac{1}{16}$-in.-diameter steel sphere			100 kg R_B = 60 kg R_F = 150 kg R_G = 100 kg R_E =	130–500f
E	$\frac{1}{8}$-in.-diameter steel sphere	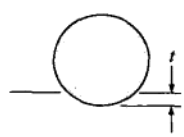			

Source: After H.W. Hayden, W.G. Moffatt, and J. Wulff, "The Structure and Properties of Materials," vol. III, Wiley, 1965, p. 12.

slipbands (Fig. 6.26*a* and *b*). The slipbands are caused by the slip or shear deformation of metal atoms on specific crystallographic planes called *slip planes*. The deformed zinc single-crystal surface illustrates the formation of slipbands very clearly since **slip** in these crystals is restricted primarily to slip on the HCP basal planes (Fig. 6.26*c* and *d*).

In single crystals of ductile FCC metals like copper and aluminum, slip occurs on multiple slip planes, and as a result the slipband pattern on the surface of these metals when they are deformed is more uniform (Fig. 6.27). A closer examination of the slipped surface of metals at high magnification shows that slip has occurred

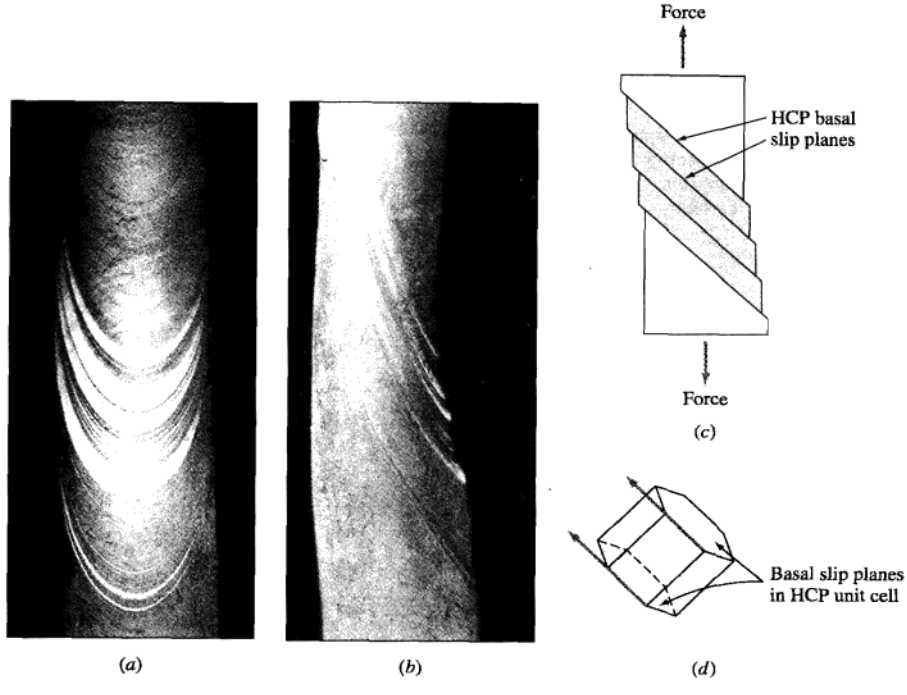

Figure 6.26
Plastically deformed zinc single crystal showing slipbands: (*a*) front view of real crystal, (*b*) side view of real crystal, (*c*) schematic side view indicating HCP basal slip planes in crystal, and (*d*) HCP unit cell indicating basal slip planes.
(*Zinc single-crystal photos courtesy of Prof. Earl Parker of the University of California at Berkeley.*)

on many slip planes within the slipbands (Fig. 6.28). These fine steps are called *slip lines* and are usually about 50 to 500 atoms apart, whereas slipbands are commonly separated by about 10,000 atom diameters. Unfortunately, the terms "slipband" and "slip line" are often used interchangeably.

6.5.2 Plastic Deformation in Metal Crystals by the Slip Mechanism

Figure 6.29 shows a possible atomic model for the slippage of one block of atoms over another in a perfect metal crystal. Calculations made from this model determine that the strength of metal crystals should be about 1000 to 10,000 times greater than their observed shear strengths. Thus, this mechanism for atomic slip in large real metal crystals must be incorrect.

Figure 6.27
Slipband pattern on surface of copper single crystal after 0.9 percent deformation. (Magnification 100×.)
[*After F.D. Rosi. Trans. AIME,* **200**:*1018 (1954).*]

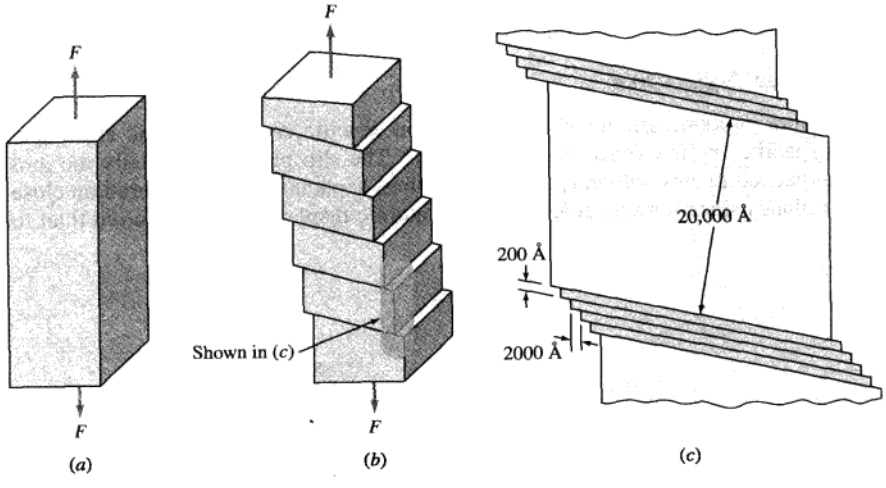

Figure 6.28
The formation of slipbands during plastic deformation. (*a*) A single crystal under a tensile force. (*b*) Slipbands appear when the applied stress exceeds the yield stress. Blocks of crystal slide past each other. (*c*) The shaded region of (*b*) has been magnified. Slip occurs on a large number of closely packed slip planes that are parallel. This region is called a *slipband* and appears as a line at lower magnification.
(Eisenstadt, M., "Introduction to Mechanical Properties of Materials: An Ecological Approach," 1st ed., 1971. Reprinted by permission of Pearson Education, Inc., Upper Saddle River, NJ.)


Animation

In order for large metal crystals to deform at their observed low shear strengths, a high density of crystalline imperfections known as *dislocations* must be present. These dislocations are created in large numbers ($\sim 10^6$ cm/cm^3) as the metal solidifies, and when the metal crystal is deformed, many more are created so that a highly deformed crystal may contain as high as 10^{12} cm/cm^3 of dislocations. Figure 6.30 shows schematically how an *edge dislocation* can produce a unit of slip under a low *shear stress.* A relatively small amount of stress is required for slip by this process since only a small group of atoms slips over each other at any instant.

An analogous situation to the movement of a dislocation in a metal crystal under a shear stress can be envisaged by the movement of a carpet with a ripple in it across a very large floor. Moving the carpet by pulling on one end may be impossible because of the friction between the floor and the carpet. However, by putting a ripple in the carpet (analogous to a dislocation in a metal crystal), the carpet may be moved by pushing the ripple in the carpet one step at a time across the floor (Fig. 6.30*d*).

Dislocations in real crystals can be observed in the transmission electron microscope in thin metal foils and appear as lines due to the atomic disarray at the dislocations that interfere with the transmission path of the electron beam of the microscope. Figure 6.31 shows a cellular wall pattern of dislocations created by lightly deforming an aluminum sample. The cells are relatively free from dislocations but are separated by walls of high dislocation density.

6.5.3 Slip Systems

Dislocations produce atomic displacements on specific crystallographic slip planes and in specific crystallographic slip directions. The slip planes are usually the most densely packed planes, which are also the farthest separated. Slip is favored on close-packed planes since a lower shear stress for atomic displacement is required than for

Figure 6.29
Large groups of atoms in large metal crystals do *not* slide over each other simultaneously during plastic shear deformation, as indicated in this figure, since the process requires too much energy. A lower-energy process involving the slippage of a small group of atoms takes place instead.

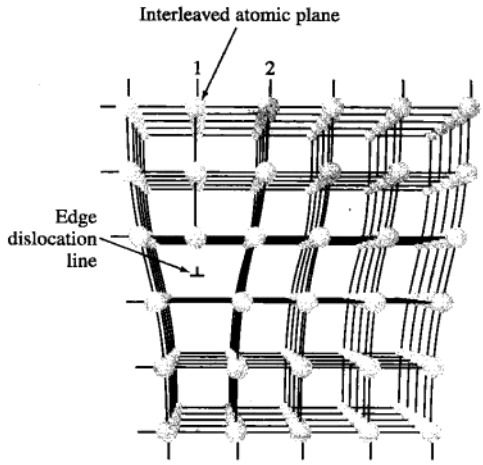

(*a*) An edge dislocation, pictured as formed by an extra half plane of atoms.

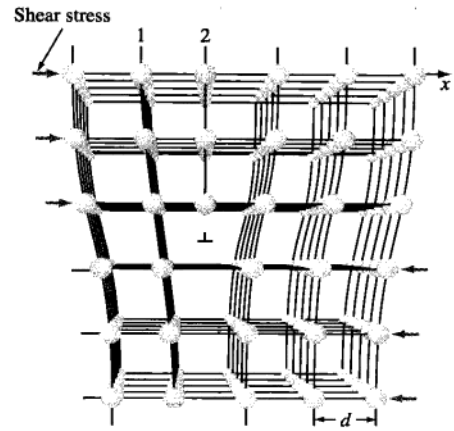

(*b*) A low stress causes a shift of atomic bonds to free a new interleaved plane.

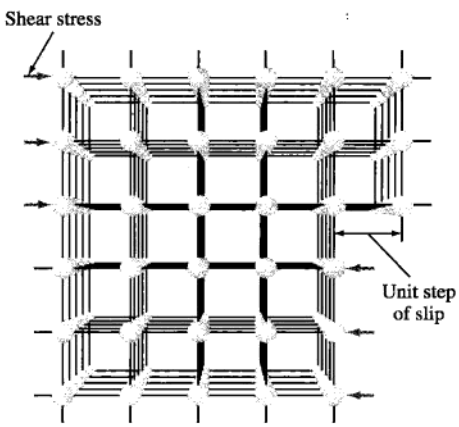

(*c*) Repetition of this process causes the dislocation to move across the crystal.

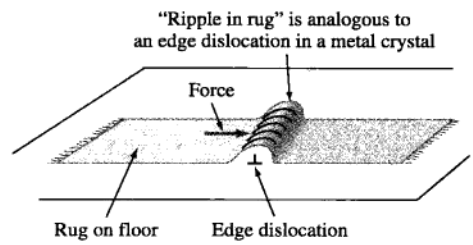

(*d*)

Figure 6.30
Schematic illustration of how the motion of an edge dislocation produces a unit step of slip under a low shear stress. (*a*) An edge dislocation, pictured as formed by an extra half plane of atoms. (*b*) A low stress causes a shift of atomic bonds to free a new interleaved plane. (*c*) Repetition of this process causes the dislocation to move across the crystal. This process requires less energy than the one depicted in Fig. 6.28.


Animation

(*From A.G. Guy, "Essentials of Materials Science," McGraw-Hill, 1976, p. 153.*)
(*d*) The "ripple in the rug" analogy. A dislocation moves through a metal crystal during plastic deformation in a manner similar to a ripple that is pushed along a carpet lying on a floor. In both cases, a small amount of relative movement is caused by the passage of the dislocation or ripple, and hence a relatively low amount of energy is expended in this process.

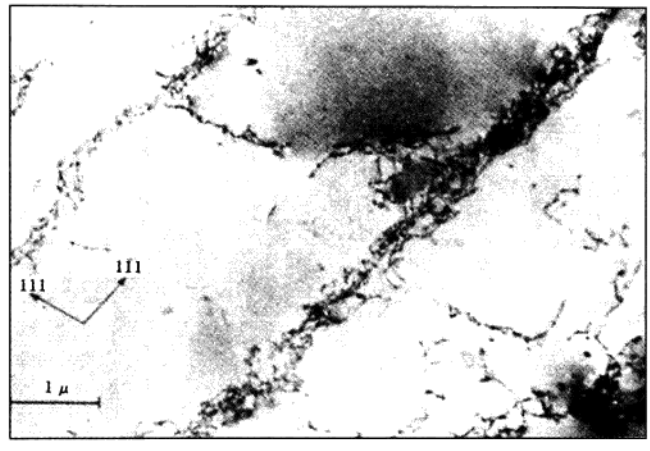

Figure 6.31
Dislocation cell structure in a lightly deformed aluminum sample as revealed by transmission electron microscopy. The cells are relatively free from dislocations but are separated by walls of high dislocation density.
(After P.R. Swann, in G. Thomas and J. Washburn, [eds.], "Electron Microscopy and Strength of Crystals," Wiley, 1963, p. 133.)

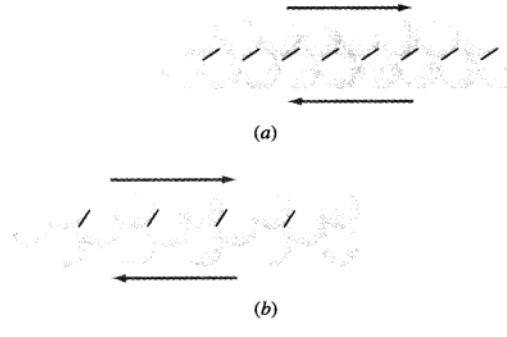

Figure 6.32
Comparison of atomic slip on (*a*) a close-packed plane and (*b*) a non–close-packed plane. Slip is favored on the close-packed plane because less force is required to move the atoms from one position to the next closest one, as indicated by the slopes of the bars on the atoms. Note that dislocations move one atomic slip step at a time.
(From A.H. Cottrell, The Nature of Metals, "Materials," Scientific American, September 1967, p. 48. Illustration © Enid Kotschnig. Reproduced by permission of Enid Kotschnig.)

less densely packed planes (Fig. 6.32). However, if slip on the close-packed planes is restricted due to local high stresses, for example, then planes of lower atomic packing can become operative. Slip in the close-packed directions is also favored since less energy is required to move the atoms from one position to another if the atoms are closer together.

A combination of a slip plane and a slip direction is called a **slip system. Slip** in metallic structures occurs on a number of slip systems that are characteristic for each crystal structure. Table 6.3 lists the predominant slip planes and slip directions for FCC, BCC, and HCP crystal structures.

For metals with the FCC crystal structure, slip takes place on the close-packed {111} octahedral planes and in the $\langle 1\bar{1}0 \rangle$ close-packed directions. There are eight {111} octahedral planes in the FCC crystal structure (Fig. 6.33). The (111) type planes at opposite faces of the octahedron that are parallel to each other are considered the same type of (111) slip plane. Thus, there are only four different types of (111) slip planes in the FCC crystal structure. Each (111)-type plane contains three $[1\bar{1}0]$-type slip directions. The reverse directions are not considered different slip directions. Thus, for the FCC lattice there are 4 slip planes × 3 slip directions = 12 slip systems (Table 6.3).

The BCC structure is *not* a close-packed structure and does not have a predominant plane of highest atomic packing like the FCC structure. The {110} planes

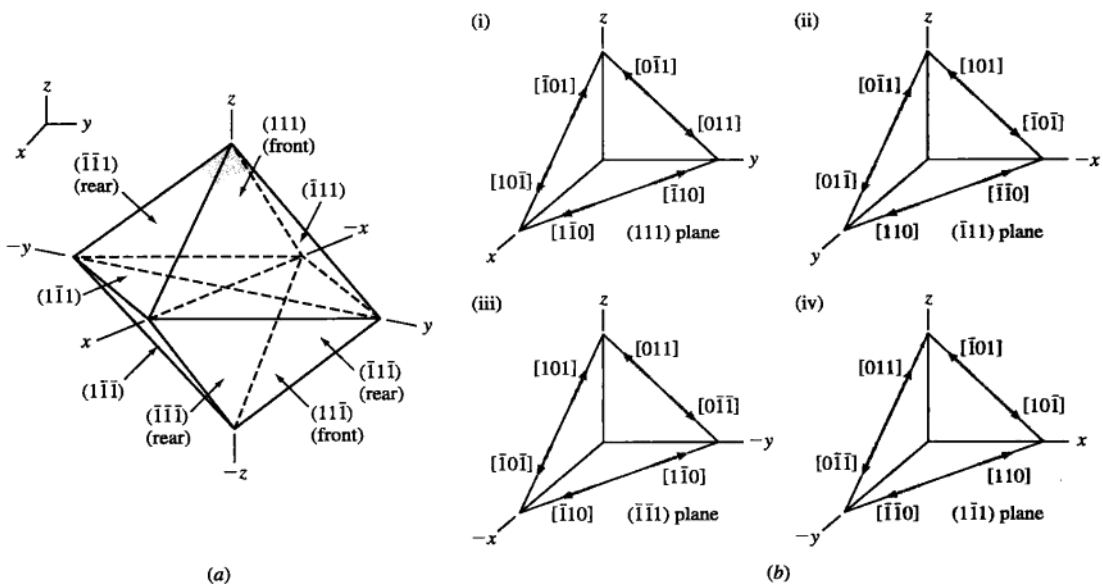

Figure 6.33
Slip planes and directions for the FCC crystal structure. (*a*) Only four of the eight {111} octahedral planes are considered slip planes since planes opposite each other are considered the same slip plane. (*b*) For each slip plane there are three $\langle 1\bar{1}0 \rangle$ slip directions since opposite directions are considered as only one slip direction. Note that slip directions are only shown for the upper four slip planes of the octahedral FCC planes. Thus, there are 4 slip planes × 3 slip directions, giving a total of 12 slip systems for the FCC crystal structure.

Table 6.3 Slip systems observed in crystal structures

Structure	Slip plane	Slip direction	Number of slip systems	
FCC: Cu, Al, Ni, Pb, Au, Ag, γFe, . . .	{111}	$\langle 1\bar{1}0 \rangle$	4 × 3 = 12	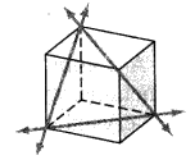
BCC: αFe, W, Mo, β brass	{110}	$\langle \bar{1}11 \rangle$	6 × 2 = 12	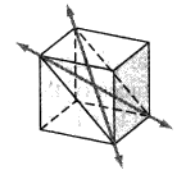
αFe, Mo, W, Na	{211}	$\langle \bar{1}11 \rangle$	12 × 1 = 12	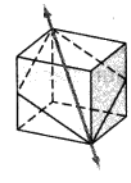
αFe, K	{321}	$\langle \bar{1}11 \rangle$	24 × 1 = 24	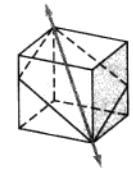
HCP: Cd, Zn, Mg, Ti, Be, . . .	{0001}	$\langle 11\bar{2}0 \rangle$	1 × 3 = 3	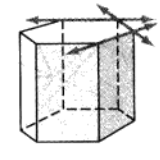
Ti (prism planes)	$\{10\bar{1}0\}$	$\langle 11\bar{2}0 \rangle$	3 × 1 = 3	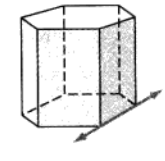
Ti, Mg (pyramidal planes)	$\{10\bar{1}1\}$	$\langle 11\bar{2}0 \rangle$	6 × 1 = 6	

Source: After H.W. Hayden, W.G. Moffatt, and J. Wulff, "The Structure and Properties of Materials," vol. III, Wiley, 1965, p. 100.

have the highest atomic density, and slip commonly takes place on these planes. However, slip in BCC metals also occurs on {112} and {123} planes. Since the slip planes in the BCC structure are not close-packed as in the case of the FCC structure, higher shear stresses are necessary for slip in BCC than in FCC metals. The slip direction in BCC metals is always of the $\langle \bar{1}11 \rangle$ type. Since there are six (110)-type slip planes of which each can slip in two $[\bar{1}11]$ directions, there are $6 \times 2 = 12$ $\{110\}\langle \bar{1}11 \rangle$ slip systems.

In the HCP structure, the basal plane (0001) is the closest-packed plane and is the common slip plane for HCP metals such as Zn, Cd, and Mg that have high c/a ratios (Table 6.3). However, for HCP metals such as Ti, Zr, and Be that have low c/a ratios, slip also occurs commonly on prism $\{10\bar{1}0\}$ and pyramidal $\{10\bar{1}1\}$ planes. In all cases, the slip direction remains $\langle 11\bar{2}0 \rangle$. The limited number of slip systems in HCP metals restricts their ductilities.

6.5.4 Critical Resolved Shear Stress for Metal Single Crystals

The stress required to cause slip in a pure-metal single crystal depends mainly on the crystal structure of the metal, its atomic bonding characteristics, the temperature at which it is deformed, and the orientation of the active slip planes with respect to the shear stresses. Slip begins within the crystal when the shear stress on the slip plane in the slip direction reaches a required level called the *critical resolved shear stress*, τ_c. Essentially, this value is the yield stress of a single crystal and is equivalent to the yield stress of a polycrystalline metal or alloy determined by a stress-strain tensile test curve.

Table 6.4 lists values for the critical resolved shear stresses of some pure-metal single crystals at room temperature. The HCP metals Zn, Cd, and Mg have low critical resolved shear stresses ranging from 0.18 to 0.77 MPa. The HCP metal titanium,

Table 6.4 Room-temperature slip systems and critical resolved shear stress for metal single crystals

Metal	Crystal structure	Purity (%)	Slip plane	Slip direction	Critical shear stress (MPa)
Zn	HCP	99.999	(0001)	$[11\bar{2}0]$	0.18
Mg	HCP	99.996	(0001)	[1120]	0.77
Cd	HCP	99.996	(0001)	$[11\bar{2}0]$	0.58
Ti	HCP	99.99	(1010)	$[11\bar{2}0]$	13.7
		99.9	(1010)	$[11\bar{2}0]$	90.1
Ag	FCC	99.99	(111)	$[1\bar{1}0]$	0.48
		99.97	(111)	$[1\bar{1}0]$	0.73
		99.93	(111)	$[1\bar{1}0]$	1.3
Cu	FCC	99.999	(111)	$[1\bar{1}0]$	0.65
		99.98	(111)	$[1\bar{1}0]$	0.94
Ni	FCC	99.8	(111)	$[1\bar{1}0]$	5.7
Fe	BCC	99.96	(110)	$[\bar{1}11]$	27.5
			(112)		
			(123)		
Mo	BCC	. . .	(110)	$[\bar{1}11]$	49.0

Source: After G. Dieter, "Mechanical Metallurgy," 2nd ed., McGraw-Hill, 1976, p. 129.

on the other hand, has a very high τ_c of 13.7 MPa. It is believed that some covalent bonding mixed with metallic bonding is partly responsible for this high value of τ_c. Pure FCC metals such as Ag and Cu have low τ_c values of 0.48 and 0.65 MPa, respectively, because of their multiple slip systems.

6.5.5 Schmid's Law

The relationship between a uniaxial stress acting on a cylinder of a pure metal single crystal and the resulting resolved shear stress produced on a slip system within the cylinder can be derived as follows. Consider a uniaxial tensile stress σ acting on a metal cylinder, as shown in Fig. 6.34. Let A_0 be the area normal to the axial force F, and A_1 the area of the slip plane or shear area on which the resolved shear force F_r is acting. We can orient the slip plane and slip direction by defining the angles ϕ and λ. ϕ is the angle between the uniaxial force F and the normal to the slip plane area A_1, and λ is the angle between the axial force and the slip direction.

In order for dislocations to move in the slip system, a sufficient resolved shear stress acting in the slip direction must be produced by the applied axial force. The resolved shear stress is

$$\tau_r = \frac{\text{shear force}}{\text{shear area (slip plane area)}} = \frac{F_r}{A_1} \tag{6.15}$$

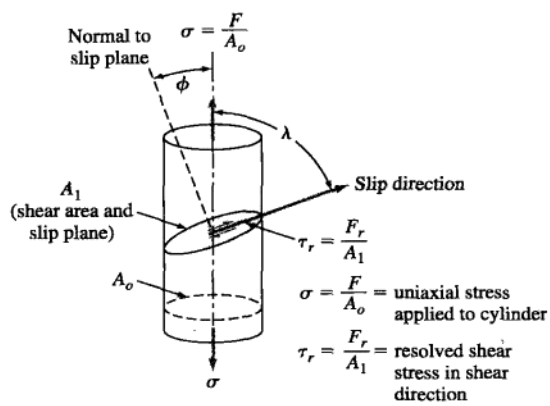

Figure 6.34
Axial stress σ can produce a resolved shear stress τ_r and cause dislocation motion in slip plane A_1 in the slip direction.

The resolved shear force F_r is related to the axial force F by $F_r = F\cos\lambda$. The area of the slip plane (shear area) $A_1 = A_0/\cos\phi$. By dividing the shear force $F\cos\lambda$ by the shear area $A_0/\cos\phi$, we obtain

$$\tau_r = \frac{F\cos\lambda}{A_0/\cos\phi} = \frac{F}{A_0}\cos\lambda\cos\phi = \sigma\cos\lambda\cos\phi \qquad (6.16)$$

which is called *Schmid's law.* Let us now consider an example problem to calculate the resolved shear stress when a slip system is acted upon by an axial stress.

EXAMPLE PROBLEM 6.9

Calculate the resolved shear stress on the (111) $[0\bar{1}1]$ slip system of a unit cell in an FCC nickel single crystal if a stress of 13.7 MPa is applied in the [001] direction of a unit cell.

■ Solution

By geometry, the angle λ between the applied stress and the slip direction is 45°, as shown in Fig. EP6.9*a*. In the cubic system, the direction indices of the normal to a crystal plane are the same as the Miller indices of the crystal plane. Therefore, the normal to the (111) plane that is the slip plane is the [111] direction. From Fig. EP6.9*b*,

$$\cos\phi = \frac{a}{\sqrt{3}a} = \frac{1}{\sqrt{3}} \quad \text{or} \quad \phi = 54.74°$$

$$\tau_r = \sigma\cos\lambda\cos\phi = (13.7\text{ MPa})(\cos 45°)(\cos 54.74°) = 5.6\text{ MPa} \blacktriangleleft$$

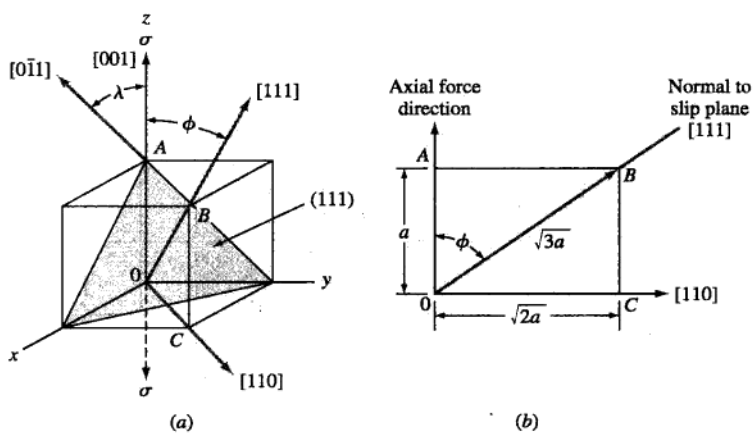

Figure EP6.9
An FCC unit cell is acted upon by a [001] tensile stress producing a resolved shear stress on the (111) $[0\bar{1}1]$ slip system.

6.5.6 Twinning

A second important plastic deformation mechanism that can occur in metals is **twinning.** In this process a part of the atomic lattice is deformed so that it forms a mirror image of the undeformed lattice next to it (Fig. 6.35). The crystallographic plane of symmetry between the undeformed and deformed parts of the metal lattice is called the *twinning plane.* Twinning, like slip, occurs in a specific direction called the *twinning direction.* However, in slip the atoms on one side of the slip plane all move equal distances (Fig. 6.30), whereas in twinning the atoms move distances proportional to their distance from the twinning plane (Fig. 6.35). Figure 6.36 illustrates the basic difference between slip and twinning on the surface of a metal after deformation. Slip leaves a series of steps (lines) (Fig. 6.36*a*), whereas twinning leaves small but well-defined regions of the crystal deformed (Fig. 6.36*b*). Figure 6.37 shows some deformation twins on the surface of titanium metal.


Virtual Lab

Twinning only involves a small fraction of the total volume of the metal crystal, and so the amount of overall deformation that can be produced by twinning is small. However, the important role of twinning in deformation is that the lattice orientation changes that are caused by twinning may place new slip systems into favorable orientation with respect to the shear stress and thus enable additional slip to occur. Of the three major metallic unit-cell structures (BCC, FCC, and HCP), twinning is most important for the HCP structure because of its small number of slip systems. However, even with the assistance of twinning, HCP metals like zinc and magnesium are still less ductile than the BCC and FCC metals that have more slip systems.

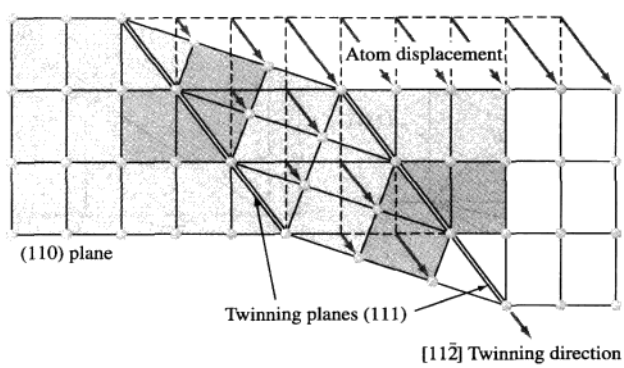

Figure 6.35
Schematic diagram of the twinning process in an FCC lattice.
(From H.W. Hayden, W.G. Moffatt and J. Wulff, "The Structure and Properties of Materials," vol. III, Wiley, 1965, p. 111.)

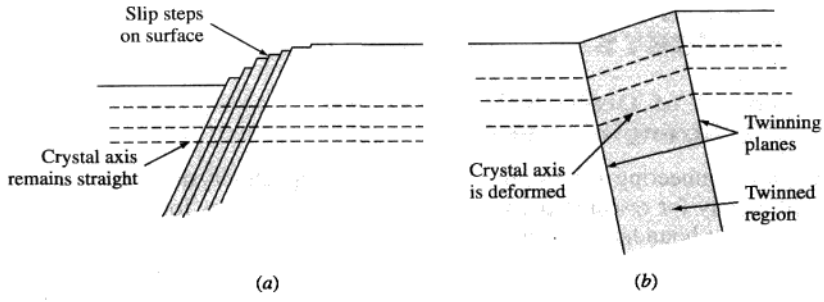

Figure 6.36
Schematic diagram of surfaces of a deformed metal after (*a*) slip and (*b*) twinning.

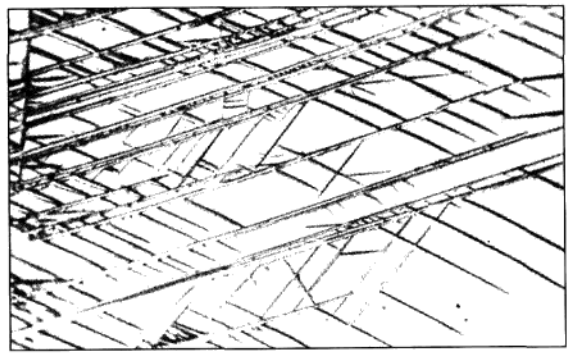

Figure 6.37
Deformation twins in unalloyed (99.77%) titanium. (Magnification 150×.)
[*After F.D. Rosi, C.A. Dube, and B.H. Alexander, Trans. AIME,* **197**:*259 (1953).*]

Deformation twinning is observed at room temperature for the HCP metals. Twinning is found in the BCC metals such as Fe, Mo, W, Ta, and Cr in crystals that were deformed at very low temperatures. Twinning has also been found in some of these BCC metal crystals at room temperature when they have been subjected to very high strain rates. The FCC metals show the least tendency to form deformation twins. However, deformation twins can be produced in some FCC metals if the stress level is high enough and the temperature sufficiently low. For example, copper crystals deformed at 4 K at high stress levels can form deformation twins.

6.6 PLASTIC DEFORMATION OF POLYCRYSTALLINE METALS

6.6.1 Effect of Grain Boundaries on the Strength of Metals

Almost all engineering alloys are polycrystalline. Single-crystal metals and alloys are used mainly for research purposes and only in a few cases for engineering applications.[8] Grain boundaries strengthen metals and alloys by acting as barriers to dislocation movement except at high temperatures, where they become regions of weakness. For most applications where strength is important, a fine grain size is desirable, and so most metals are fabricated with a fine grain size. In general, at room temperature, fine-grained metals are stronger, harder, tougher, and more susceptible to strain hardening. However, they are less resistant to corrosion and creep (deformation under constant load at elevated temperatures; see Sec. 7.4). A fine grain size also results in a more uniform and isotropic behavior of materials. In Sec. 4.5, the ASTM grain size number and a method to determine the average grain diameter of a metal using metallography techniques were discussed. These parameters allow us to make a relative comparison of grain density and therefore grain boundary density in metals. Accordingly, for two components made of the same alloy, the component that has a larger ASTM grain size number or a smaller average grain diameter is stronger. The relationship between strength and grain size is of great importance to engineers. The well known *Hall–Petch equation,* Eq. 6.16, is an empirical (based on experimental measurements and not on theory) equation that relates the yield strength of a metal, σ_y, to its average grain diameter d as follows:

$$\sigma_y = \sigma_0 + k/(d)^{1/2} \qquad \textbf{(6.17)}$$

where σ_0 and k are constants related to the material of interest. A similar effect exists between hardness (Vickers microhardness test) and grain size. The equation clearly shows that as grain diameter decreases, the yield strength of the material increases. Considering that the conventional grain diameters may range from a few hundred microns to a few microns, one may expect a significant change in strength through grain refinement. The values for σ_0 and k for selected materials are given in Table 6.5. It is important to note that the Hall–Petch equation does not apply to (1) extremely coarse or extremely fine grain sizes and (2) metals used at elevated temperatures.

Figure 6.38 compares the tensile stress-strain curves for single-crystal and polycrystalline unalloyed copper at room temperature. At all strains, the polycrystalline copper is stronger than the single-crystal copper. At 20 percent strain, the tensile strength of the polycrystalline copper is 40 ksi (276 MPa) as compared to 8 ksi (55 MPa) for single-crystal copper.

---

[8]Single-crystal turbine blades have been developed for use in gas turbine engines to avoid grain boundary cracking at high temperatures and stresses. See F.L. Ver Snyder and M.E. Shank, *Mater. Sci. Eng.,* 6:213–247(1970).

Table 6.5 Hall–Petch relationship constants for selected materials

	σ_0 (MPa)	k (MPa · $m^{1/2}$)
Cu	25	0.11
Ti	80	0.40
Mild steel	70	0.74
Ni_3Al	300	1.70

Source: www.tf.uni-kiel.de/matwis/matv/pdf/chap_3_3.pdf

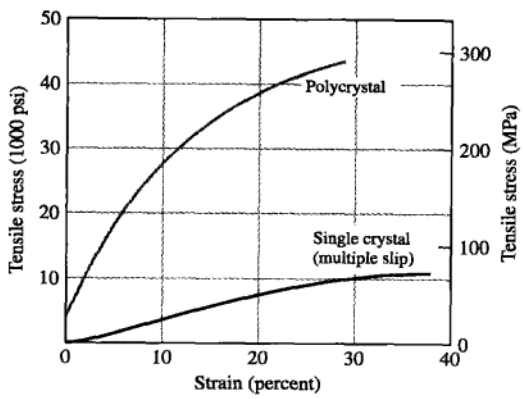

Figure 6.38
Stress-strain curves for single-crystal and polycrystalline copper. The single crystal is oriented for multiple slip. The polycrystal shows higher strength at all strains.
(After M. Eisenstadt, "Introduction to Mechanical Properties of Materials," Macmillan, 1971, p. 258.)

During the plastic deformation of metals, dislocations moving along on a particular slip plane cannot go directly from one grain into another in a straight line. As shown in Fig. 6.39, slip lines change directions at grain boundaries. Thus, each grain has its own set of dislocations on its own preferred slip planes, which have different orientations from those of neighboring grains. As the number of grains increases and grain diameter becomes smaller, dislocations within each grain can travel a smaller distance before they encounter the grain boundary, at which point their movement is terminated (dislocation pileup). It is for this reason that

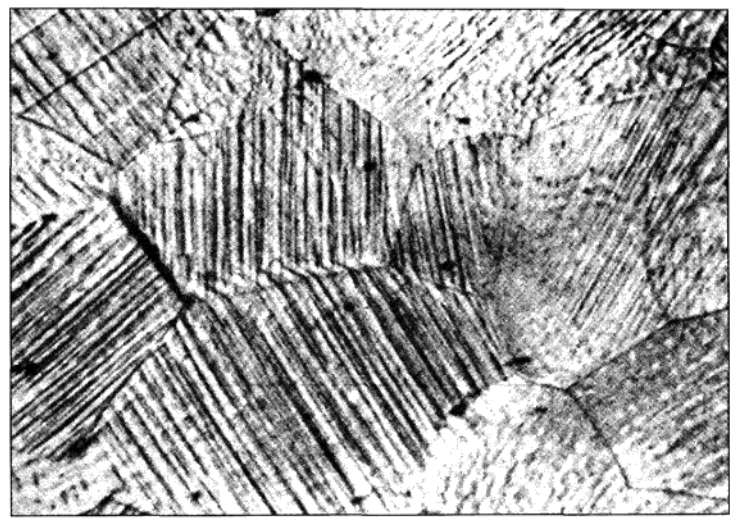

Figure 6.39
Polycrystalline aluminum that has been plastically deformed. Note that the slipbands are parallel within a grain but are discontinuous across the grain boundaries. (Magnification 60×.)
(After G.C. Smith, S. Charter, and S. Chiderley of Cambridge University.)

fine-grained materials possess a higher strength. Figure 6.40 shows clearly a high-angle grain boundary that is acting as a barrier to dislocation movement and has caused dislocations to pile up at the grain boundary.

6.6.2 Effect of Plastic Deformation on Grain Shape and Dislocation Arrangements

Grain Shape Changes with Plastic Deformation Let us consider the plastic deformation of annealed samples[9] of unalloyed copper that have an equiaxed grain structure. Upon cold plastic deformation, the grains are sheared relative to each other by the generation, movement, and rearrangement of dislocations. Figure 6.41 shows the microstructures of samples of unalloyed copper sheet that was cold-rolled to reductions of 30 and 50 percent. Note that with increased cold rolling the grains are more elongated in the rolling direction as a consequence of dislocation movements.

[9]Samples in the annealed conditions have been plastically deformed and then reheated to such an extent that a grain structure in which the grains are approximately equal in all directions (equiaxed) is produced.

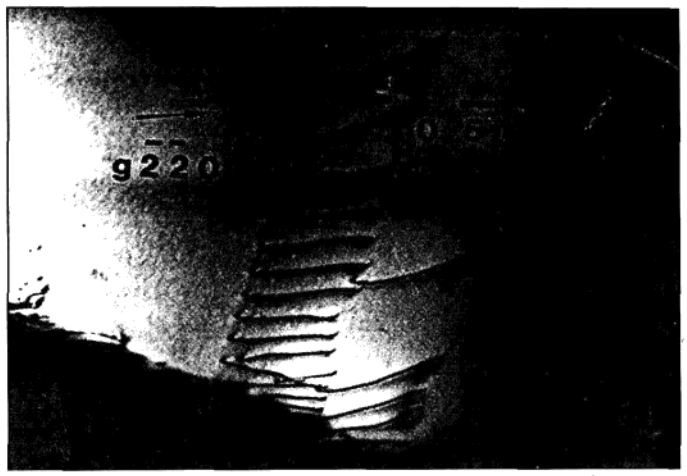

Figure 6.40
Dislocations piled up against a grain boundary as observed with a transmission electron microscope in a thin foil of stainless steel. (Magnification 20,000×.)
[After Z. Shen, R.H. Wagoner, and W.A.T. Clark, Scripta Met., 20: 926 (1986).]

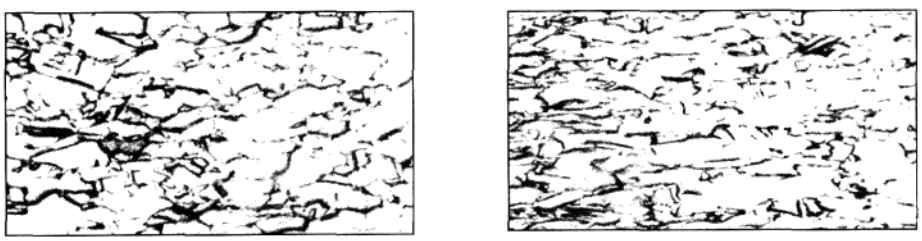

(*a*) (*b*)

Figure 6.41
Optical micrographs of deformation structures of unalloyed copper that was cold-rolled to reductions of (*a*) 30 percent and (*b*) 50 percent. (Etch: potassium dichromate; magnification 300×.)
(After J.E. Boyd in "Metals Handbook," vol. 8: "Metallography, Structures, and Phase Diagrams," 8th ed., American Society for Metals, 1973, p. 221. Reprinted with permission from ASM International. All rights reserved. www.asminternational.org.)

Dislocation Arrangement Changes with Plastic Deformation The dislocations in the unalloyed copper sample after 30 percent plastic deformation form cell-like configurations with clear areas in the centers of the cells (Fig. 6.42*a*). With increased

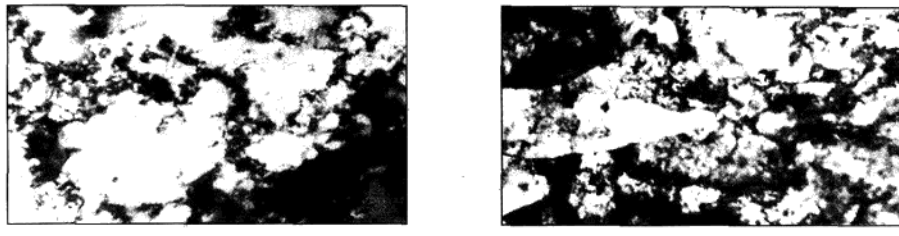

(*a*) (*b*)

Figure 6.42
Transmission electron micrographs of deformation structures of unalloyed copper that was cold-rolled to reductions of (*a*) 30 percent and (*b*) 50 percent. Note that these electron micrographs correspond to the optical micrographs of Fig. 6.41. (Thin-foil specimens, magnification 30,000×.)
(After J.E. Boyd in "Metals Handbook," vol. 8: "Metallography, Structures, and Phase Diagrams," 8th ed., American Society for Metals, 1973, p. 221. Reprinted with permission from ASM International. All rights reserved. www.asminternational.org.)

cold plastic deformation to 50 percent reduction, the cell structure becomes denser and elongated in the direction of rolling (Fig. 6.42*b*).

6.6.3 Effect of Cold Plastic Deformation on Increasing the Strength of Metals

As shown by the electron micrographs of Fig. 6.42, the dislocation density increases with increased cold deformation. The exact mechanism by which the dislocation density is increased by cold working is not completely understood. New dislocations are created by the cold deformation and must interact with those already existing. As the dislocation density increases with deformation, it becomes more and more difficult for the dislocations to move through the existing "forest of dislocations," and thus the metal work or strain hardens with increased cold deformation.

When ductile metals such as copper, aluminum, and α iron that have been annealed are cold-worked at room temperature, they strain-harden because of the dislocation interaction just described. Figure 6.43 shows how cold working at room temperature increases the tensile strength of unalloyed copper from about 30 ksi (200 MPa) to 45 ksi (320 MPa) with 30 percent cold work. Associated with the increase in tensile strength, however, is a decrease in elongation (ductility), as observed in Fig. 6.43. With 30 percent cold work, the elongation of unalloyed copper decreases from about 52 to 10 percent elongation.

Cold working or **strain hardening** is one of the most important methods for strengthening some metals. For example, pure copper and aluminum can be strengthened significantly only by this method. Thus, cold-drawn unalloyed copper wire can be produced with different strengths (within certain limitations) by varying the amount of strain hardening.

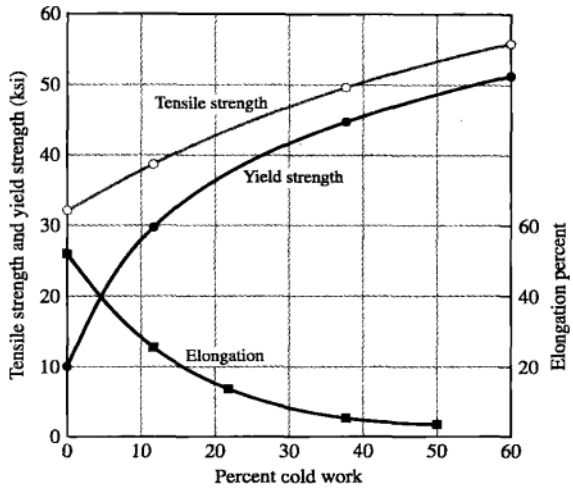

Figure 6.43
Percent cold work versus tensile strength and elongation for unalloyed oxygen-free copper. Cold work is expressed as a percent reduction in cross-sectional area of the metal being reduced.

EXAMPLE PROBLEM 6.10

We wish to produce a 0.040-in.-thick sheet of oxygen-free copper with a tensile strength of 45 ksi. What percent cold work must the metal be given? What must the starting thickness of the metal be before cold rolling?

■ **Solution**

From Fig. 6.43, the percent cold work must be 25 percent. Thus, the starting thickness must be

$$\frac{x - 0.040 \text{ in.}}{x} = 0.25$$

$$x = 0.053 \text{ in.} \blacktriangleleft$$

6.7 SOLID-SOLUTION STRENGTHENING OF METALS

Another method besides cold working by which the strength of metals can be increased is **solid-solution strengthening.** The addition of one or more elements to a metal can strengthen it by the formation of a solid solution. The structure of *substitutional* and *interstitial solid solutions* has already been discussed in Sec. 4.3 and should be referred to for review. When substitutional (solute) atoms are mixed in the solid state with those of another metal (solvent), stress fields are created around each

solute atom. These stress fields interact with dislocations and make their movement more difficult, and thus the solid solution becomes stronger than the pure metal.

Two important factors in solid-solution strengthening are:

1. *Relative-size factor.* Differences in atomic size of solute and solvent atoms affect the amount of solid-solution strengthening because of the crystal lattice distortions produced. Lattice distortions make dislocation movement more difficult and hence strengthen the metallic solid solution.
2. *Short-range order.* Solid solutions are rarely random in atomic mixing, and some kind of short-range order or clustering of like atoms takes place. As a result, dislocation movement is impeded by different bonding structures.

In addition to these factors, there are others that also contribute to solid-solution strengthening but will not be dealt with in this book.

As an example of solid-solution strengthening, let us consider a solid solution alloy of 70 wt % Cu and 30 wt % Zn (cartridge brass). The tensile strength of unalloyed copper with 30 percent cold work is about 48 ksi (330 MPa) (Fig. 6.43). However, the tensile strength of the 70 wt % Cu–30 wt % Zn alloy with 30 percent cold work is about 72 ksi (500 MPa) (Fig. 6.44). Thus, solid-solution strengthening in this case produced an increase in strength in the copper of about 24 ksi (165 MPa). On the other hand, the ductility of the copper by the 30 percent zinc addition after 30 percent cold work was reduced from about 65 to 10 percent (Fig. 6.44).

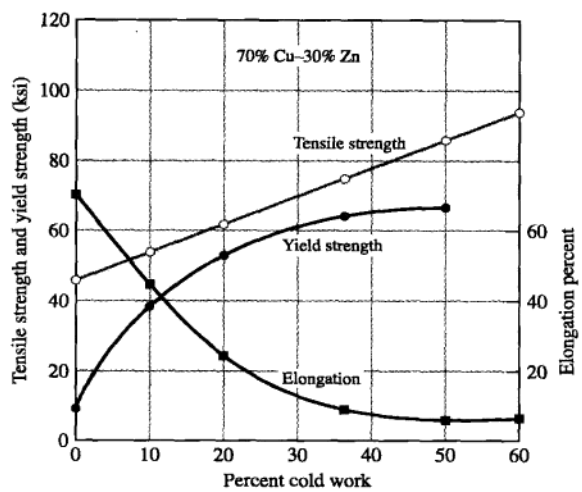

Figure 6.44
Percent cold work versus tensile strength and elongation for 70 wt % Cu–30 wt % Zn alloy. Cold work is expressed as a percent reduction in cross-sectional area of the metal being reduced (see Eq. 6.2).

6.8 RECOVERY AND RECRYSTALLIZATION OF PLASTICALLY DEFORMED METALS

In previous sections the effect of plastic deformation on the mechanical properties and microstructural features of metals was discussed. When metal-forming processes such as rolling, forging, extrusion, and others are performed cold, the work material has many dislocations and other defects, and the grains are stretched and deformed; as a result, the worked metal is significantly stronger but less ductile. Many times the reduced ductility of the cold-worked metal is undesirable, and a softer metal is required. To achieve this, the cold-worked metal is heated in a furnace. If the metal is reheated to a sufficiently high temperature for a long enough time, the cold-worked metal structure will go through a series of changes called (1) **recovery,** (2) **recrystallization,** and (3) **grain growth.** Figure 6.45 shows these structural changes schematically as the temperature of the metal is increased along with the corresponding changes in mechanical properties. This reheating treatment that softens a cold-worked metal is called **annealing,** and the terms *partial anneal* and *full anneal* are often used to refer to degrees of softening. Let us now examine these structural changes in more detail, starting with the heavily cold-worked metal structure.

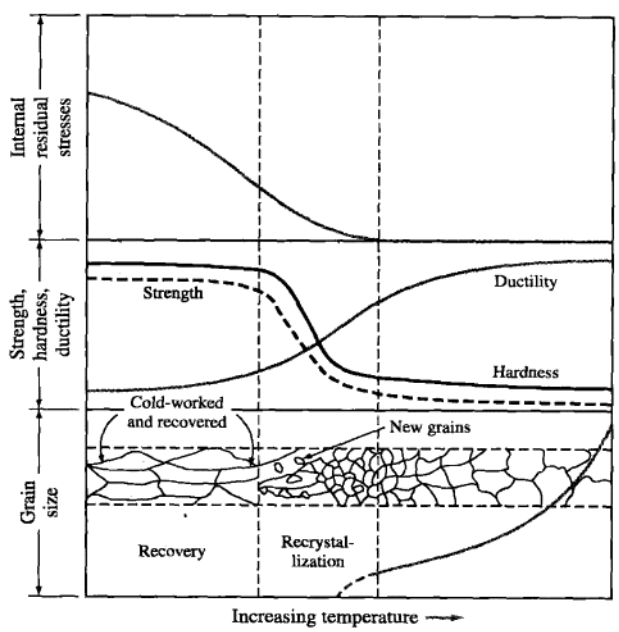

Figure 6.45
Effect of annealing on the structure and mechanical property changes of a cold-worked metal.
(Adapted from Z.D. Jastrzebski, "The Nature and Properties of Engineering Materials," 2nd ed., Wiley, 1976, p. 228.)

6.8.1 Structure of a Heavily Cold-Worked Metal before Reheating

When a metal is heavily cold-worked, much of the strain energy expended in the plastic deformation is stored in the metal in the form of dislocations and other imperfections such as point defects. Thus a strain-hardened metal has a higher internal energy than an unstrained one. Figure 6.46*a* shows the microstructure (100×) of an Al−0.8% Mg alloy sheet that has been cold-worked with 85 percent reduction. Note that the grains are greatly elongated in the rolling direction. At higher magnification (20,000×), a thin-foil transmission electron micrograph

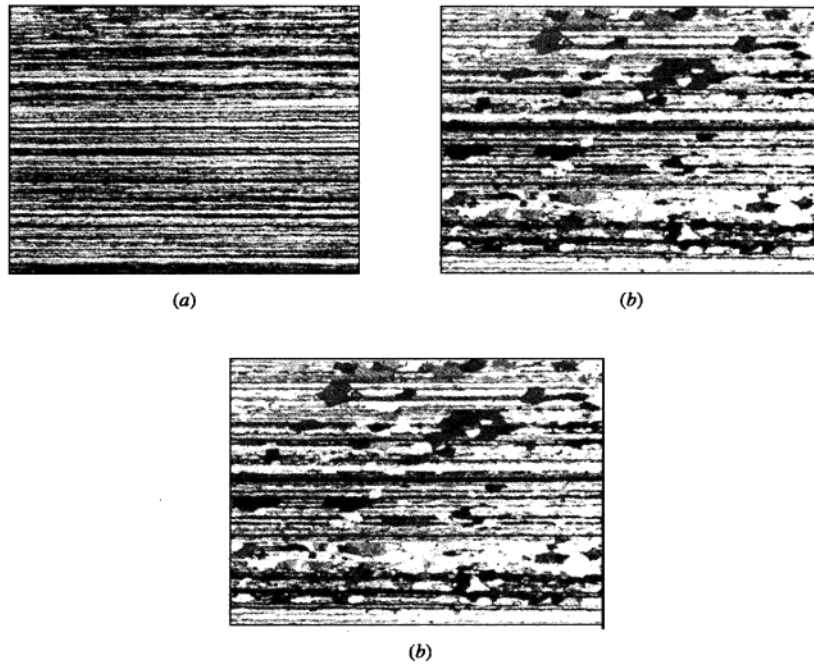

Figure 6.46
Aluminum alloy 5657 (0.8% Mg) sheet showing microstructures after cold rolling 85 percent and subsequent reheating (optical micrographs at 100× viewed under polarized light). (*a*) Cold-worked 85 percent; longitudinal section. Grains are greatly elongated. (*b*) Cold-worked 85 percent and stress-relieved at 302ºC (575ºF) for 1 h. Structure shows onset of recrystallization, which improves the formability of the sheet. (*c*) Cold-worked 85 percent and annealed at 316ºC (600ºF) for 1 h. Structure shows recrystallized grains and bands of unrecrystallized grains.
(After "Metals Handbook," vol. 7, 8th ed., American Society for Metals, 1972, p. 243. Reprinted with permission from ASM International. All rights reserved. www.asminternational.org.)

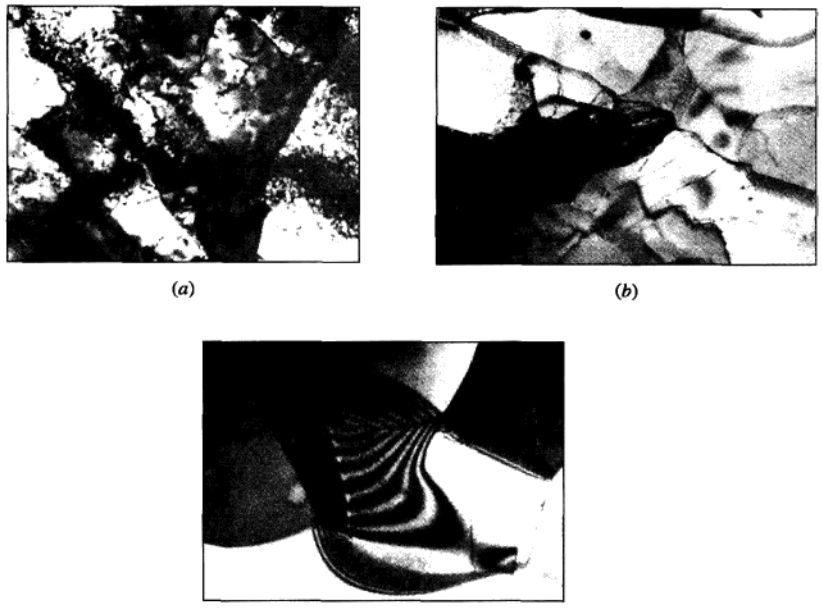

(*a*) (*b*)

(*c*)

Figure 6.47
Aluminum alloy 5657 (0.8% Mg) sheet showing microstructures after cold rolling 85 percent and subsequent reheating. The microstructures shown in this figure were obtained by using thin-foil transmission electron microscopy. (Magnified 20,000×.) (*a*) Sheet was cold-worked 85 percent; micrograph shows dislocation tangles and banded cells (subgrains) caused by cold working extensively. (*b*) Sheet was cold-worked 85 percent and subsequently stress-relieved at 302°C (575°F) for 1 h. Micrograph shows dislocation networks and other low-angle boundaries produced by polygonization. (*c*) Sheet was cold-worked 85 percent and annealed at 316°C (600°F) for 1 h. Micrograph shows recrystallized structure and some subgrain growth.
(After "Metals Handbook," vol. 7, 8th ed., American Society for Metals, 1972, p. 243. Reprinted with permission from ASM International. All rights reserved. www.asminternational.org.)

(Fig. 6.47) shows the structure to consist of a cellular network with cell walls of high dislocation density. A fully cold-worked metal has a density of approximately 10^{12} dislocation lines/cm^2.

6.8.2 Recovery

When a cold-worked metal is heated in the recovery temperature range that is just below the recrystallization temperature range, internal stresses in the metal are relieved (Fig. 6.45). During recovery, sufficient thermal energy is supplied to allow

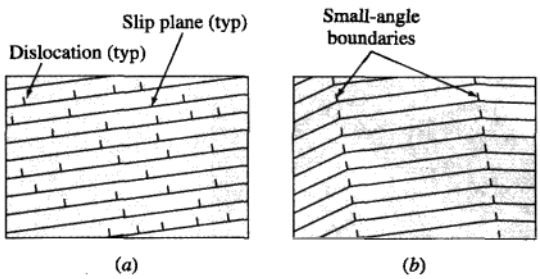

Figure 6.48
Schematic representation of polygonization in a deformed metal. (*a*) Deformed metal crystal showing dislocations piled up on slip planes. (*b*) After recovery heat treatment, dislocations move to form small-angle grain boundaries. (*After L.E. Tanner and I.S. Servi, in "Metals Handbook," vol. 8, 8th ed., American Society for Metals, 1973, p. 222.*)

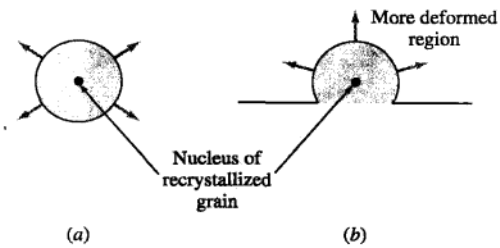

Figure 6.49
Schematic model of the growth of a recrystallized grain during the recrystallization of a metal. (*a*) Isolated nucleus expanded by growth within a deformed grain. (*b*) Original high-angle grain boundary migrating into a more highly deformed region of metal.

the dislocations to rearrange themselves into lower-energy configurations (Fig. 6.48). Recovery of many cold-worked metals (such as pure aluminum) produces a subgrain structure with low-angle grain boundaries, as shown in Fig. 6.48*b*. This recovery process is called *polygonization*, and often it is a structural change that precedes recrystallization. The internal energy of the recovered metal is lower than that of the cold-worked state since many dislocations are annihilated or moved into lower-energy configurations by the recovery process. During recovery the strength of a cold-worked metal is reduced only slightly but its ductility is usually significantly increased (Fig. 6.45).

6.8.3 Recrystallization

Upon heating a cold-worked metal to a sufficiently high temperature, new strain-free grains are nucleated in the recovered metal structure and begin to grow (Fig. 6.46*b*), forming a recrystallized structure. After a long enough time at a temperature at which recrystallization takes place, the cold-worked structure is completely replaced with a recrystallized grain structure, as shown in Fig. 6.46*c*.

Primary recrystallization occurs by two principal mechanisms: (1) an isolated nucleus can expand with a deformed grain (Fig. 6.49*a*) or (2) an original high-angle grain boundary can migrate into a more highly deformed region of the metal (Fig. 6.49*b*). In either case, the structure on the concave side of the moving boundary is strain-free and has a relatively low internal energy, whereas the structure on the convex side of the moving interface is highly strained with a high dislocation density and high internal energy. Grain boundary movement is therefore

away from the boundary's center of curvature. Thus, the growth of an expanding new grain during primary recrystallization leads to an overall decrease in the internal energy of the metal by replacing deformed regions with strain-free regions.

The tensile strength of a cold-worked metal is greatly decreased and its ductility increased by an annealing treatment that causes the metal structure to be recrystallized. For example, the tensile strength of a 0.040-in. (1-mm) sheet of 85% Cu–15% Zn brass that had been cold-rolled to 50 percent reduction was decreased from 75 to 45 ksi (520 to 310 MPa) by annealing 1 h at 400°C (Fig. 6.50*a*). The

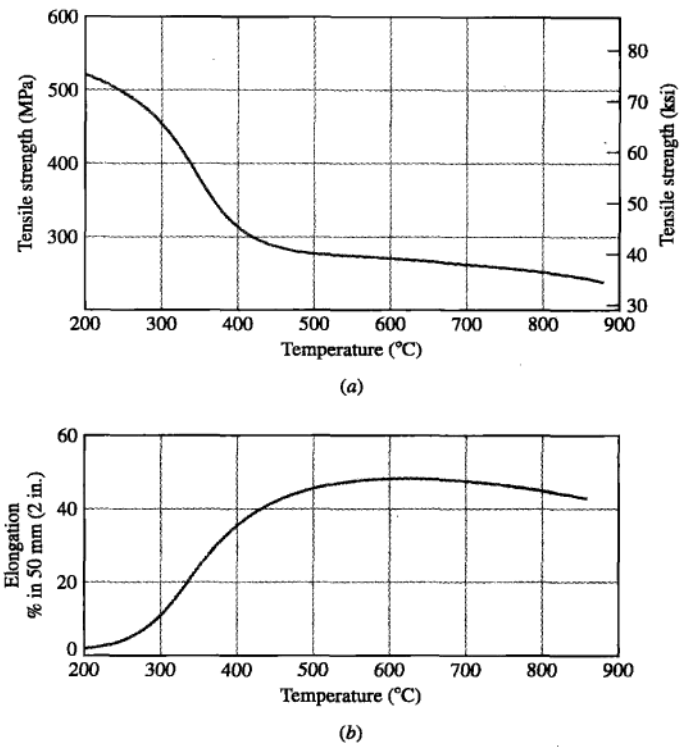

Figure 6.50
Effect of annealing temperature on (*a*) the tensile strength and (*b*) elongation of a 50 percent cold-rolled 85% Cu–15% Zn, 0.040-in. (1 mm) thick sheet. (Annealing time was 1 h at temperature.)
(After "Metals Handbook," vol. 2, 9th ed., American Society for Metals, 1979, p. 320.)

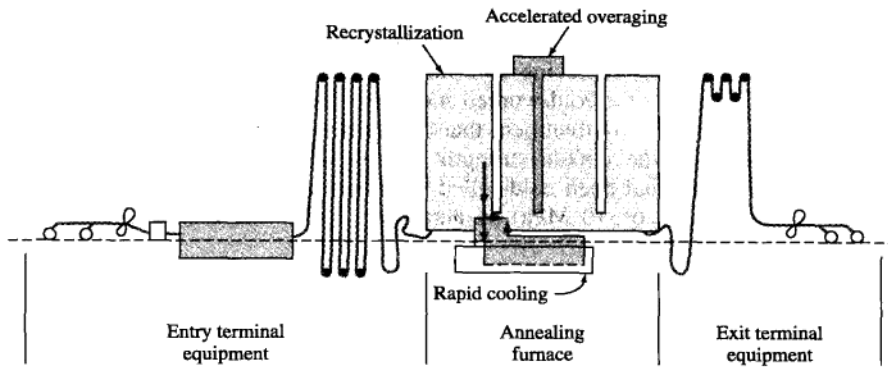

Figure 6.51
Continuous annealing schematic diagram.
(After W.L. Roberts, "Flat Processing of Steel," Marcel Dekker, 1988.)

ductility of the sheet, on the other hand, was increased from 3 to 38 percent with the annealing treatment (Fig. 6.50*b*). Figure 6.51 shows a schematic diagram of a continuous annealing process for sheet steel.

Important factors that affect the recrystallization process in metals and alloys are (1) amount of prior deformation of the metal, (2) temperature, (3) time, (4) initial grain size, and (5) composition of the metal or alloy. The recrystallization of a metal can take pace over a range of temperatures, and the range is dependent to some extent on the variables just listed. Thus, one cannot refer to the recrystallization temperature of a metal in the same sense as the melting temperature of a pure metal. The following generalizations can be made about the recrystallization process:

1. A minimum amount of deformation of the metal is necessary for recrystallization to be possible.
2. The smaller the degree of deformation (above the minimum), the higher the temperature needed to cause recrystallization.
3. Increasing the temperature for recrystallization decreases the time necessary to complete it (see Fig. 6.52).
4. The final grain size depends mainly on the degree of deformation. The greater the degree of deformation, the lower the annealing temperature for recrystallization and the smaller the recrystallized grain size.
5. The larger the original grain size, the greater the amount of deformation required to produce an equivalent recrystallization temperature.
6. The recrystallization temperature decreases with increasing purity of the metal. Solid-solution alloying additions always increase the recrystallization temperature.

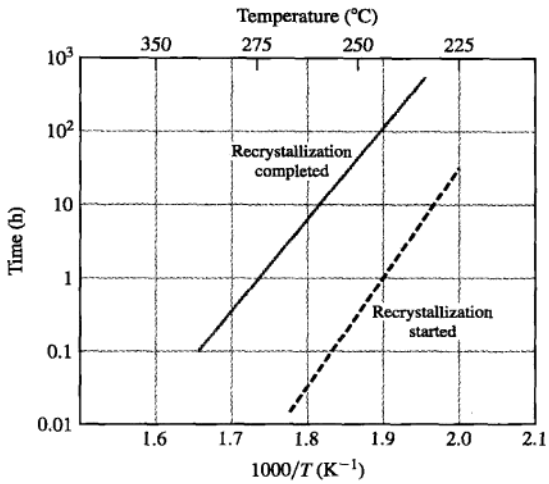

Figure 6.52
Time-temperature relations for the recrystallization of 99.0% Al cold-worked 75 percent. The solid line is for recrystallization finished and the dashed line for recrystallization started. Recrystallization in this alloy follows an Arrhenius-type relationship of ln t versus $1/T(K^{-1})$.
(After "Aluminum," vol. 1, American Society for Metals, 1967, p. 98.)

EXAMPLE PROBLEM 6.11

If it takes 9.0×10^3 min to recrystallize a piece of copper at 88°C and 200 min at 135°C, what is the activation energy for the process, assuming the process obeys the Arrhenius rate equation and the time to recrystallize $= Ce^{-Q/RT}$, where $R = 8.314$ J/(mol · K) and T is in kelvins?

■ **Solution**

$$t_1 = 9.0 \times 10^3 \text{ min}; T_1 = 88°C + 273 = 361 \text{ K}$$

$$t_2 = 200 \text{ min}; T_2 = 135°C + 273 = 408 \text{ K}$$

$$t_1 = Ce^{Q/RT_1} \quad \text{or} \quad 9.0 \times 10^3 \text{ min} = Ce^{Q/R(361 \text{ K})} \tag{6.17}$$

$$t_2 = Ce^{Q/RT_2} \quad \text{or} \quad 200 \text{ min} = Ce^{Q/R(408 \text{ K})} \tag{6.18}$$

Dividing Eq. 6.17 by 6.18 gives

$$45 = \exp\left[\frac{Q}{8.314}\left(\frac{1}{361} - \frac{1}{408}\right)\right]$$

$$\ln 45 = \frac{Q}{8.314}(0.00277 - 0.00245) = 3.80$$

$$Q = \frac{3.80 \times 8.314}{0.000319} = 99{,}038 \text{ J/mol or } 99.0 \text{ kJ/mol} \blacktriangleleft$$

6.9 SUPERPLASTICITY IN METALS

A careful examination of Fig. 6.23 shows that most metals, even those that are classified as ductile, undergo a limited amount of plastic deformation prior to fracture. For example, mild steel undergoes 22 percent elongation before fracture in uniaxial tensile tests. As discussed in Sec. 6.1, many metal-forming operations are performed at elevated temperatures in order to achieve a higher degree of plastic deformation by increasing the ductility of the metal. **Superplasticity** refers to the ability of some metal alloys, such as some aluminum and titanium alloys, to deform as much as 2000 percent at elevated temperatures and slow loading rates. These alloys do not behave superplastically when loaded at normal temperatures. For example, annealed Ti alloy (6Al-4V) elongates close to 12 percent prior to fracture in a conventional tensile test at room temperature. The same alloy, when tested at elevated temperatures (840°C to 870°C) and at very low loading rates ($1.3 \times 10^{-4}\,s^{-1}$), can elongate as much as 750 to 1170 percent. To achieve superplasticity, the material and the loading process must meet certain conditions:

1. The material must possess very fine grain size (5–10 μm) and be highly strain-rate sensitive.
2. A high loading temperature greater than 50 percent of the melt temperature of the metal is required.
3. A low and controlled strain rate in the range of 0.01 to 0.0001 s^{-1} is required.[10]

These requirements are not easily achievable for all materials and therefore not all materials can attain superplastic behavior. In most cases, condition (1) is very difficult to achieve, i.e., ultrafine grain size.[11]

Superplastic behavior is an extremely useful property that can be used to manufacture complex structural components. The question is, "What is the deformation mechanism that accounts for this incredible level of plastic deformation?" In previous sections, we discussed the role of dislocations and their movements on the plastic behavior of materials under room temperature loading. As dislocations move across the grain, plastic deformation is produced. But as grain size decreases, the movement of dislocations becomes more limited and the material becomes stronger. However, metallographical analysis of materials that undergo superplastic behavior has revealed very limited dislocation activity inside the grain. This supports the fact that superplastic materials are susceptible to other deformation mechanisms such as grain boundary sliding and grain boundary diffusion. At elevated temperatures, a large amount of strain is believed to be accumulated by the sliding and rotation of individual grains or clusters of grains relative to each other. There is also a belief that grain boundary sliding is accommodated by a gradual change in grain shape as matter is moved by diffusion across the grain boundary. Figure 6.53 shows the microstructure of Pb–Sn eutectic alloy before (Fig. 6.53*a*) and after superplastic deformation (Fig. 6.53*b*). It is clear from the figure that grains are equiaxed before and after the deformation; sliding and rotation of the grains are noticeable.

---

[10]High strain rate ($>10^{-2}\,s^{-1}$) superplasticity has been reported in some aluminum alloys.

[11]Static and dynamic recrystallization, mechanical alloying, and other techniques are used to create ultrafine grain structure.

Many manufacturing processes exist that take advantage of the superplastic behavior of materials to produce complex components. Blow forming is one such process in which a superplastic material is forced under gas pressure to deform and take the shape of a die. Figure 6.54 shows the hood of the automobile that is made from superplastically formed aluminum alloy using the blow-forming method. Also, superplastic behavior can be combined with diffusion bonding (a metal-joining method) to produce structural components with limited material waste.

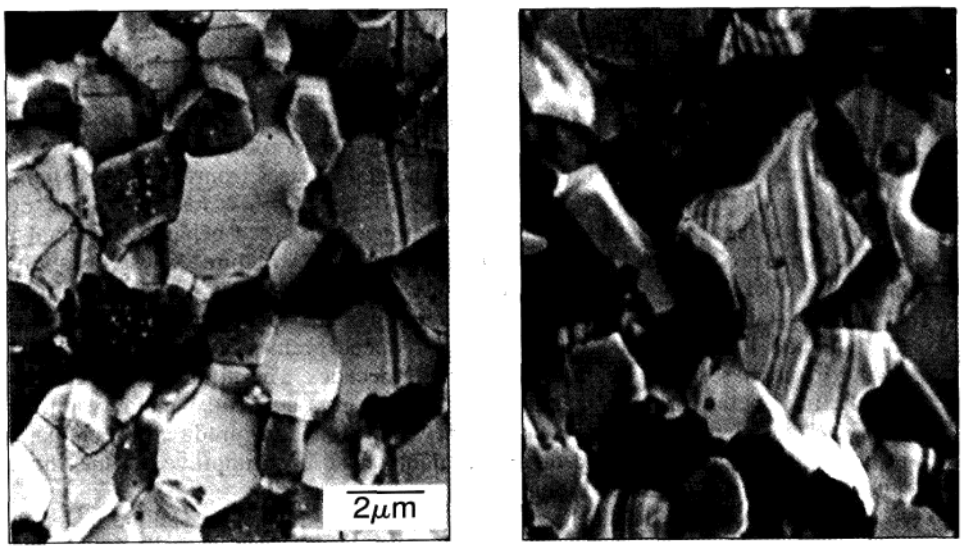

(*a*) (*b*)

Figure 6.53
Superplastic deformation in Pb–Sn eutectic alloy (*a*) before and (*b*) after deformation.

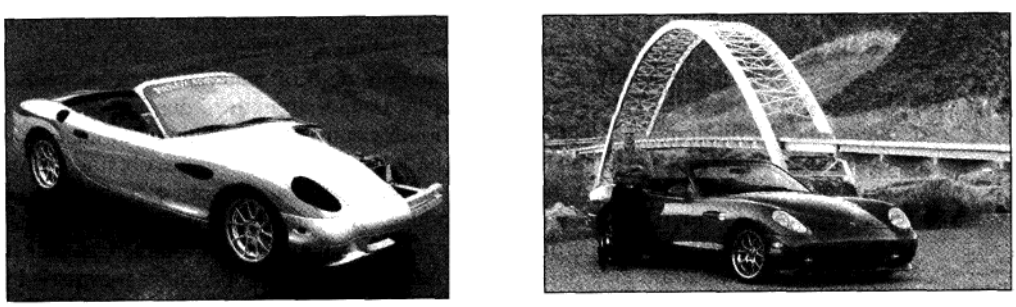

(*a*) (*b*)

Figure 6.54
The hood for the automobile made of superplastic aluminum using the blow-molding method.
(Courtesy of Panoz Auto.)

6.10 NANOCRYSTALLINE METALS

In Chap. 1, the concept of nanotechnology and nanostructured materials was introduced. Any material with length scale features below 100 nm is classified as *nanostructured.* According to this definition, all metals with average grain diameters less than 100 nm are considered nanostructured or nanocrystalline. The question is, "What are the advantages of **nanocrystalline metals**?" Metallurgists have always been aware that by reducing the grain size, a harder, stronger, and tougher metal may be produced as evidenced by the Hall–Petch equation (6.16). It has also been known that at ultrafine grain size levels (not necessarily nanocrystalline) and under certain temperature and loading rate conditions, some materials can deform plastically to many times their conventional levels, i.e., they achieve superplasticity.

Noting the characteristics attributed to ultrafine grain sizes and extrapolating the Hall–Petch equation for nanocrystalline metals, one can foresee some extraordinary possibilities. Consider the possibility that, according to the Hall–Petch equation, if the average grain diameter of a metal decreases from 10 μm to 10 nm, its yield strength will increase by a factor of 31. Is this possible? How do nanograins affect the ductility, toughness, fatigue, and creep behavior of metals? How can we produce bulk metals with nanocrystalline structure? These questions and others like them are the driving force in research and development in the field of nanocrystalline metals. Therefore, at least in metal-manufacturing industries, the potential for improved properties with reduced grain size or dispersing secondary nanophases has been known for many decades. The difficulty has been in developing metal-forming techniques that can produce truly nanocrystalline ($d < 100$ nm) metals. In recent decades, new techniques for producing such materials have been developed and older techniques have been improved. Thus, those studying these materials are enthusiastic.

It has been reported that the modulus of elasticity of nanocrystalline materials is comparable to bulk microcrystalline materials for grain sizes exceeding 5 nm. For d less than 5 nm, a decrease in the modulus of elasticity of metals such as nanocrystalline iron has been reported. It is not completely clear why such a drop in the modulus of elasticity occurs; one may find a reason by considering that for such small grains, the majority of the atoms are positioned on the surface of the grain (as opposed to inside the grain) and therefore along the grain boundary. This is completely opposite to what is found in microcrystalline materials.

As discussed previously, the hardness and strength of materials increase with a decrease in grain size. This increase in hardness and strength is due to dislocation pileup and the hindrance of dislocation motion for conventional grains. For nanocrystalline materials, most available data are based on hardness values obtained from nanohardness tests. This is mostly due to the fact that tensile specimens with nanocrystalline structure are hard to produce. But since strength and hardness are closely correlated, nanohardness tests are acceptable at this time. It has been established that as grain size decreases to around 10 nm, the hardness increases by factors of four to six for nanocrystalline copper and six to eight for nanocrystalline nickel when compared to large grained metals ($d > 1$ μm). Although this is an